

Student Researched and Developed High Power Rocket

A Technical Report submitted to the Department of Mechanical and Aerospace Engineering

Presented to the Faculty of the School of Engineering and Applied Science
University of Virginia • Charlottesville, Virginia

In Partial Fulfillment of the Requirements for the Degree
Bachelor of Science, School of Engineering

Aymon Daud

Spring, 2024

Technical Project Team Members

Ardan Abraham	Andy Delgado	Duraan Miskinyar	Dylan Tran
Jake Bales	Tim Edinger	Miriam Morse	Peter Zappia
Alexandria Barnard-Davignon	Noah Hassett	Jason Nguyen	
Leo Bashaw	Jordyn Hicks	Aiden Ogle	
Tucker Benton	Niklas Holle	Thomas Ortega	
Marc Brightwell	Dylan House	Aaron Osborne	
Joe Burton	Claire Kent	Johannes Quapil	
Christopher Camacho	Connor Lothrop	Shane Sawyer	
Aymon Daud	Olivia Lyall	Daniel Tohti	

Executive Summary	5
Project and Team Organization	7
Introduction	8
Problem Definition	8
Aerospace Context	9
Functional Requirements / Specifications	9
Design Approach.....	9
Design	11
Aerodynamics and Structures.....	11
Nosecone	11
Description.....	11
Analysis.....	13
Fins	17
Description.....	17
Analysis.....	18
Couplers.....	22
Description.....	22
Analysis.....	24
Body.....	25
Description.....	25
Analysis.....	26
Mechatronics and Controls.....	26
Electronics	26
Description.....	26
Analysis.....	27
Avionics Bay	29
Description.....	29
Analysis.....	29
Parachute Deployment.....	30

Description.....	30
Analysis.....	30
Payload	31
Description.....	31
Analysis.....	32
Propulsion.....	41
Motor Selection	41
Motor Design.....	45
Analysis.....	54
Prototype.....	56
Aerodynamics and Structures.....	56
Purpose	56
Description and Implementation	56
Manufacturing and Fabrication	57
Nosecone.....	57
Fins.....	60
Integration.....	63
Body.....	64
Mechatronics and Controls.....	66
Electronics	66
Purpose.....	66
Description and Implementation	66
Testing and Results	68
Avionics Bay	74
Purpose.....	74
Description and Implementation	74
Manufacturing and Fabrication	75
Testing and Results	75
Parachute Deployment and Separation	76

Purpose.....	76
Description and Implementation.....	76
Manufacturing and Fabrication.....	76
Testing and Results.....	77
Payload.....	78
Purpose.....	78
Description and Implementation.....	78
Fabrication and Materials Selection.....	81
Testing Results.....	83
Propulsion.....	83
Purpose.....	83
Description and Implementation.....	83
Manufacturing and Fabrication.....	85
Testing Results.....	86
Risk and Liability.....	88
Ethical Issues.....	90
Impact on the Environment.....	91
Cost and Engineering Economics.....	92
Codes and Standards.....	93
Conclusion.....	94
Acknowledgements.....	94
References.....	96
Appendices.....	98

Executive Summary

The goal of this project was to design, prototype, fabricate, and test a high-powered rocket capable of reaching an apogee of 4000 feet and deploying an experiment as a payload. While the ultimate goals remained the same throughout the course of this capstone, there were numerous changes to the requirements, which played a large part in how the design and fabrication processes were conducted. The final design and predicted trajectory can be seen in figures 1 and 2 below. The initial requirements were based on those of the Intercollegiate Rocket Engineering Competition, and then those of the Battle of the Rockets at Tripoli Central Virginia. Ultimately, the members of the capstone decided to forgo participation in competitions, as it restricted our ability to use student-made designs. We agreed that it was more important to get the experience of creating our own components entirely from scratch than it was to see our rocket launched. Despite not being able to launch, it is our hope that our work will provide a valuable knowledge base for our class as we enter the workforce, as well as for future classes working on similar projects.

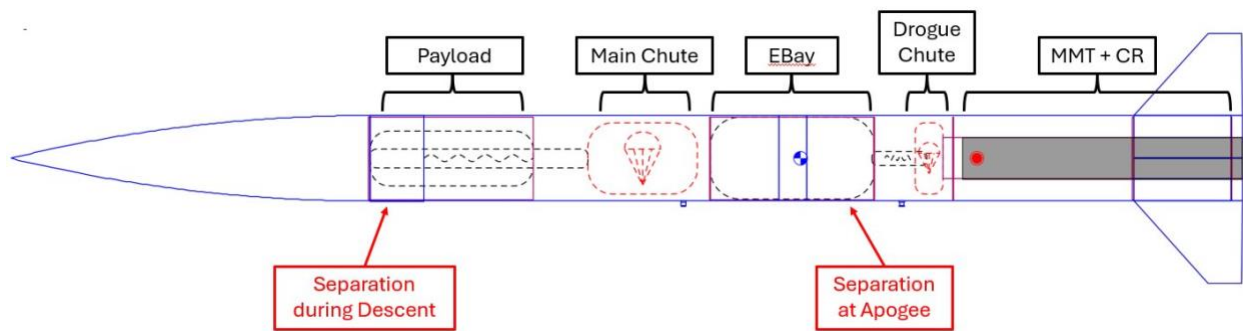


Figure 1. Labeled Final Open Rocket Model

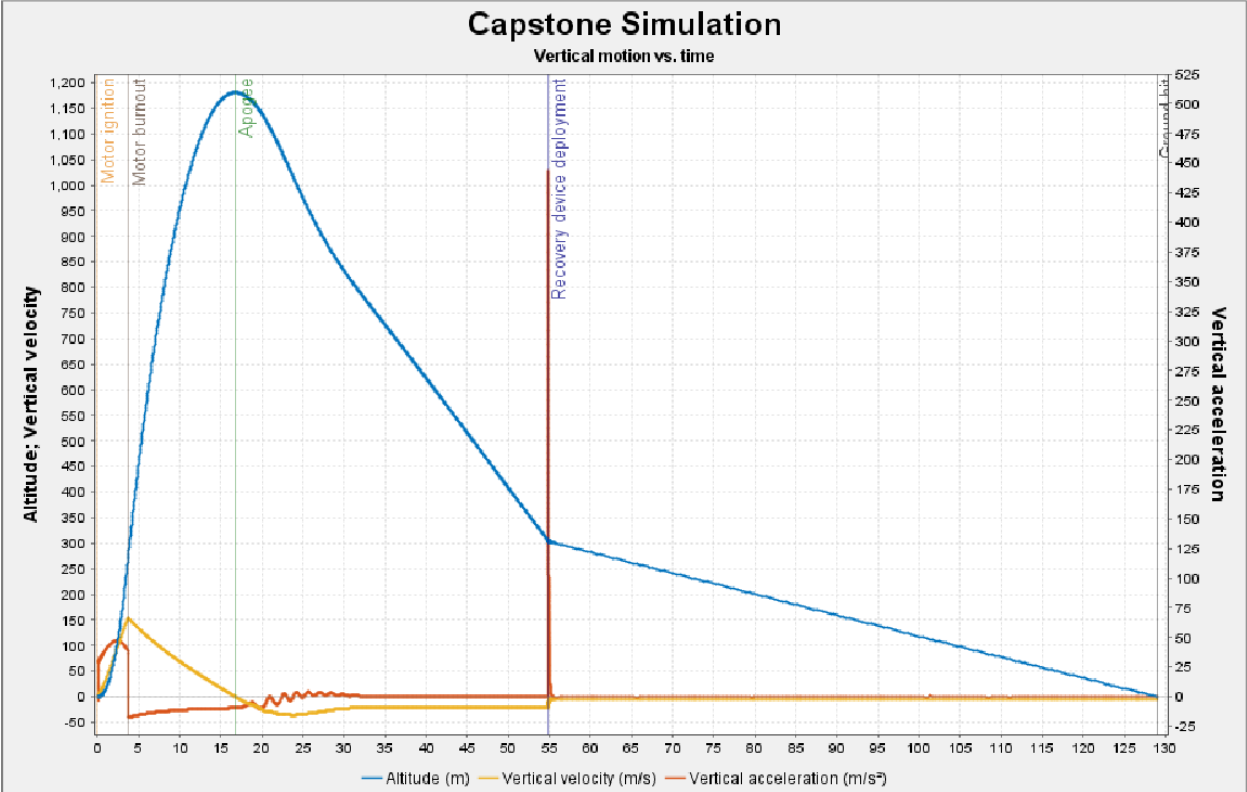
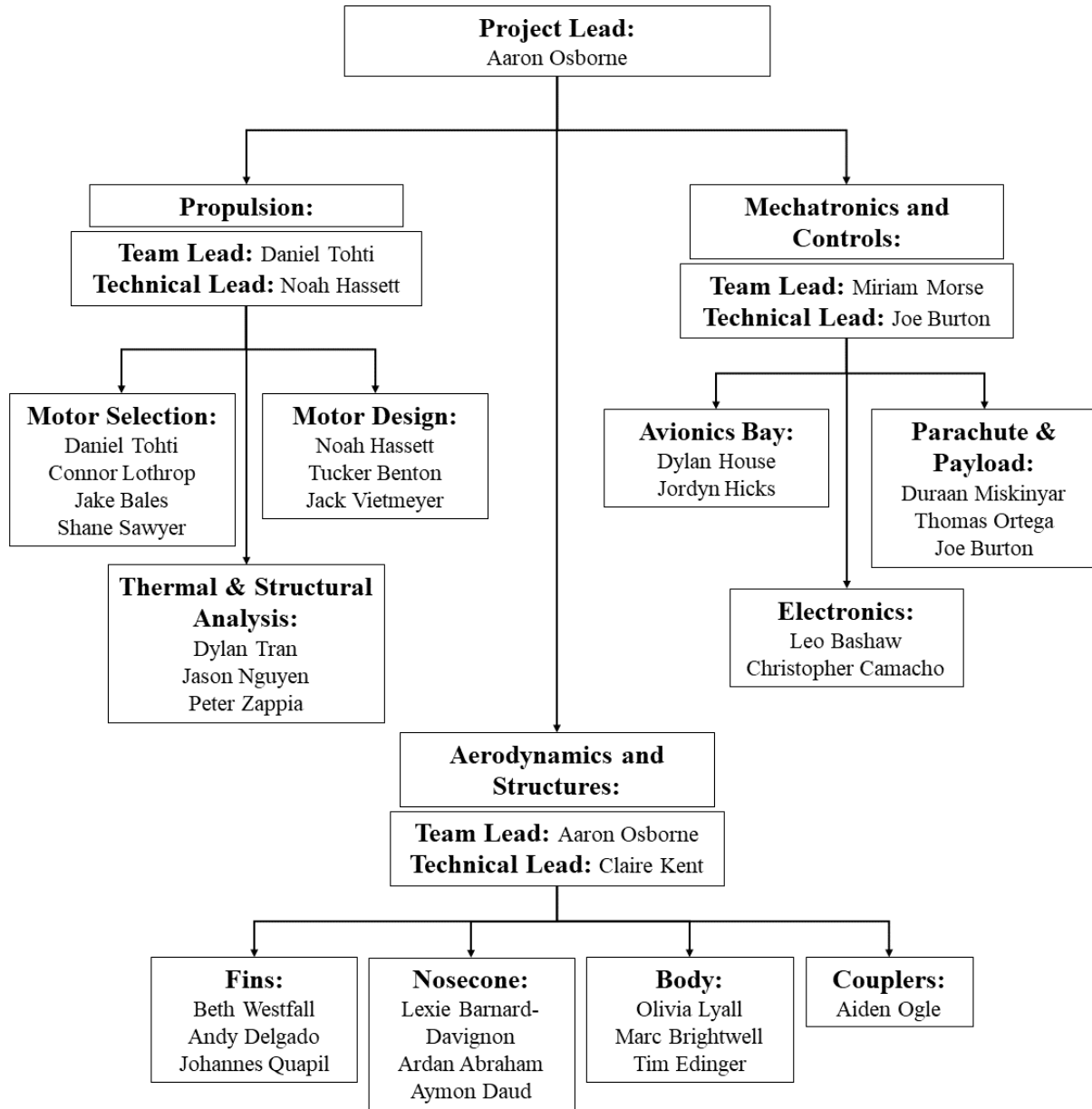


Figure 2. Final Open Rocket Simulation Data.

Project and Team Organization



Team composition was decided by the students. Each student indicated a top choice for a team to join, and leadership, which were chosen by the professors, finalized the members. Then, within the teams, each student selected a sub team based on technical interests. Communication

both within teams and between teams was facilitated by regular updates, communication through team leads, as well as direct communication between individuals.

Introduction

Problem Definition

While the specific technical requirements have significantly fluctuated over the duration of the Spacecraft Design Capstone, the core objectives have remained the same. The goal of this project was to design, develop, prototype, and ultimately fabricate and test a high-power rocket capable of performing an experiment with its payload. The rocket must have a recovery mechanism and land safely, posing no danger in its launch or fabrication process. The rocket must be able to successfully handle the high temperatures generated during firing of the motor without suffering unacceptable damages to the systems or structures of the rocket. The capstone aimed to deepen the class's understanding of rocket design and prototyping, and the necessary safety precautions. The difficulty of this problem comes from the numerous design decisions which all must be made in tandem. The most obvious example of this are the fin and nose cone designs; these two aerodynamic surfaces are necessary to ensure efficiency and stability, but their designs have large impacts on one another. This presents difficulties when trying to quickly iterate through design choices, as each component has many others contingent upon its design specifications. Furthermore, difficulty quickly arose during fabrication while attempting to meet the level of precision necessary for these and all other elements. Current practice usually involves outsourcing much of this manufacturing and design to suppliers. However, we elected not to follow this approach and instead seek the vital experience of manufacturing our own nosecone, fins, body tubes, avionics bay, and SRAD (Student Researched and Designed) motor.

Many specific requirements of the rocket, such as the 30cm x 10cm x 10cm payload size, are legacies of the initial project objective. During the capstone, our technical requirements shifted dramatically to accommodate three separate sets of criteria. Initially, the rocket was designed to abide by the IREC (Intercollegiate Rocket Engineering Competition) guidelines, which were well documented and easy to follow. However, as it became known that the capstone could not compete in addition to UVA's Rocketry Club, as universities are limited to one submission, these criteria had to change. Instead, the capstone elected to launch at the Battle of the Rockets at Tripoli Central Virginia. This option was appealing for its relative convenience, as well as the open channels of communication established with Tripoli TAP members Ben and Elaine Russell, as well as the site's prefect, Sean Hanlon. However, launching at this location would require the rocket to be significantly downsized and simplified, as these members had concerns regarding the capstone's level of experience. The deadline for launch also posed

significant time constraints which did not align with the course's schedule. Ultimately, the capstone class voted not to attempt the launch and instead focused on documenting the design and fabrication performed to allow future years to continue the project.

Aerospace Context

This project objective, as well as high-power rocketry in general, serve to represent the kind of work done in the aerospace industry. Working to achieve this definite goal required skills ranging from technical to budgeting, communication, planning, and risk analysis. In many ways, this project is most representative of the work many UVA aerospace engineers will go on to perform. High-power rocketry offers intense areas of focus which take years for universities to develop, including applications such as removable fins and SRAD motors. By beginning this capstone, the class has laid a solid foundation on which future years can build. This project presents a means to directly apply coursework in areas which pose many risks and require high degrees of fidelity. By striving to achieve these goals, the capstone both propels the stature of the University of Virginia as a rocketry school and expands our own knowledge in these specialized areas.

Functional Requirements / Specifications

Requirements for the rocket are as follows. It must carry a payload to a target altitude of 4,000 ft. while maintaining stability. Structural system requirements include being able to withstand the loads experienced during takeoff and flight and completing two separation events to facilitate parachute and payload deployment. Mechatronics system requirements include being able to sense when the rocket is at apogee, communicating live data back to the ground, and enabling the execution of separation events. Payload deployment must occur at apogee. The parachute must be deployed at a time that ensures a non-destructive terminal velocity. Propulsion system requirements include being able to achieve an altitude of 4,000 ft. and being able to withstand the forces and thermal conditions associated with launch and flight.

Design Approach

Our design approach differed significantly from convention for two primary reasons. Firstly, the number of technical requirements which changed during the class caused each new iteration of the rocket to differ significantly from the previous. Secondly, all this design work

was performed with no baseline, as the capstone had not been active for years and many of the current students had yet to be exposed to high power rocketry. Our process began with the simplest design possible—abiding by the IREC guidelines—and then adding components or capabilities as they became necessary. For example, it was quickly decided two separation events would be necessary to deploy the drogue chute, the payload, and the main chute. This approach also permitted us to quickly backtrack or change the design as new requirements became apparent. We iterated through many alternative design solutions in this process, documenting these changes in our dated OpenRocket files. These included designs which placed the payload aft of the avionics bay; it quickly became clear this would cause issues during payload deployment. We also iterated through designs which included removable fins or a completely SRAD motor. Many of these choices were products of our inexperience with the timeline required for such design choices; under the guidance of Ben and Elaine Russell, we elected not to pursue removable fins. Our approach also involved studying design choices made for similar Level 3 rockets, such as that of the UVA Rocketry Club or documented designs by other colleges online. This permitted us to understand how such a problem is usually approached, and in what areas we might want to deviate.

Our thermal management design approach also changed significantly throughout the life of the project. In the first two months of design, the Propulsion team believed that it would be allowed to produce its own propellant and motor design for the motor. As such, the thermal team conducted calculations and simulations of the ability of the motor designs to handle the thermal output of the ignited propellant. When the team was informed by UVA Health and Safety that under no circumstances would it be allowed to produce propellant, the design approach changed significantly. The Propulsion team decided due to this constraint to select a commercial off-the-shelf motor to use for the rocket. From this point on the only thermal design approach necessary was to validate that the purchased rocket motor would be able to handle its own thermal load.

We elected to measure the success of our rocket simply by the completion of our prototype. As it became evident a launch would likely not be feasible, we instead chose to test our components individually to gauge their success, as documented in the Testing and Results section. This achievable goal indicated that our research could be of direct aid to students in future years, who likely would need to perform more cohesive testing prior to a launch. This design approach posed several risks which had to be addressed. In addition to the physical risks inherent to fabrication, several design steps were contingent on the completion of others, ultimately delaying the process. This risk extended to the fabrication process too, as the order of assembly was vital to successfully completing the prototype. The capstone was also reliant upon the completion of machine shop training, which proved difficult to schedule.

Cost and timeline predictions were necessary for the successful competition of the capstone. Estimates from the Preliminary Design Review placed the total cost at \$5,000, most of this taken up by the Aero-Structures team for the required body materials and the purchase of the

chosen motor. This prediction was somewhat accurate; however, the final total cost fell to \$6,043. As predicted, most of these costs came from the Aero-Structures team, and this deviation in cost can be attributed to the body tubes the team was forced to pivot to. This cost could have been further optimized, as some parts went unutilized as the team was forced to make design changes. Timeline estimates were also relatively accurate; the Preliminary Design Review (Appendix E) accurately indicated that design would conclude and that parts would be ordered in December, fabrication of priority components would be done by March, and subsystems would be fully integrated by the end of April. This prediction was inaccurate in that it was made to account for the scheduled Tripoli launch, which was elected against. More accurate timelines developed for the Critical Design Review (Appendix F) were closely adhered to; the only deviation came from safety concerns which prevented competition and integration of the nose cone in time for the Final Design Review.

These design reviews were vital to the capstone's success and were markers of our progress throughout the year. Through these, progression could be directly measured and presented. Each design review reflected the many changes the rocket underwent, also allowing for each team to communicate their progress to one another. The reviews ensured design and fabrication work was completed on schedule as a group, and these timelines were updated as needed. Since these presentations are the most distilled form of what we've learned, they are also likely to be the most helpful to future students working on the capstone. Presentations such as these from other universities offered much guidance during our own design process.

Design

Aerodynamics and Structures

Nosecone

Description

The final design of the nosecone aspect of the aerodynamic structure is an ogive shape. A nosecone is the outer, forwardmost section of the sounding rocket. To effectively reach the desired apogee, the design of the nosecone must account for a reduction in drag. In total, computational fluid dynamics (CFD) analysis showed that the final design had a drag of 82.31 N. The chosen nosecone has a height of 65.82 cm and a diameter of 15.67 cm for a height to diameter ratio of 4.2 as shown in Figure 3.



Figure 3. Final ogive nosecone design and dimensions.

The initial design included an aluminum insert for attachment to the body tube component as shown in Figure 4. However, further iterations prior to beginning manufacturing led the design to change to an internal coupler being inserted into the nosecone with epoxy and then attached to the body. In order to implement this design, an additional 10 cm cylindrical extension was added to the nosecone in the manufacturing stage as shown in Figure 5. This left the final design to have the dimensions specified previously with an extended cylindrical piece.

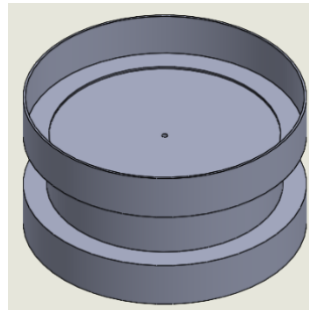


Figure 4. Image of design concept for initial aluminum insert.

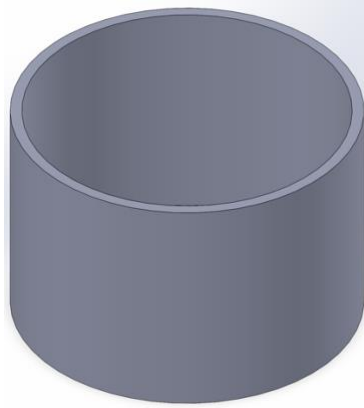


Figure 5. Final design for extension piece for nosecone integration with rocket.

Analysis

The ogive shape of the nosecone was chosen due to its reduced drag properties. Initially, using equations as shown in Table C1 in Appendix C obtained from Crowell Sr's 1996 publication, the elliptical, parabolic, and ogive shapes were modeled. A selection of the three initial shapes modeled and analyzed are shown in Figure 6. These three nosecone shapes were chosen due to research suggesting that they were the shapes that yielded the least amount of drag. Initially, each shape was modeled with different length to diameter ratios using computer aided design (CAD) software and computational fluid dynamics (CFD) analysis to determine which design yields the least drag given the flight conditions. In total, this went through two major iterations of CAD and CFD.

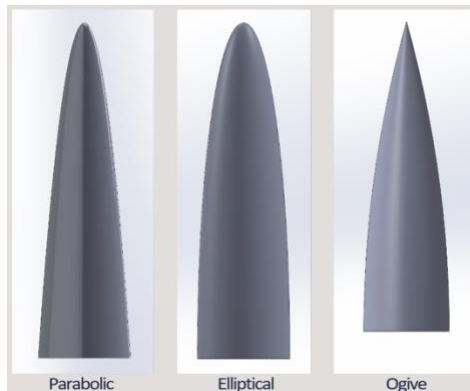


Figure 6. Image of each of the initial nosecone shapes considered

During the first iteration, three of each nosecone shape, parabolic, elliptical, and ogive were created in SolidWorks, the CAD software used. Based on integration concerns with the body component, the diameter was set at 16.5 cm which was an early estimate. For each model, we implemented Crowell's equations for the given shape and set the height at height to diameter

ratios, also known as fineness ratios, at 3:1, 4:1, and 5:1. From this, we used our CAD models to conduct CFD analysis on each shape and fineness ratio. Prior to conducting the final CFD analysis, an additional CAD model for each component was made. To simplify the CFD, an airbox was made around each model and then the model was cut out and removed from the total airbox as shown in Figure 7. When placing it in the CFD software, Autodesk CFD, the velocity of the airflow was set at 189 m/s. This velocity was chosen since this was what was calculated to be the maximum velocity of the rocket at any given time during the flight. For consistency, each part imported into the CFD program was given the same boundary conditions. Additionally, the drag force was then found by finding the force on the part in the direction of the air flow in which the velocity was originally set.

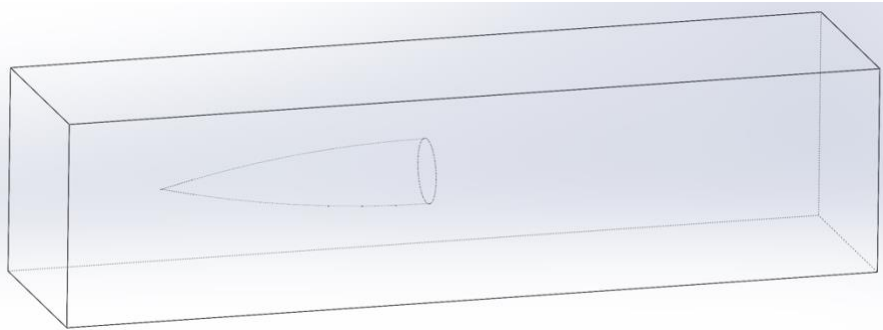


Figure 7. Image of airbox with cutout nosecone setup.

The results of this first iteration of CFD indicated that the parabolic nosecone shape had significantly higher drag values than either the elliptical or ogive nosecone shapes which were both similar to one another as shown in Figure 8. The full results of the first iteration of CFD are shown in Table C2 in Appendix C. Due to this, the parabolic nosecone shape was eliminated from consideration in future iterations.

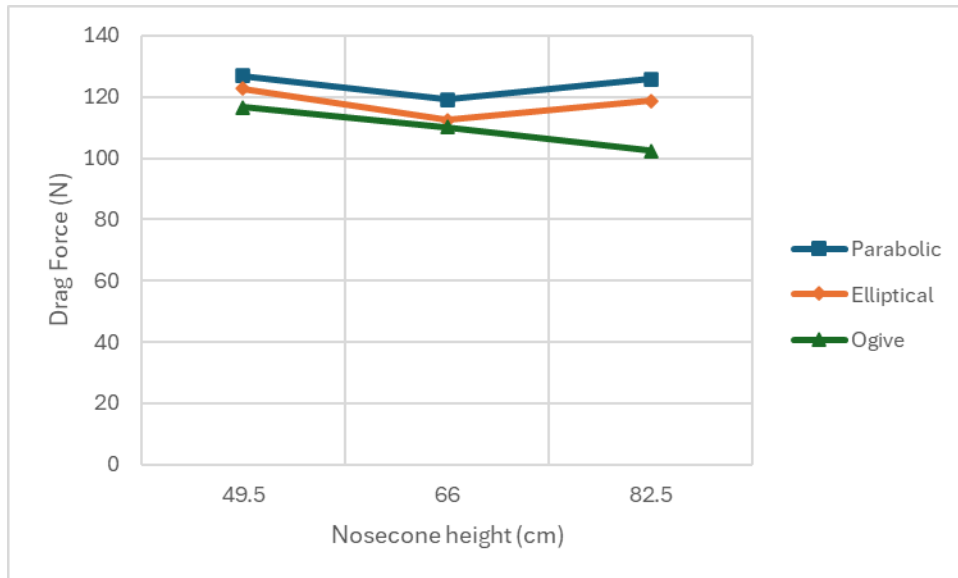


Figure 8. Graph of first iteration nosecone drag results.

The second iteration of CAD and CFD for the nosecone followed. During this iteration, six designs of each with fineness ratios of 4, 4.2, 4.4, 4.6, 4.8, and 5. These ratios were chosen due to the values in iteration one for both of these nosecone shapes being closer and for the values of the 4 and 5 ratios being lower than that of the ratio of 3 that was also conducted. For this iteration, and the final design, the diameter was changed to account for changes in diameter of the body component. The final outer diameter was designed to be 15.67 cm. A similar process for the CAD of the elliptical and ogive nosecone shapes as that of iteration one occurred. The velocity of the air flow in the direction of interest was left at 189 m/s as during iteration one since this expected value was not changed when the CFD for this iteration was conducted. If the velocity was changed at a later date, it was not expected that the differences yielded would not be significant enough to affect our results and would likely maintain the same pattern of high to low drag.

The results from this iteration of CFD allowed us to choose our final design. An example of the nosecone after the CFD was completed is shown in Figure 9. As shown in Figure 10 and expanded on with the full results shown in Table C3 in Appendix C, the ogive nosecone had, on average, significantly lower drag values when compared to the values obtained for the elliptical nosecone shape. This indicated that a nosecone of an ogive shape would, on average, experience the lower drag value for the fineness ratios of interest. This caused us to eliminate the elliptical nosecone shape and look more closely at the ogive nosecone shape CFD results. As shown in Table C3 in Appendix C, the fineness ratios of 4.2, 4.4, and 5 had drag values close to one another, with the ratio of 5 having the lowest drag value overall. However, when determining our final design, we had concerns over the height of the nosecone with a fineness ratio of 5 since it

was at least 10 cm larger than the other two. For the ogive shape, larger heights result in thinner tips. In the manufacturing stage, we were concerned this would prove to be an issue since we planned to use a wet layup method with carbon fiber. This caused us to choose the ogive nosecone with a fineness ratio of 4.2 which had the second best drag value overall which was only 0.121 N lower than that with a ratio of 5. This difference was determined to be minimal and the possible risks with choosing the one with a ratio of 5 were too significant to justify choosing it.



Figure 9. CFD results from Autodesk CFD for chosen nosecone design.

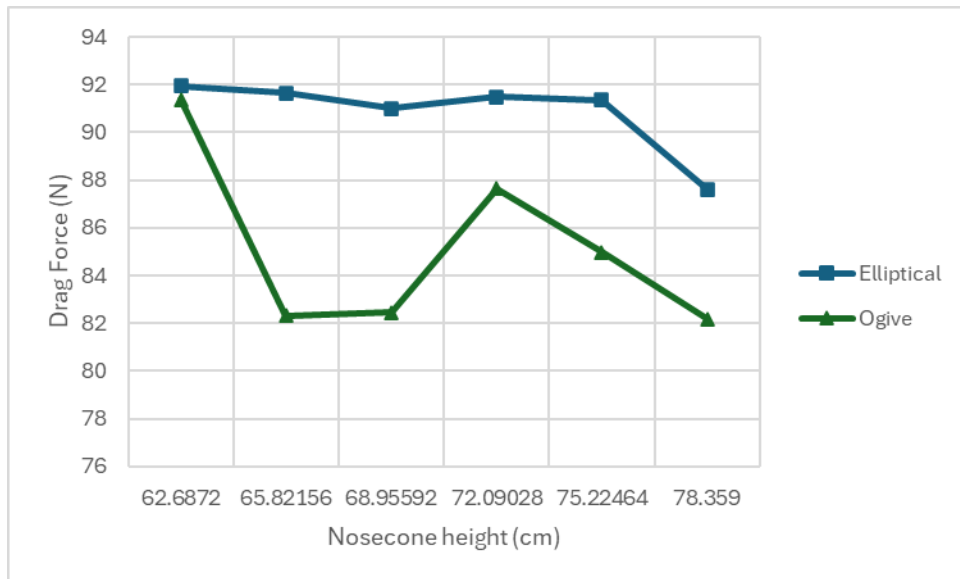


Figure 10. Graph of second iteration nosecone drag results.

As shown in Figures 8 and 10 and in Tables C2 and C3 in Appendix C, the chosen design of an ogive nosecone shape with a fineness ratio of 4.2, height of 65.82 cm, and a diameter of

15.67 cm had one of the lowest drag values of all of the iterations of CFD conducted and the least amount of risk when compared to similar results.

Fins

Description

In the beginning of the design process, research was conducted on the fin designs of the most successful teams in competitions over the last several years as well as related published research. The main topics we needed to research were performance requirements, overall shape, airfoil shape, active/passive fins, replaceable/permanent fins, and attachment mechanism. In studying the IREC rules and requirements, we determined our design requirements to be as follows: Center of Pressure must be between 1-2 rocket diameters aft of the Center of Gravity (rocket cannot be unstable or over-stable), fins must be replaceable within 30 minutes if they are designed to be replaced, active fins must not be actively guided but rather simply correct stability, rocket velocity must not exceed fin flutter velocity, and all dimensions must be recorded (Spaceport America Cup, 2023). For the overall shape, airfoil shape, type of fins, and attachment we studied several different articles and technical reports from other teams (Acosta, 2019, Pektas, 2019, Sankalp, 2022, Fraley, 2018, Milligan, 2017). From their results, it was seen that the clipped delta shape was most used for subsonic sounding rockets, with each team doing a slight variation on that general shape. For reduced drag, and to avoid a potentially large lift force, we chose a trapezoidal airfoil shape. Choosing the trapezoidal airfoil furthermore allowed us to simplify the manufacturing process and facilitated the alignment process during integration. Each paper researched also mentioned the number of fins, of which we chose 4 smaller fins rather than 3 larger fins. The reason behind this choice was primarily simplicity in manufacturing as well.

Due to the extra parameters to consider with active fins (wiring, manufacturing of control surfaces, subsystem would have to correct automatically, etc.), we also decided, for this first iteration of a sounding rocket as a Capstone project, to have passive fins rather than active. We considered replaceable fins for most of our design process, but after counseling with some technical advisors from the rocket community, they suggested that for a first time creating a rocket, we should use permanent fins, but can pursue replaceable fins (via screws as we had been planning) in a future project. After combining the gathered information and performing CFD simulations (in the analysis section) of different proposed airfoil shapes at multiple Reynolds Numbers, the team decided on a final design with a clipped delta shape, trapezoidal airfoil, and dimensions shown in Figure 11 below:

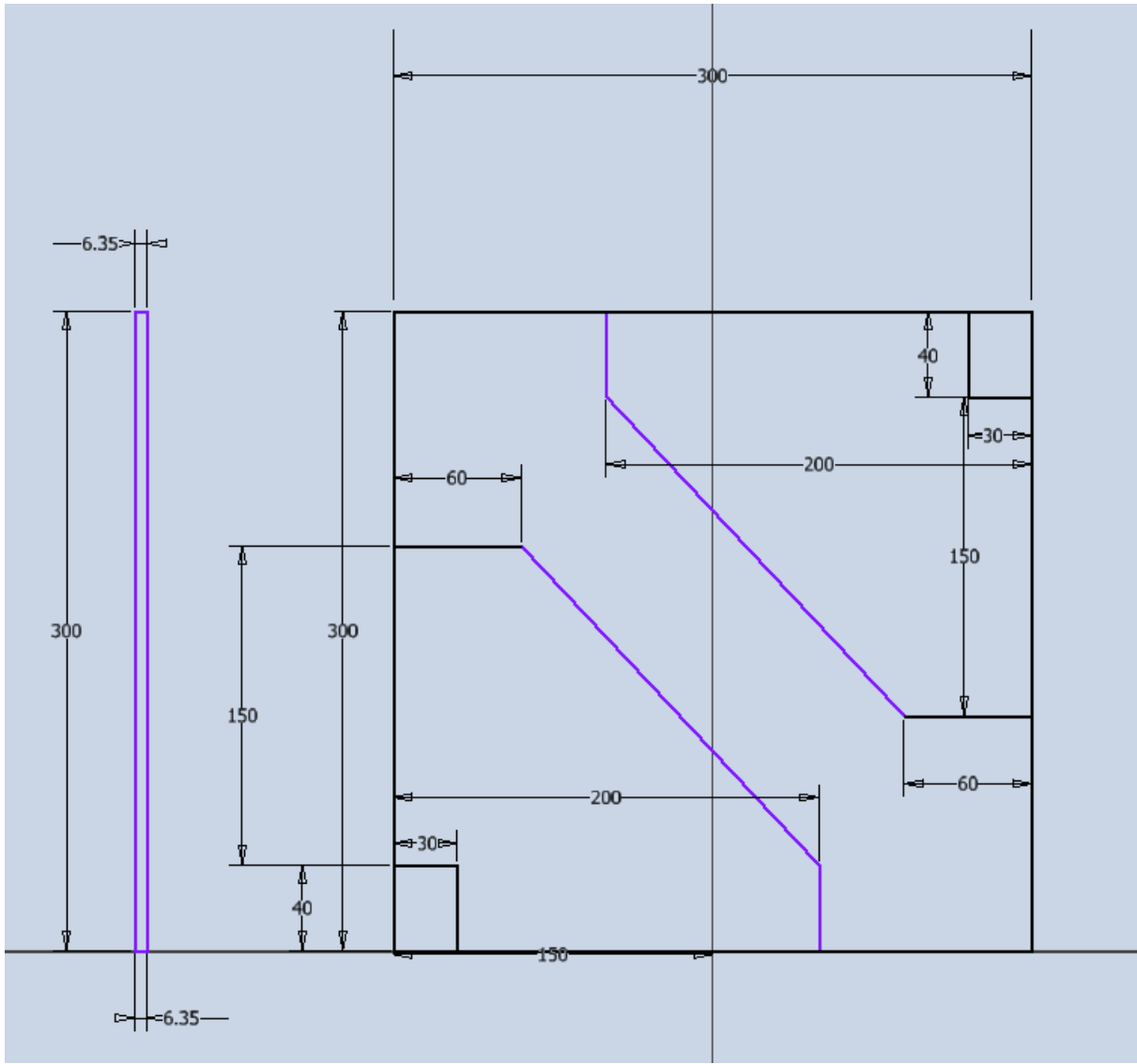


Figure 11. Final dimensions, numbers in mm, cut out of a 300mm x 300mm Carbon Fiber plate

Analysis

For an in-depth analysis of the viability of the fin design, three methods were used to analyze effectiveness and safety: AutoCAD CFD simulations, Matlab code theoretical analyses, and Open Rocket comprehensive analysis. Within the fins team, the design process implemented these three methods in an iterative loop: one team member would check the Open Rocket files for updates to gather the data from the other sub teams to feed to another member, that member would input that rocket data in a Matlab code (Appendix B) to generate a potential range of dimensions for a fin, another member would use some of these dimensions in AutoCAD Inventor

to create or update a fin prototype, another member would use that prototype in an AutoCAD CFD simulation. As the specified rocket dimensions and mass distribution changed over time, this iterative process facilitated the process of determining the new fin dimensions.

Several prototypes and iterations were conducted to better optimize the fins by decreasing drag and increasing stability whilst staying within the design requirements. The Open Rocket program would show how the fin fits with the whole rocket, providing relevant Center of Gravity (CG) and Center of Pressure (CP) data, and allow us to make the fin better as a part of a system. The Matlab code confirms this data and adds the flutter velocity as a factor to avoid, and then suggests new parameters to account for it. The CFD simulation shows forces on each surface, revealing which fin would be the most aerodynamically efficient. From this analysis, a promising design could be reliably chosen.

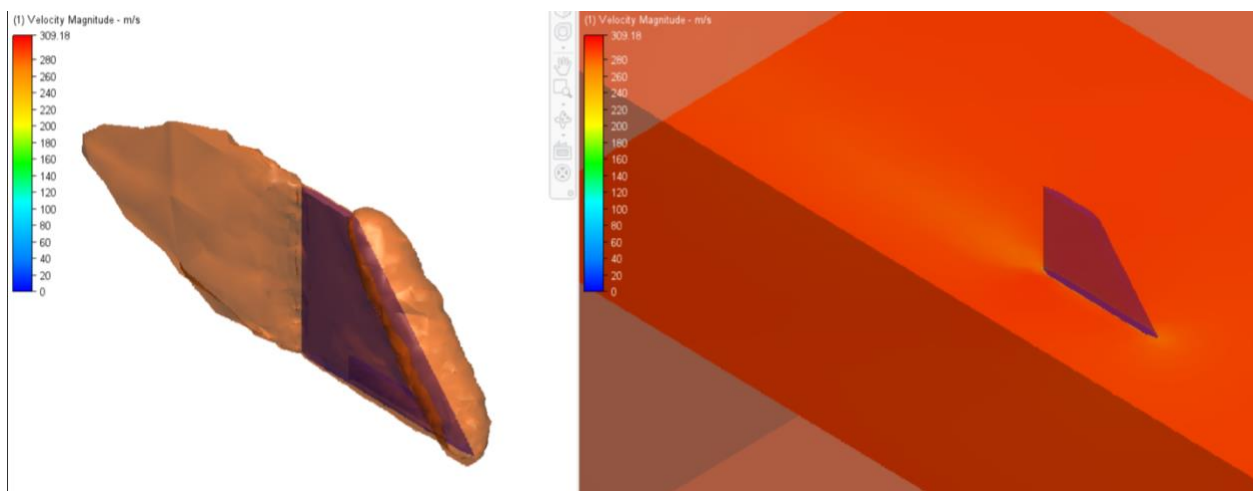


Figure 12. Final CFD results of our last design iteration before the large changes

Unfortunately, after an optimized fin was chosen, the entire internal anatomy of the rocket shifted, moving the CG, causing us to redo the fin design and run further tests, which then had to be redone due to a change in fin attachment. After the many design changes, analyses were run on the final design and recorded in Table 1 below:

Design No.		Dimension Dataset from Matlab								
Parameter	Semispan	Root Thickness	Tip Thickness	Root chord length	Tip chord length	Tip to Root Length	Edge Half Angle	Center of Pressure	CG-CP	Flutter Velocity (V)
Unit	[m]	[m]	[m]	[m]	[m]	[m]	[°]	[m]	[m]	[m/s]
1A	0.14	0.008	0.008	0.18	0.06	0.12	15	2.419	0.309	1493
1B	0.14	0.008	0.006	0.18	0.06	0.12	15	2.419	0.309	1222
1C	0.14	0.006	0.006	0.18	0.06	0.12	15	2.419	0.309	970
1D	0.14	0.006	0.004	0.18	0.06	0.12	15	2.419	0.309	738
2A	0.15	0.006	0.006	0.14	0.05	0.09	15	2.418	0.308	2036
2B	0.14	0.007	0.005	0.18	0.06	0.12	15	2.419	0.309	1434
2C	0.135	0.006	0.006	0.22	0.06	0.16	15	2.417	0.307	1138
2D	0.131	0.006	0.006	0.3	0.07	0.23	15	2.41	0.3	749
3A	0.15	0.006	0.006	0.18	0.06	0.12	15	2.48	0.29	???
Final	0.145	0.00635	0.00635	0.18	0.06	0.12	15	2.1985	0.3285	995
Design No.		AutoCAD CFD				OpenRocket				
Parameter	Drag Force	Lift Force	Moment	Max V-air			New CG	New CP	Max V-fin	Altitude
Unit	[N]	[N]	[N*m]	[m/s]			[cm]	[cm]	[m/s]	[m]
1A	47.4	-19.22	-2	314.561			212	243	286	2634
1B	41.4	-17.03	-4.14	315.778			212	243	288	2656
1C	34.679	-14	-1.063	309.18			211	243	290	2685
1D	28.7	-11.64	-1.872	309.16			210	243	293	2713
2A	39.7	-12.04	-1.18	311.65			211	245	290	2671
2B	34.75	-14.36	-2.231	303.829			211	243	290	2685
2C	31.44	-15.9	-0.6644	307.901			211	240	290	2695
2D	27.76	-16.2	-4.17	309.04			212	237	287	2682
Final	17.1	-6.1	-0.89	257			187	218	200	1679

Table 1: Final performance characteristics of our designs, note the final design in blue with a much different altitude requirement and maximum velocity in the air.

With the flutter velocity nearly four times that of the maximum velocity of the air, drag and lift significantly reduced, and the CP well within stability parameters, the final profile design was chosen. There were various similar iterations ran for different airfoil shapes, including differing half angles for the trapezoidal airfoil, and it was determined that 15 degrees was an appropriate angle (as a higher angle would induce more drag and a lower angle would risk cracking at the tip upon landing, which we also simulated in SolidWorks).

Parallel to the fin shape research, the possibilities in fin attachment were investigated. The fin attachment mechanisms were evaluated as detachable fins offer multiple advantages: Due to higher adaptability, different fin shapes could be tested on the rocket, and fins could be replaced when damaged on ground impact. However, due to design restrictions, the fins were manufactured as non-detachable. The following paragraphs aim to give an overview of the fin attachment mechanisms used. The first attachment design, depicted in the figure below, featured interlocking aluminum brackets that were connected via screws. The main issues with this design were the low capacity of the mechanism to transfer moments (around the longitudinal axis of the rocket) that would push the leading edge of the fin to either side. Furthermore, the screwheads

and nuts would be highly exposed to the outside air stream, increasing the drag of the rocket and therefore decreasing the apogee height.

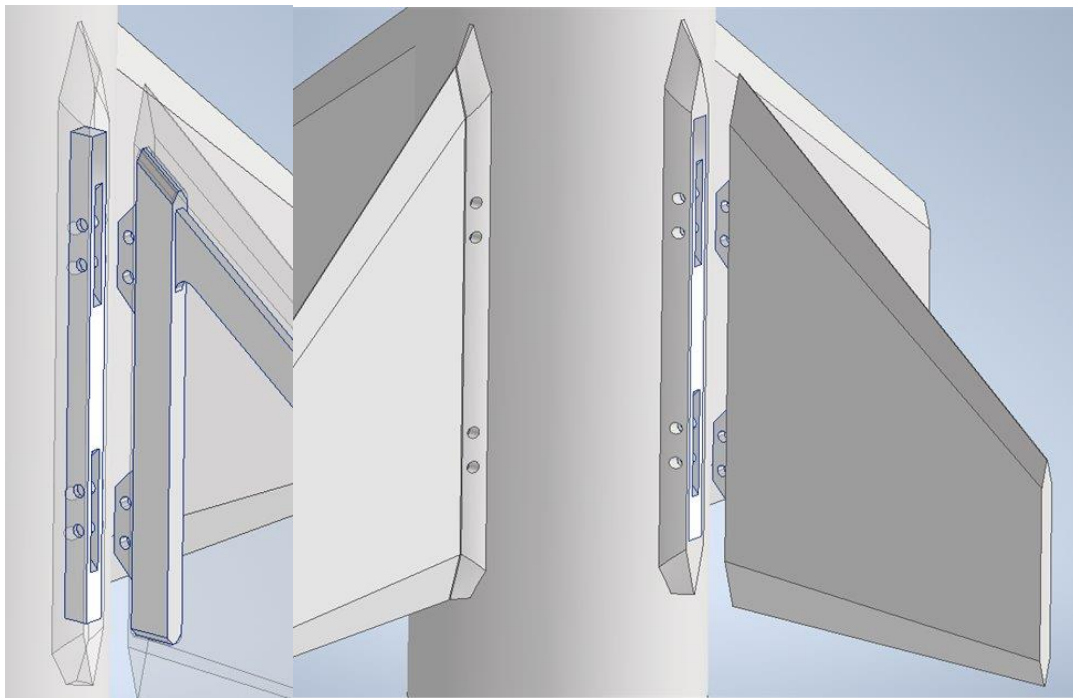


Figure 13. First version of the fin attachment mechanism

The second attachment design (depicted in the figure below) used a sliding mechanism with the motor centering rings to transfer the moments and forces in a more effective way. Bent metal sheets were attached to the fin to allow an aerodynamically optimized employment of the screws, with only the screwheads exposed to the outside of the rocket. The nuts on the metal sheets intended to secure the fin assembly to the body frame after sliding the assembly in were held in place and stopped from rotating by 3D-printed PETG parts. This design allowed the fins to be either molded or fabricated from a solid carbon fiber plate, which increased the flexibility of the manufacturing process.

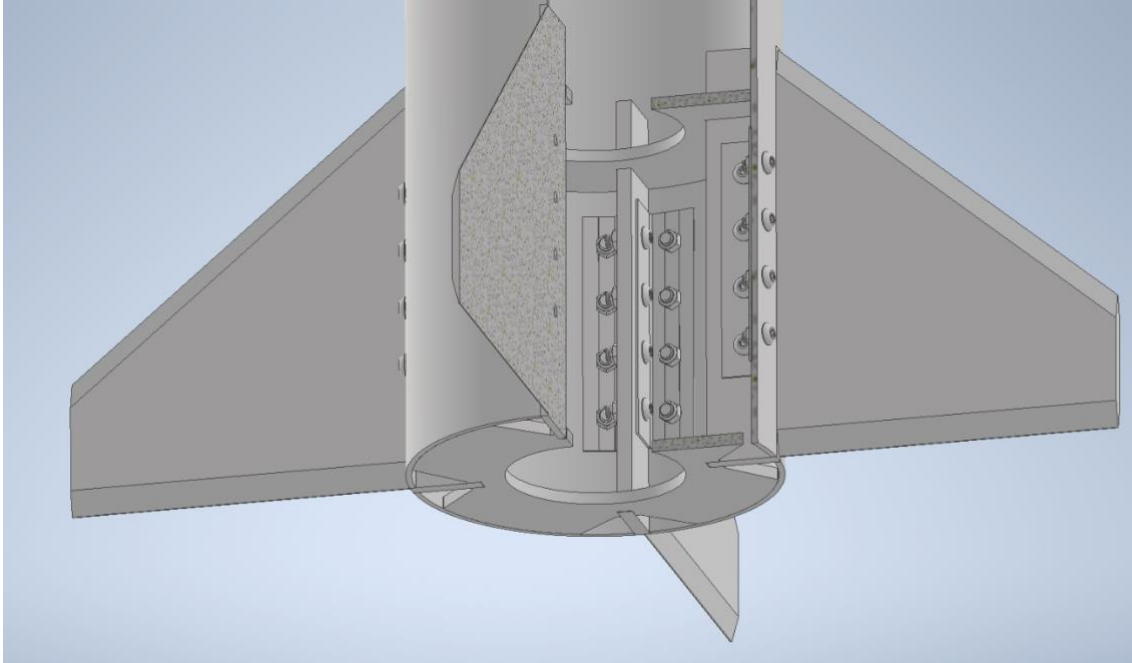


Figure 14. Sliding attachment mechanism, quarter-cut to show the connection between body, motor centering rings and fins.

As mentioned above, the decision was made to abandon the approach with detachable fins in favor of fixed fins due to the requirement of glued-in fins by the board members of the Tripoli Rocketry Association. This reduced the assembly's complexity and allowed us to focus on the other parts of the manufacturing process. Furthermore, it decreased the weight and cost of parts. The acquired knowledge of attachment mechanisms may be used in future projects and was therefore included in this report.

Couplers

Description

The couplers system was designed to maximize stiffness between body tube sections while minimizing weight and material used. For this purpose, an inner tube design was selected, as it provides the best force and weight distribution while maintaining a low profile within the body tube to accommodate the avionics bay. The length of the coupler tube was maximized to better distribute bending moments experienced during flight to provide greater stiffness to the weaker body joints. A minimum shoulder length of one body diameter was selected based on recommendations from literature. This length additionally allowed for the use of OTS fiberglass one foot coupler tubes to be used without length modification, and an outer diameter of 6 inches for the couplers were selected in conjunction with the body team. Fiberglass was selected as the

main coupler and bulkhead material for its strength-to-weight ratio and its RF permeability. Figures 15 and 16 show an assembly view of the final coupler design, with the components colored as follows: yellow - separation thrust ring, blue - separation piston, orange - bulkheads, green -avionics plate, tan - coupler tube, red - avionics thrust ring, gray - body tube placeholders.

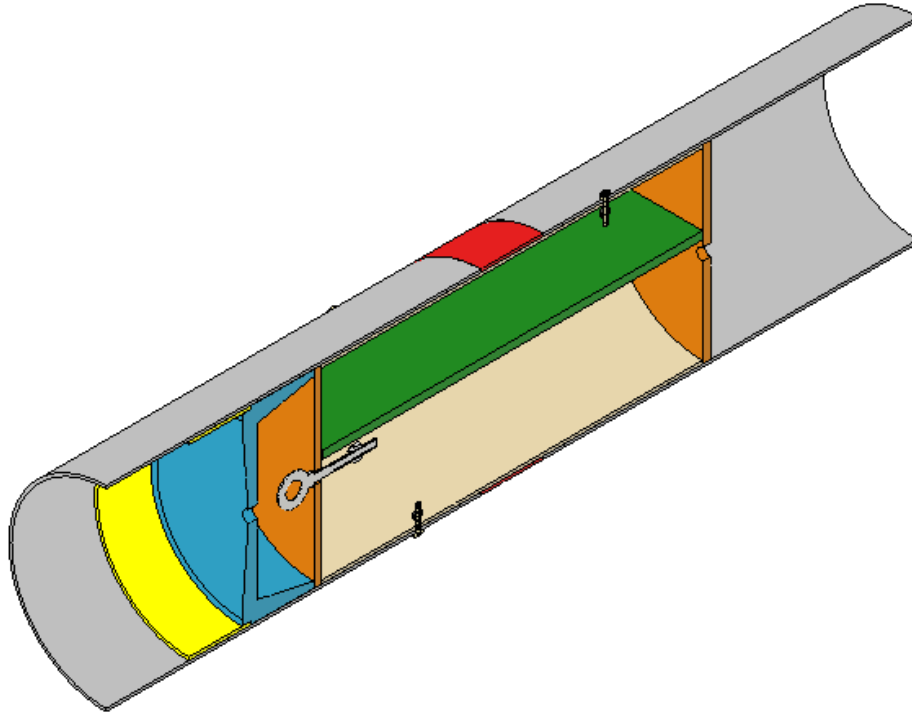


Figure 15. Half-section view of the avionics coupler assembly.

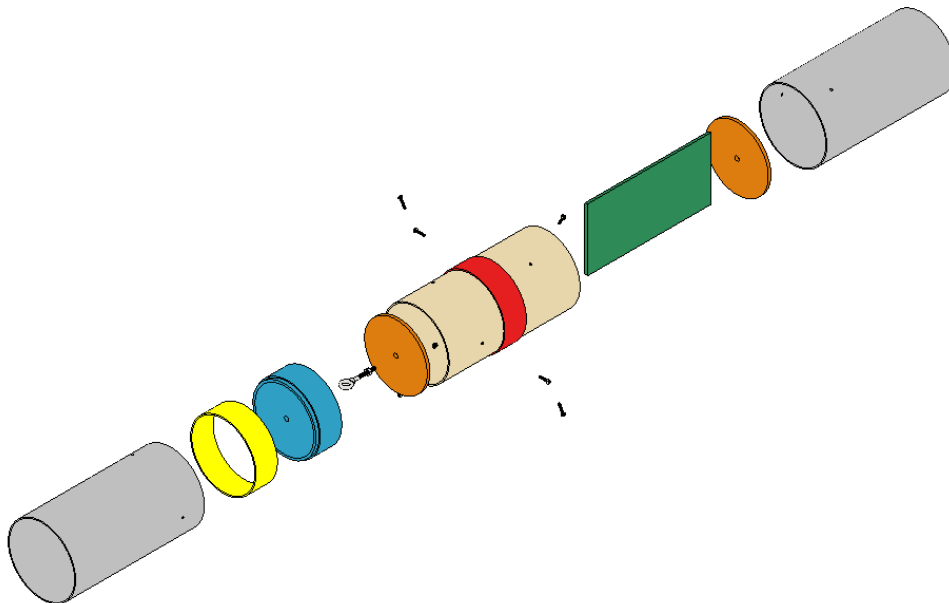


Figure 16. Exploded view of the avionics coupler assembly.

The final rocket design required the avionics coupler to function as a separation joint for the deployment of a drogue parachute, and steps were taken to facilitate a controlled and repeatable separation event. A separation piston-based design was chosen to minimize the amount of black powder (BP) necessary to ensure reliable separation and to minimize the presence of combustion byproducts in the drogue chute bay. This separation piston was chosen to be additively manufactured using ABS 3D printing to facilitate custom geometry and ease of fabrication. The original separation design featured the use of nylon shear screws to prevent premature separation in flight and to aid in the buildup of pressure during the ignition of BP charges. Subsequent testing following fabrication however revealed that the friction fit of the coupler inside the body tubes was more than sufficient to prevent unintended separation due to the long shoulder interfaces and that the use of shear screws was superfluous and potentially inhibitive. The presence of holes intended for shear screw use was deemed nonproblematic, as they are small enough to not cause significant structural or aerodynamic issues, and they can be prevented from acting as atmospheric vents by simply rotating the coupler tube within the body. Fixed joints were secured using epoxy to ensure proper strength requirements and to avoid stress concentrations caused by traditional fasteners that would be extremely problematic in anisotropic fiberglass components.

Analysis

Analysis of the couplers system was largely dedicated to ensuring proper separation, taking the form of shear screw calculations, BP charge calculations, and FEA analysis of the separation piston. Calculations were originally performed off the assumption of negligible friction resistance and the usage of three M4 nylon screws, as well as idealized combustion of 4Fg black powder. These assumptions proved to be significantly inaccurate, but the equations developed proved to provide a good basis of understanding of the balancing of design parameters and are easily adaptable to function off a friction fit mechanism with less efficient combustion. The original equations using a shear screw schema are provided in Appendix D for reference and future use. By obtaining pressure estimates of various BP charge sizes, it was possible to perform FEA analysis on the separation piston, as it is the component that is predicted to undergo the largest pressure load. Static FEA analysis was performed at a simulated pressure of 317 kPa, corresponding to an idealized estimate the pressure generated by 2 grams of 4Fg BP. The separation piston was fully constrained, representing the highest possible loading scenario in which the piston becomes jammed in the body tube. Figure 16 corresponds to the resultant safety factor analysis of the separation piston under the given loading conditions.

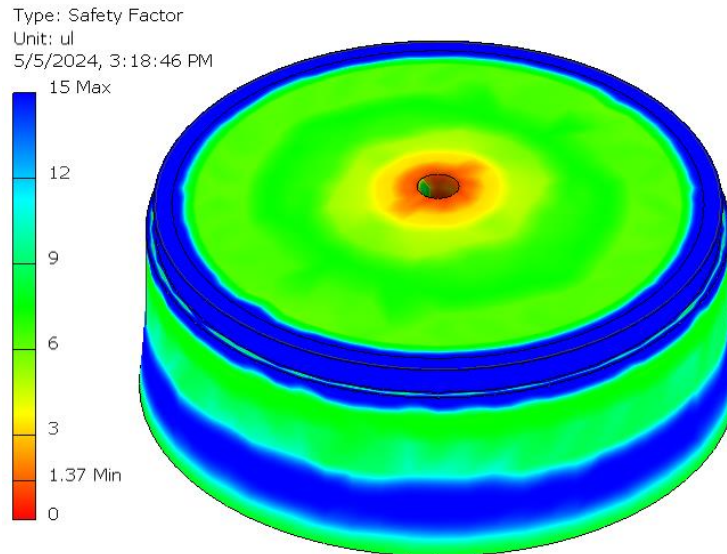


Figure 17. FEA of the Separation Piston corresponding to a pressure load of 317 kPa with fully constrained motion. The safety factor of the component is 1.37 under the worst loading condition, with failure occurring at an acceptable location.

Body

Description

The body is the outer cylindrical structure responsible for housing the motor, payload, and other essential components. Centrally located, the body serves as the portion of the rocket which the nose cone and fins are directly attached to. The primary characteristics concerning the body are strength-to-weight ratio, material construction, and overall dimensions. More specifically, the body must be properly dimensioned to fit all necessary components, strong enough to withstand all the forces during flight and propulsion, while also being light to optimize efficiency in performance. In addition, the material selected must be one that doesn't interfere with on board avionics. Stability during flight is a critical aspect largely concerning the body. Moreover, the center of gravity and center of pressure are two properties that must be constantly accounted for during the design process.

In order to optimize the design of the rocket body according to the parameters mentioned above, several methods were used. First, a comprehensive examination of previous technical reports was conducted to construct a baseline level of knowledge as well as some general guidelines concerning the design process of a rocket body. From this we were able to construct a short list of materials to consider for design, namely fiberglass, carbon fiber, and aluminum alloys. We eventually decided on fiberglass due to ease of acquisition, manufacturing, and its

high strength to weight ratio. Another important factor of the design was the length and radius of the rocket body, as well as the size of the two sections. To determine the optimal orientation of these parameters, we utilized the previously mentioned rocket simulation software, Open Rocket. Through this software we were able to iterate on these variables and determine an optimized body tube configuration for us to construct. After multiple prototypes, we decided on two body tube sections, each with an inner diameter of 15.2 cm, an outer diameter of 15.6 cm, and lengths of 75 and 80 cm for the main chute and propulsion tubes respectively. For the manufacturing process, we decided to use tubes of canvased phenolic tubing reinforced with a fiberglass sleeve and epoxy resin. This combination of materials provided a high level of strength while still remaining quite lightweight.

Analysis

Analysis of the body section was primarily done through visualization after completing the fiberglassing of each tube. Initially, after fiberglassing the first body tube, we noticed issues with the resin-epoxy mixture from air pockets that we had not fully dissipated, so the surface of the rocket ended up being very uneven. We attempted to sand this section to even it out, but quickly realized this method was not very effective. Due to time constraints, we initially planned to use this first body tube in the final design and not redo it. We went through the fiberglassing procedures for our second body tube, which had the fin slots cut out, and had much better results with smoothing out the resin-epoxy mixture since we had better tools and more time to be thorough. This tube ended up being much smoother and we found that we had more time in the semester to redo the first tube using the better techniques. We ended up with the two planned body tubes that were visually very smooth and did not deform much when we pressed down on the tube, indicating that our design was successful in strengthening the body, without adding too much mass. We were able to learn a lot about trial and error from this hands-on experience and were able to successfully integrate our design with the other subteams' designs.

Mechatronics and Controls

Electronics Description

The electronics sub team was responsible for developing the avionics circuitry and architecting the apogee-detection code. The circuitry needed to meet several high-level mission requirements. Primarily, it needed to accurately measure atmospheric pressure, temperature, and the rocket's motion. It also had to locally store this information, transmit it to ground control,

and send it to an on-board processor that could interpret the data to detect apogee and estimate the rocket's altitude. Finally, the circuitry needed to activate two separate parachute ejection charge igniters: once for the drogue parachute at apogee, and once for the main parachute at a pre-specified altitude. The avionics circuitry needed to meet these requirements in a safe and reliable manner, which necessitated that several redundancies be built into the system. The most important redundancy requirement, per our advisors and the Tripoli Launch Facility's policies, was that an OTS parachute deployment system be integrated into our SRAD avionics circuitry. Our code exists to complement the on-board circuitry, as the code is the metaphorical brain with the circuitry acting as the working force. With the sensors and deployment acting as separate mechanisms, the code allows for communication between these parts. With the circuit board powering the flight computer, the code creates the network for the sensors to be initialized, for the data collected to be stored, for parachute deployment, and radio telemetry.

Analysis

The circuit diagram pictured below is the culmination of our research and prototyping efforts. We are confident that this circuit would be reliable and is ready for PCB design, evidenced by the extensive testing and iterative design process described later in this report.

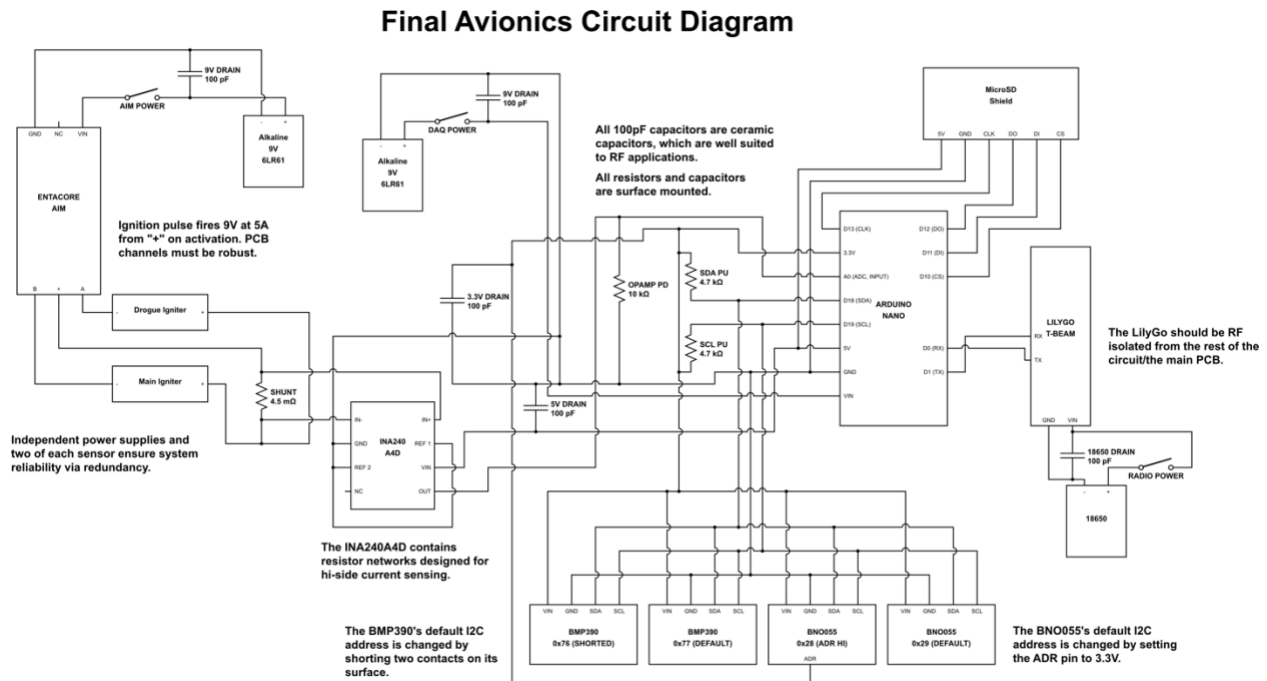


Figure 18. Avionics Circuitry – Final Design

This design is built around two main components: the Arduino Nano and the Entacore Aim. The Nano comprises the core of our SRAD avionics system: it reads sensor data, writes that data to a microSD card, and sends it to the LilyGo T-Beam (our radio). The sensors chosen are the BMP390, which measures temperature, pressure, and humidity, and the BNO055 IMU, which measures the rocket's acceleration and attitude. Two of each sensor is included for extra redundancy in the case of a hardware failure, while each of these sensors are compact, lightweight, and highly capable. The sensors and Nano are connected via the I2C communication protocol because of the connection's simplicity and the hardware's built-in I2C support. Due to the high number of sensors sharing the Arduino's I2C bus, pull up resistors are necessary to maintain the bus's voltage and prevent overloading when all four sensors are sending data simultaneously. The 4.7 kilo ohm resistor value is an industry standard and is used for that reason - if our I2C lines exceeded two feet, then this value would be decreased. To ensure that each sensor has a unique address for the Arduino to use, one of each must have its address changed from its factory default (see the notes within the diagram above). The microSD card adapter used is low-cost, reliable, and easy to connect via SPI. The radio is chosen because of its high power, accessibility through the MAE department, and its inclusion of a GPS module for built-in tracking and safety; there is also extensive related documentation available online.

The Entacore AIM is a one-piece OTS apogee detection and ejection charge ignition system. It is powered via a 6LR61 spec nine-volt battery that can provide adequate current to the igniters as confirmed by our tests. The Entacore AIM is used because of its simple UI, proven reliability, and the all-in-one nature of its design. The AIM has final control over ejection charge ignition - as advised and necessitated by our launch safety requirements - and therefore extra circuitry is needed to link it to the Nano for our use. To validate our apogee detection algorithms, the Nano needs to be able to detect when the AIM fires the charges and compare it to when our algorithms would have done so. The detection method used is high-side current sensing, hence the shunt resistor placed upstream of each igniter. When the AIM sends current to the charges, a small voltage drop occurs across the shunt resistor. This voltage drop must be small enough that the resistor does not overheat; however, this means that the Nano alone cannot detect the voltage drop. Therefore, the INA240A4D operational amplifier is used to amplify this voltage drop so that the Arduino can detect it. The INA240A4D is specifically designed for high side current sensing and has a gain factor of 200. Our 9V battery can source five amps; using ohm's law this equates to a voltage drop of 0.0225 volts across our 4.5 milliohm resistor. After being amplified 200 times, this voltage drop is sent to the Nano as 4.5 volts, which is just below the five-volt maximum that a Nano pin can handle. A standard 10 kilo ohm pull down resistor connects the op-amp's output to ground, which ensures that the Arduino does not read any erroneous voltages when the AIM is not sending current to the igniters.

Other safety and reliability measures can be seen in the circuit diagram. First, the AIM, Nano, and LilyGo each have independent power supplies which drastically reduces the likelihood of parachute non-deployment and data loss. Second, each of these devices has its own power switch to ensure that the team has complete control over when systems are activated, which allows us to save power and avoid premature triggering of ejection charges. Finally, standard 100 picofarad capacitors connect each power line to ground - these capacitors act as drains for AC signal noise that could be induced in our circuits by radio waves. All capacitors are specified as ceramic-type capacitors, which are well suited for RF drain applications.

Our code is constructed in two parts, with one dealing with radio telemetry and another handling data storage, sensor reading, and general board initializations. This came about due to the nature of our development and testing, where the sensors were tested separately from the radio transmitters, leading to isolated code made specifically for each. In the future, these codes should be consolidated once the radio is configured, as two codes cannot run at the same time on the board.

Avionics Bay Description

The avionics bay is a cylindrical design that optimizes performance and functionality. Within this casing are an arranged array of components, organized to ensure operation and reliability. At the center of the avionics bay are three threaded rods that traverse through two robust plates, anchoring the structure securely and providing a stable foundation for the intricate system within. This arrangement not only ensures structural integrity but also facilitates efficient distribution of weight and forces, crucial for withstanding the rigors of launch and flight.

Analysis

Within the cylinder design, there will be six high-performance batteries carefully positioned to maximize space, while ensuring ample power supply for the mission. Mounted perpendicular to the threaded rods is a vertical plate, serving as the backbone for the integration of the circuit board and sensors. This vertical orientation optimizes space, allowing for the compact arrangement of components while ensuring easy access for maintenance tasks.

The circuit board serves as the central system of the avionics bay. It is positioned alongside the circuit board where sensors will be placed. These sensors include GPS, temperature, and accelerometers. The cylindrical design of the avionics bay offers several distinct advantages for our application. Its shape minimizes aerodynamic drag during flight, reducing energy consumption and enhancing overall efficiency. This aerodynamic profile also

reduces the risk of destabilizing forces during ascent and descent phases. This shape allows for easy access for maintenance and integration tasks and enables scalability and future expansion of the avionics system to accommodate evolving mission requirements. Moreover, the cylindrical structure offers inherent structural integrity and stability, essential for withstanding the dynamic loads and vibrations experienced during launch and flight. The design of the avionics bay ensures the electronic components are shielded from external shocks and environmental hazards, aiding in their functionality and longevity.

Parachute Deployment

Description

The parachute deployment and body separation system's outlined specifications were to ensure the total separation of the couplers from the rocket body, be able to deploy parachutes on separation, not damage the rocket body or its internal components, and be controlled by an off-the-shelf altimeter, with the capability to integrate with the telemetry circuitry. The ignition cycle would occur once at apogee to release the drogue parachute, and again to release the main parachute at a lower altitude when the rocket has slowed down. The use of the drogue parachute is to slow down the rocket to a manageable descent velocity, so less drift occurs when the main parachute is ejected.

Analysis

The ignition system requires a pressure differential within a sealed volume in order to induce separation. The method chosen given the parameters of this project was to use a black powder charge ignited via an electrical signal controlled by the rocket's electronics bay. Due to material and supply chain deficiencies, 3FG black powder was chosen instead of the desired 4FG, with 4FG being much finer, resulting in a faster and smoother burn rate. The black powder will be ignited by passing a current through a nichrome filament, which has a high resistivity and would heat the charge to its combustion point. The charge would connect to the electrical bay via 2 mm copper wiring, which was chosen for its low resistivity to compensate for losses within the nichrome element. The mass of black powder required was determined using a modified version of the ideal gas law shown in Equation 1 below, where the given mass (grams) was given by plugging in the pressure required for separation into the modified equation, with pressure being calculated by finding the force required for separation, and dividing it by the internal surface area where the charge is housed, in this case between the separation piston and bulkhead, given these

values, the pressure required for separation is approximately 30 psi, leading to a target mass of 1.6 grams.

$$\text{Grams}(BP) = \frac{454\text{grams}}{1\text{lbf}} \times \frac{\text{Pressure}(\text{psi}) \times \text{Volume}(\text{inches}^3)}{266 \frac{\text{inches} \cdot \text{lbf}}{\text{lbm}} \times 3307 \circ R}$$

Eq. 1

The parachutes' diameters were found using Equation 2 below to match the area required to get a specified final velocity of 3 m/s at landing by assuming a circular profile of the parachute and applying the relevant drag coefficient equation to gravitational potential energy.

$$A = \frac{mg}{\frac{1}{2}V^2pC_d}$$

Eq. 2

Given the target final velocity, we estimated a 4 ft diameter for the drogue parachute, with the main parachute having a diameter of approximately 14 ft. The parachutes will be purchased OTS, and are made of ripstop nylon. Given the nylons low density and high tensile strength (660 N / 5 cm²), it made the best choice for the material used. Additionally, due to the different diameters of fibers used in the fabric, the parachute shouldn't tear if any other components get tangled within. Due to delays in shipping, empirical testing of the parachutes could not take place.

Payload *Description*

The rocket's objective is to deploy a glider payload at an apogee of 4,000 ft. Once deployed, the glider's objective is to descend in a controlled and stable manner, landing within the designated launch facility area. The glider also has a secondary objective of serving as a platform for future capstone projects. Later capstone projects may introduce more advanced features, such as it being autonomous and actively controlled, to enable more advanced mission objectives, such as surveying a region and gliding to a target landmark.

The glider must be passively stable and foldable to satisfy the mission objectives. This is because the glider won't have any control surfaces meaning it won't be actively controlled. Additionally, it needs to fit within the rocket's payload bay of 3U or 10cm x 10cm x 30cm. To ensure the deployable glider satisfies these criteria the following design approach was taken: Airfoil Research, XFLR5 Batch Airfoil Analysis, XFLR5 Wing Analysis, Terminal Velocity

Analysis, SolidWorks CAD, SolidWorks CFD, SolidWorks FEA, Static Stability Calculator, and 3D-Printed Prototype.

Although there are a total of nine stages in the design approach, only the last four stages are both iterative and cyclical. The first four stages intend to narrow the design options so that the last four phases can focus on optimizing the design.

Analysis

Variable definitions:

m = mass of glider

g = 9.81 m/s²

p = density of air

v = terminal velocity of the glider

CD = drag coefficient

CL = lift coefficient

AW = area of the wings

AA = area of the ailerons

AB = largest cross-sectional area of the glider on plane perpendicular to flight direction

θ = glide angle or the direction of **v** taken as the angle from horizontal

LCG = moment arm between center of wing lift and center of gravity

LA = moment arm between center of wing lift and center of aileron lift

Nine analyses occurred, one for each stage of the design process. However, before any analysis occurred a concept for a foldable glider had to be established. Given the constraints of the rocket payload bay of 3U, two concepts were identified. The first concept was a blended wing body design (BWB) that would maximize the glider's total wing area. The second concept was a rectangular planform wing (RPW) design that would maximize the glider's aspect ratio. Since both ideas appeared to have merit, both concepts were analyzed. The goal was to establish which concept would be better suited to accomplish the mission objectives. Figure 19 and Figure 20 depict these concepts.

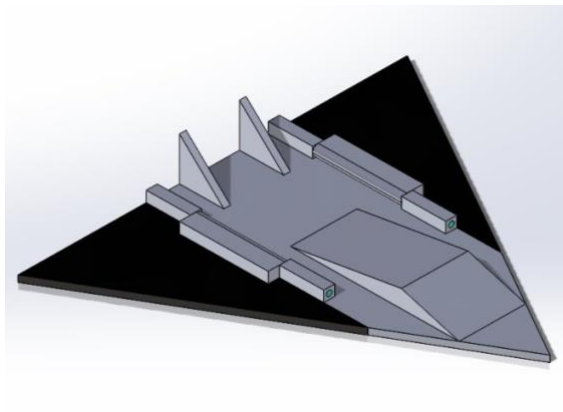
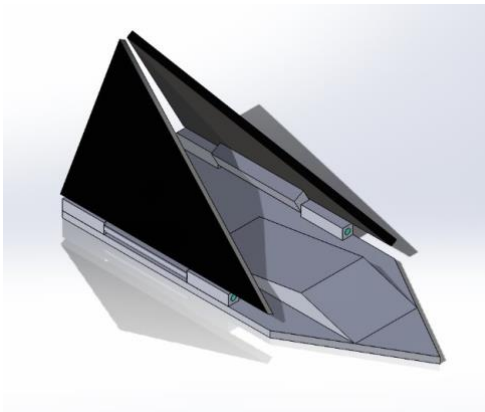


Figure 19. Foldable BWB glider concept. The left image depicts the glider’s configuration in the payload bay. The right image depicts the glider’s cruise condition configuration.

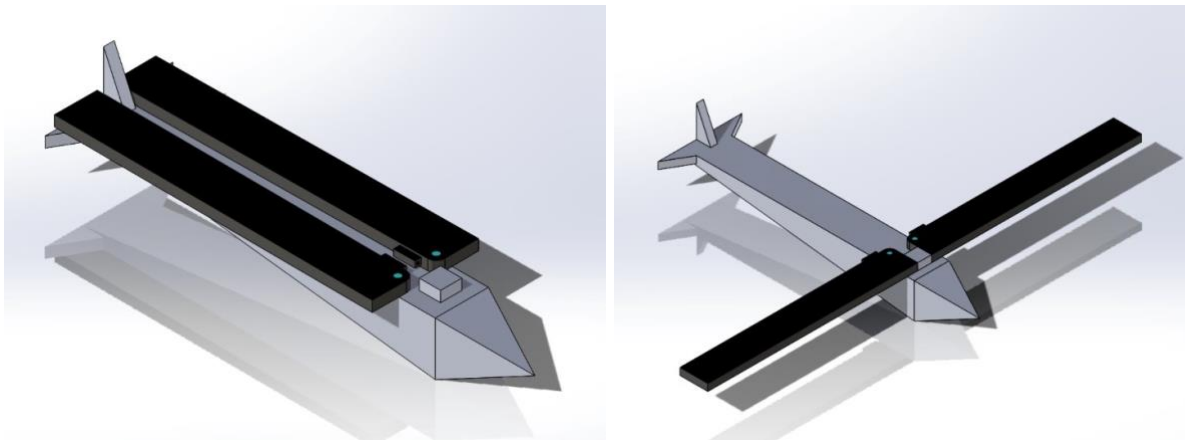


Figure 20. Foldable RPW glider concept. The left image depicts the glider’s configuration in the payload bay. The right image depicts the glider’s cruise condition configuration.

The first analysis conducted was Airfoil Research. This involved compiling a list of airfoils typically used in gliders or sailplanes. Specifically, airfoils used in low Reynolds number applications such as RC planes as it most similar in scale. As seen in Table 2, this research yielded four options.

Table 2: List of suitable airfoil options based on research.

Airfoil Options
SD7037
Clark Y
E205
AG35

The second analysis conducted was the XFLR5 Batch Airfoil Analysis. The objective of the XFLR5 Batch Airfoil Analysis was to select an airfoil that would maximize the performance of passive stability as well as efficiency at cruise condition. This analysis was conducted for a range of Reynolds number of 60,000 to 150,000 and a range of angle of attack of -5.0 to 10.0. Three performance parameters that were considered: lift coefficient, drag coefficient, and moment coefficient. The results are shown in Figure 21 below. Each color on the graph represents a different airfoil. Lines of color represent the same airfoil at a different Reynolds number. The right graph analyzes cruise condition performance while the left graph analyzes passive stability performance. Ultimately, the SD7037 airfoil was selected because it had the overall best performance. The SD7037 airfoil is depicted in a mustard color in Figure 21.

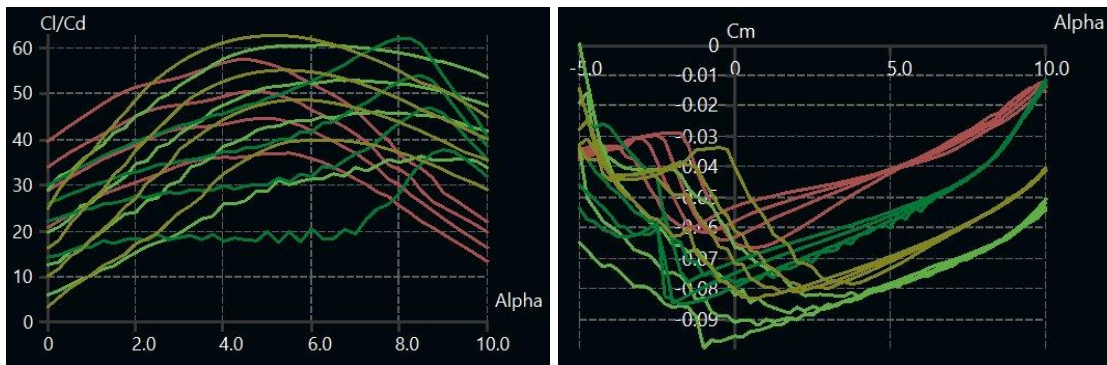


Figure 21. Graphs comparing the four airfoil options.

The third analysis conducted was the XFLR5 Wing Analysis. The objective of the XFLR5 Wing Analysis was to optimize the design of the wings for the two foldable glider options. This analysis evaluated wing geometry by solving a simplified version of the Navier-Stokes equations. Figure 22 below outlines the main assumptions the solver employed.

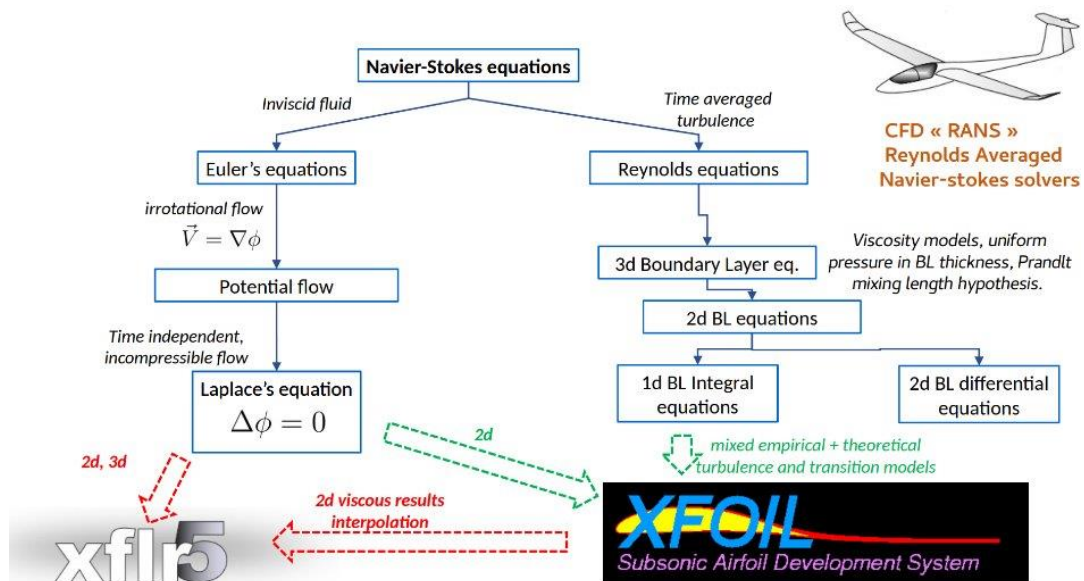


Figure 22. Assumptions made by the XFLR5 Wing Analysis Solver.

Four performance parameters that were considered: lift coefficient, drag coefficient, moment coefficient, and total lift. These parameters were then used to slowly increase the performance of the wings by altering aspects of the wing such as wingspan, sweep angle, dihedral angle, and twist angle that proved to be beneficial.

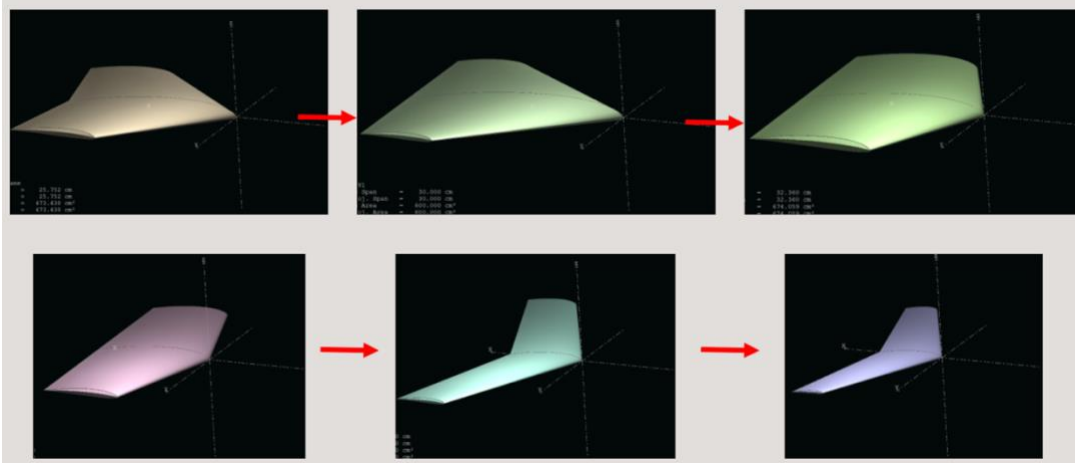


Figure 23. Wing design iterations for the BWB glider. The design in the bottom right image is the most optimized design.

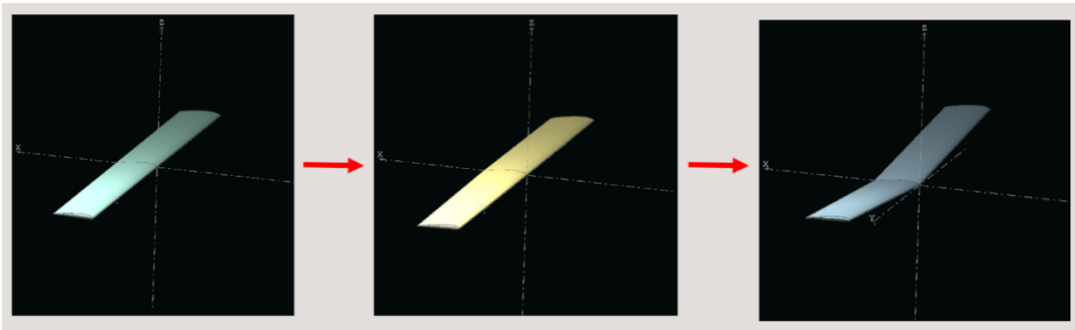


Figure 24. Wing design iterations for the RPW glider. The design in the bottom right image is the most optimized design.

Overall, this analysis suggested that both designs were feasible. However, the BWB design performed better than the RPW design. It created more lift, maximized the minimum rate of descent, maximized the moment coefficient, and was more efficient at cruise conditions.

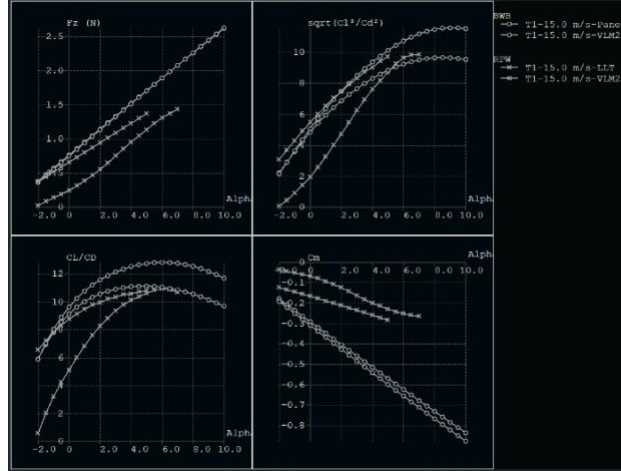


Figure 25. Comparison between final versions of the BWB glider wings and the RPW glider wings. The BWB glider performed about 10% better overall across all metrics.

The fourth analysis conducted was Terminal Velocity Analysis. The objective of the Terminal Velocity Analysis was to estimate a few features and properties of the conventional glider. This analysis was done by hand using a few assumptions at equilibrium terminal velocity gliding. First, the force of gravity pulling the glider along its path was equated to the force of drag of the glider opposing its motion. Then, the moment of the center of gravity about the center of lift was equated with the moment of the downward lift of the ailerons about the center of lift. These yield Equations 3 and 4 below.

$$mg \sin(\theta) = \frac{1}{2} \rho C_D A_W v^2 \quad \text{Eq. 3}$$

$$mg \cos(\theta) L_{CG} = \frac{1}{2} \rho C_L A_A v^2 L_A \quad \text{Eq. 4}$$

Solving for the terminal velocity and glide angle result in Equations 5 and 6 below.

$$\theta = \tan^{-1} \left(\frac{C_D A_B L_{CG}}{C_L A_A L_A} \right) \quad \text{Eq. 5}$$

$$v = \sqrt{\frac{2mg \sin \theta}{\rho C_D A_B}} \quad \text{Eq. 6}$$

The final constraint is that the total lift must be equal to the gravitational component opposing the lift and to the downward force of the ailerons, yielding Equation 7.

$$mg \cos(\theta) + \frac{1}{2} \rho C_L A_A v^2 = \frac{1}{2} \rho C_L A_W v^2 \quad \text{Eq. 7}$$

Rearranging this equation and substituting into Equation 4, the final relation in Equation 8 below is reached.

$$\frac{L_A}{L_{CG}} = \frac{A_A}{A_W - A_A}$$

Eq. 8

In order to yield steady state terminal velocity conditions, equation 6 must be satisfied. This analysis is limited as it hinges on a steady state system: the glider drifting at terminal velocity with all forces and moments at equilibrium. In reality, a glider will encounter unsteady forces and conditions; turbulent wind, deformation and flexing of the glider itself, etc. and thus this analysis excludes dynamic stability and focuses on static stability.

The fifth analysis conducted was SolidWorks CAD. The XFLR5 geometry data was exported as a text file and then imported into SolidWorks via a custom script. The fuselage, vertical stabilizer, and horizontal stabilizer for the RPW glider were modeled using the terminal velocity equation relations. No fuselage was modeled for the BWB because it is integrated into the wings themselves. 3D models of each glider were created to enable CFD, FEA, and 3D printed prototypes to occur.

The sixth analysis conducted was SolidWorks CFD. SolidWorks CFD was used to improve the glider's aerodynamics. The RPW glider became more streamlined to decrease pressure drag. Finlets were added to the BWB glider's wings to mitigate wingtip vortices.

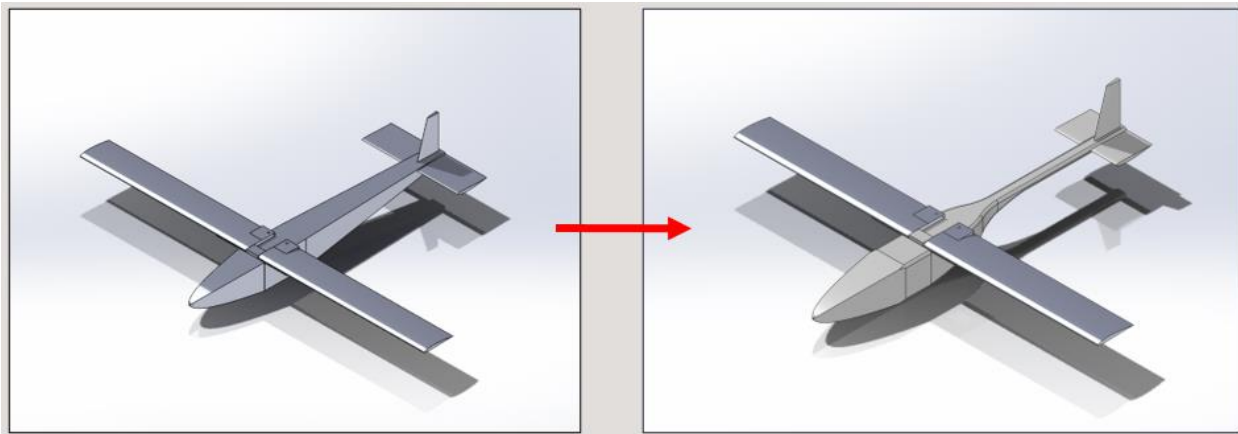


Figure 26. Impact that SolidWorks CFD had on design. The RPW glider became more streamlined to decrease pressure drag.

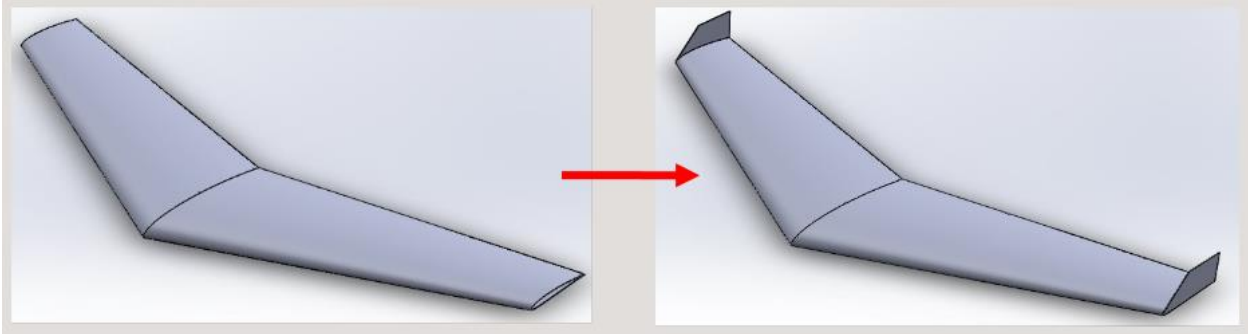


Figure 27. Impact that SolidWorks CFD had on design. The BWB glider gained winglets to decrease the effects of wingtip vortices.

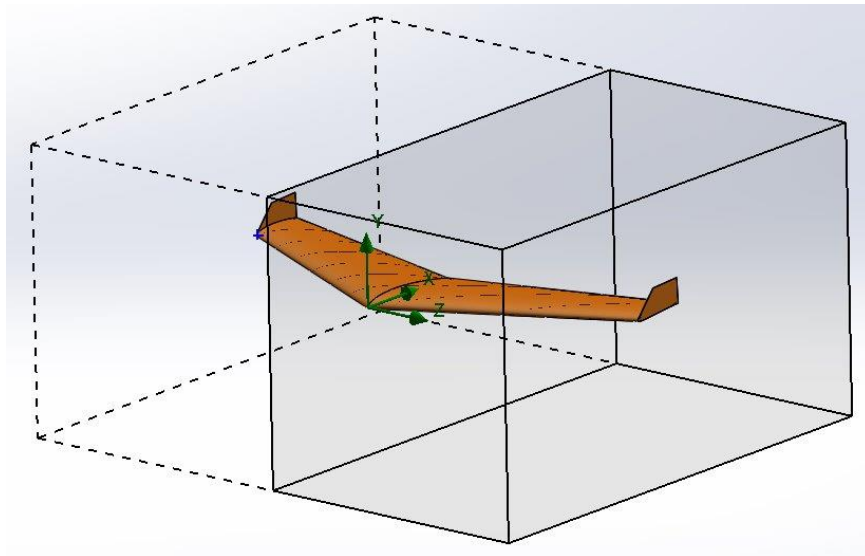


Figure 28. Symmetrical computation domain of improved BWB glider used for CFD.

The seventh analysis conducted was SolidWorks FEA. SolidWorks FEA was used to design the internal structure of the glider wings. The glider wings required an internal structure because they needed to be strong enough to support the aerodynamic loading. However, the glider also had to be light enough so that it could glide well. As such, FEA was used to ensure the design of the internal support structure of the glider's wings were as light as possible while maintaining structural integrity. Figure 29 below showcases the result of the analysis.

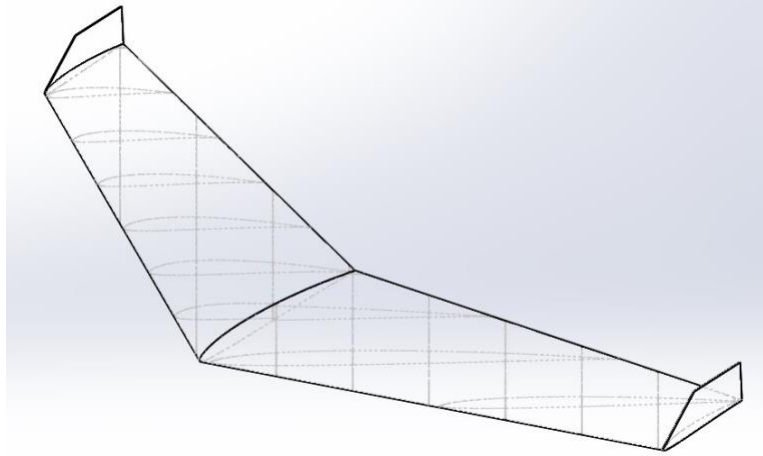


Figure 29. Internal support structure of BWB glider wings. The RPW glider used the same support structure for its wings.

The eighth analysis conducted was Static Stability Calculator. The Static Stability Calculator was used to ensure the glider was statically stable. An aircraft is statically stable if its static margin is larger than ten percent. An aircraft's static stability is dependent on three main factors: its aerodynamic center (AC), its neutral point (NP), and its center of gravity (CG). Since the glider's design had been refined after the previous analysis, its AC and NP were fixed. This meant that for the glider's static margin to be manipulated, its CG had to be altered. The Static Stability Calculator provided the location that the CG needed to be in order for it to have a static margin of ten percent. As such, once the CG location was located the CAD models were updated so that its static margin was larger than ten percent. This update would theoretically make the gliders statically stable in flight.

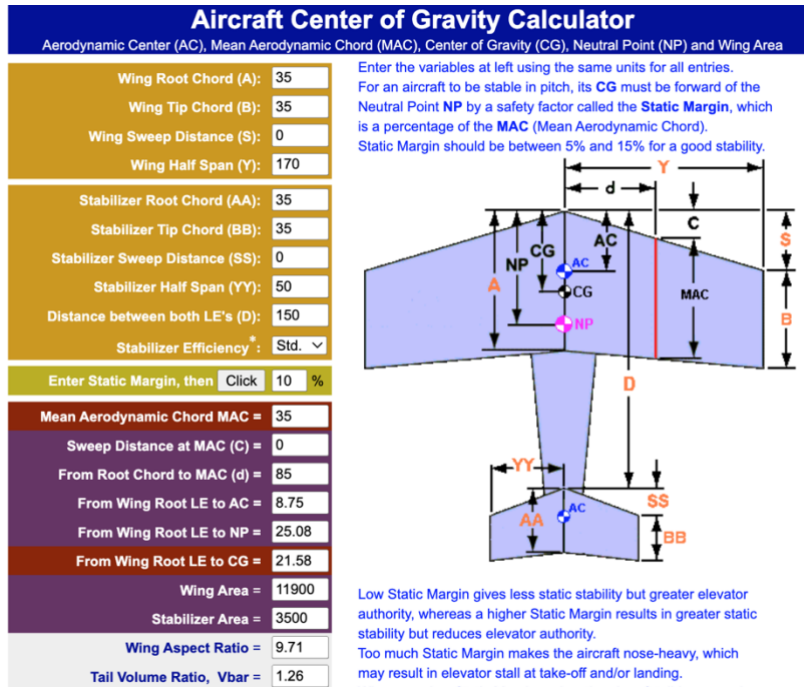


Figure 30. Example Static Stability Calculator for RPW glider. This suggests the the CG of the glider in this configuration should be approximately 2.16 cm aft of the leading edge.

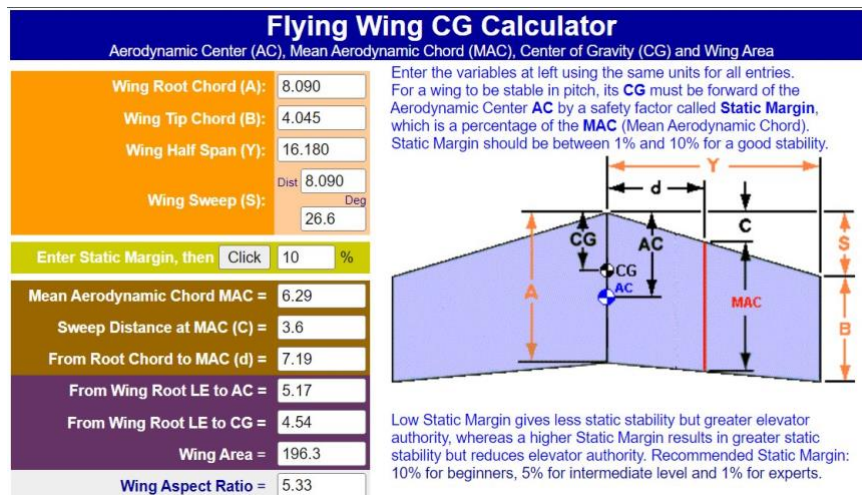


Figure 31. Static Stability Calculator for BWB glider. Suggests the CG of the glider should be 4.54 cm aft of the leading edge.

The ninth analysis conducted was the 3D-Printed Prototype. The 3D printed prototypes facilitated rapid prototyping, allowing for swift comparison with the theoretical model. This approach streamlined the iterative design process and enabled efficient validation of design concepts. The results of 3D printed prototypes are discussed in a later section.

Table 3: Summary of results for each type of analysis.

Analysis Type	Result
Airfoil Research	List of Four Airfoil Options
XFLR5 Batch Airfoil Analysis	Airfoil Selection
XFLR5 Wing Analysis	Optimized Wing Design
Terminal Velocity Analysis	RPW Glider Characteristics
SolidWorks CAD	3D Model
SolidWorks CFD	Optimized Wing/Body Design
SolidWorks FEA	Optimized Internal Wing Structure
Static Stability Calculator	Statically Stable Glider
3D Print Prototype	Test Article

Propulsion

Motor Selection

The process of selecting the appropriate motor for our rocketry capstone project involved a step-by-step process that included a mixture of commercially available propellants and open-source simulation software. Rocket Motor Components, an online vendor for high-powered rocketry, sells grains of propellant mostly made by AeroTech, a popular high-powered motor manufacturer. The propellants that were researched and analyzed all came from this website because they have scientific data on the propellants that allows us to import it to software to simulate its burn properties.

We used the software OpenMotor to assess the performance characteristics of various propellant options. All the burn properties and propellant grain dimensions acquired from the Rocket Motor Components' website were imported into OpenMotor. Each grain was a BATES grain, which is a propellant grain with a through hole and has an outer diameter of 2.493 inches and a core diameter of 0.875 inches. Our technical advisors, Ben Russell and Elaine Russell, gave us an equation to find the ideal length for propellant grains, shown in Equation 7 below.

$$L = \frac{1}{2}(3D_g + D_c) \quad \text{Eq. 9}$$

According to the calculations, the ideal length for each grain was 4.177 inches. If propellant grains were to be purchased in the future, the grains could be cut down to the calculated length. Our motor had three grains each, and each grain used a single propellant formulation, maintaining consistency and avoiding mixing propellant formulations in the motor.

In rocket motor design, several parameters are important in determining the efficiency, stability, and effectiveness of the propulsion system. The Knudsen number (Kn) is the ratio of surface burning area to nozzle throat cross-sectional area (Nakka 2022). The port/throat ratio is the relative sizes of the motor's combustion chamber exit and nozzle throat, and it is related to exhaust gas velocity and pressure. Peak mass flux is the maximum rate of mass flow through the nozzle throat during combustion, influencing propellant consumption and thrust generation (Nakka 2022). These parameters are used to evaluate the design and selection of our propellant.

With our advisors' help as Level 3 certified Tripoli members, we identified specific performance criteria that the selected motor must meet. These criteria included Kn values ranging from 200 to 275, a Port/Throat ratio over 2.00, a Peak Mass Flux below 2.00 lb/(in²*s), and a pressure range of 500 to 700 psi, along with a neutral pressure curve. Additionally, the motor was required to achieve an altitude below 4,000 feet above ground level, according to our project objectives.

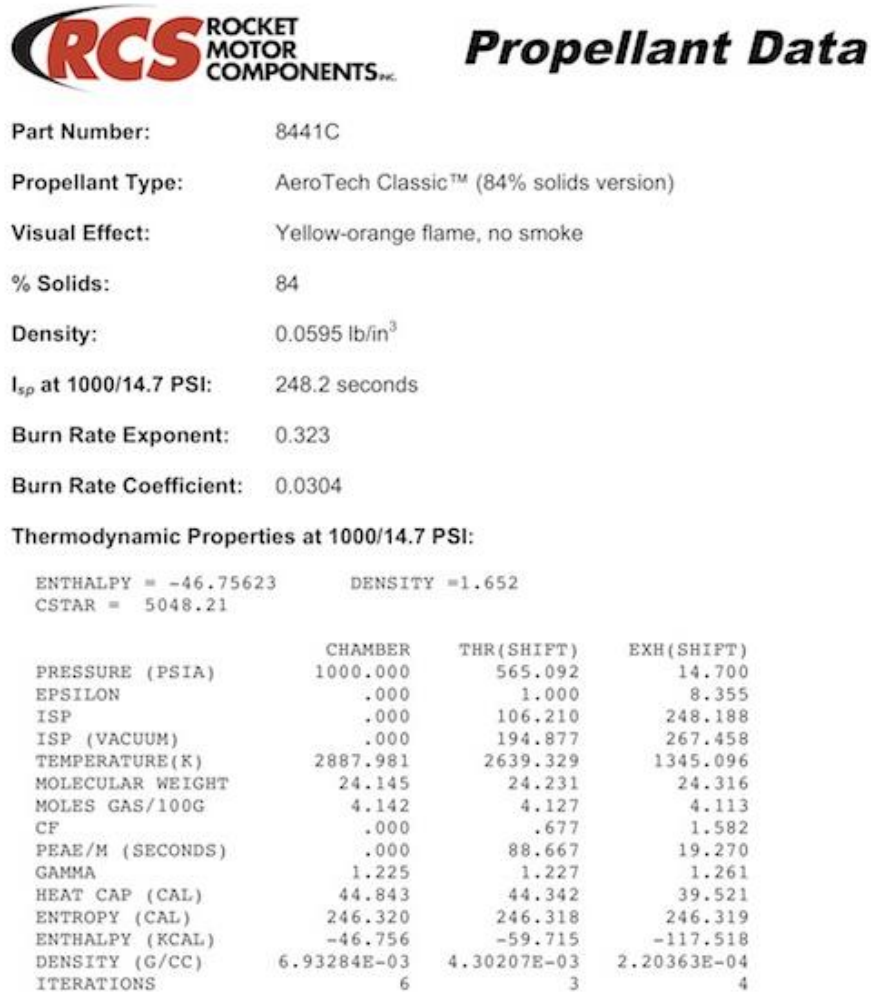
Section	Parameter	Value	Unit
Wind	Average windspeed	4.47	mph
	Standard deviation	0.447	mph
	Turbulence intensity	10	%
	Wind direction	90	°
Atmospheric conditions	Temperature	57.29	°F
	Pressure	996.09	mbar
Launch site	Latitude	38.4	° N
	Longitude	-78.1	° E
	Altitude	480	ft
Launch rod	Length	192	in
	Angle	0	°
	Direction	90	°

Buttons: Reset to default, Save as default

Figure 32. OpenRocket simulation parameters. The values were selected based on the Tripoli Central Virginia launch site, along with common wind patterns experienced there.

We used OpenMotor's compatibility with OpenRocket, a six-degree-of-freedom rocket simulator. The motor created by OpenMotor was imported to an OpenRocket model created by the Aero-Structures team, which had the weights and dimensions of each rocket component. There are several simulation parameters that can be changed, including wind speeds, turbulence intensity, altitude, launch rail length, and more. The parameters for the simulation are shown in the figure above. After designing an engine through OpenMotor and simulating a launch through

OpenRocket, the selected propellant and motor name was the AeroTech Classic Propellant L798. The propellant data sheet can be seen in the figure below.



Information represents typical values and is believed to be correct, however no warranty is expressed or implied as to the accuracy of any of the information contained herein nor is any warranty implied as to the fitness of the device described herein for any particular application. This document is not to be used for design or specification purposes. This document is uncontrolled and all information on this document is subject to change without notice or obligation.

Figure 33. Chosen propellant data sheet provided by Rocket Motor Components

The AeroTech Classic Propellant was chosen because it met the previously mentioned burn property specifications and met the project objective of bringing the rocket under 4,000 feet. Table 4 below shows the launch simulation of the rocket integrated with the motor.

Table 4: Values Acquired from Launch Simulation with Classic L798

	Value
Apogee (ft)	3877
Velocity Off Rod (ft/s)	59.6
Maximum Velocity (ft/s)	507
Maximum Acceleration (ft/s ²)	155

Some key results of the simulation include a velocity off rod of over 50 ft/s and a maximum velocity of 507 ft/s. The velocity off rod value is important because it prevents weathercocking, a phenomenon where winds could tip the rocket on its second rail button after the first rail button exits the rail. Meanwhile, the relatively low maximum velocity (less than Mach 0.5) adds simplicity to the design because staying in the subsonic region lowers the structural and aerodynamic strains the rocket would have to withstand. The figure below shows the burn properties of the Classic L798.

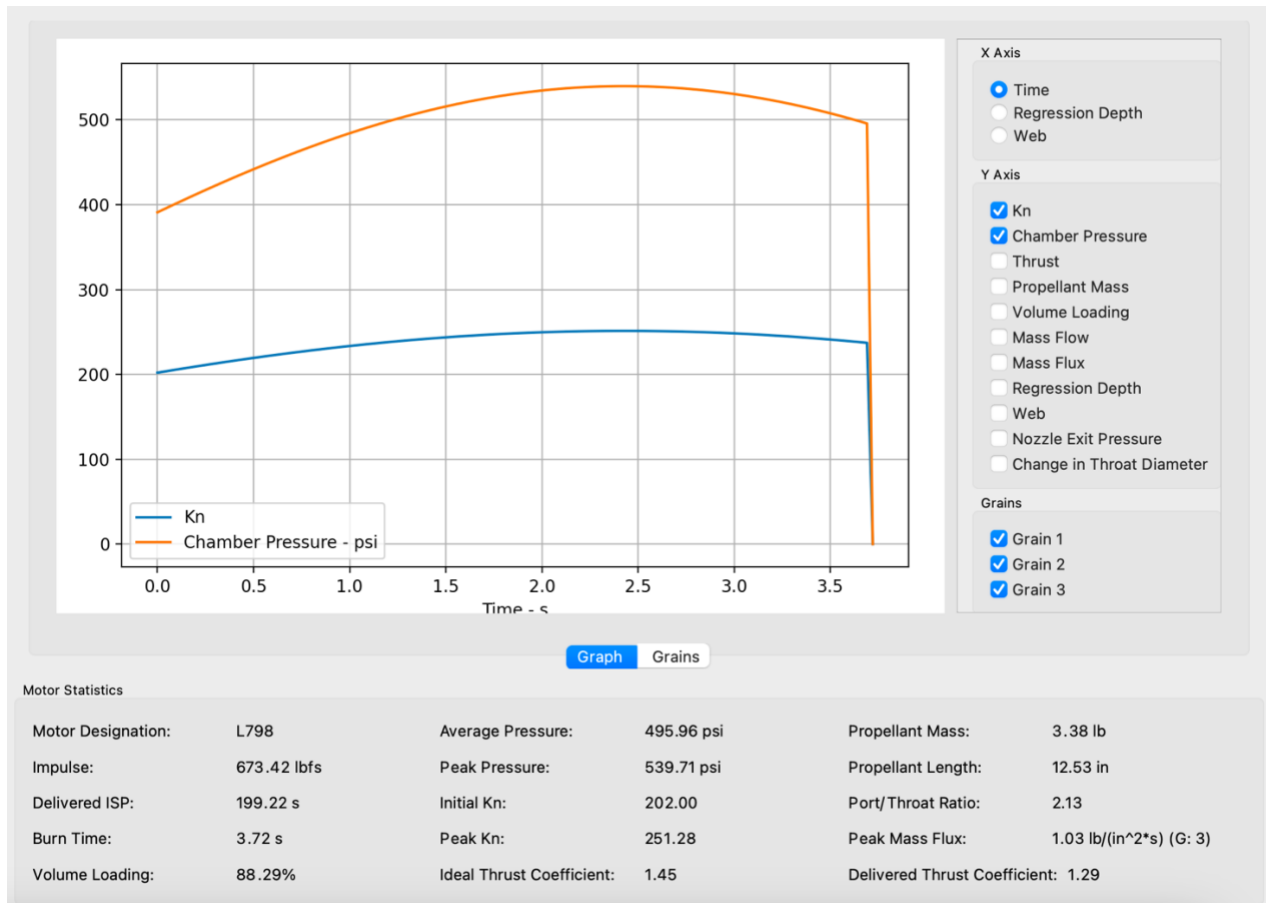


Figure 34. Burn properties of the Classic L798 motor

The Classic L798 is the result of design criteria backed by student research and a careful selection process that sets the rocket up for success and meets the project objective for the capstone.

Motor Design

The motor went through various iterations to match the requirements and specifications of the design as the project evolved. The first design was an M class motor secured with bolts and was designed to have a custom grain. The purpose for the generous size of the motor is because of a high initial estimate for total weight of the rocket, as well as a 5000 feet (about 1.52 km) desired altitude, both of which were changed later during the project. The motor had 2.5mm (about 1/8in) thick walls, and was designed for a pressure of 1000psi, with a safety factor of three and a 150mm (about 5.91 in) outer diameter. Before the modeling stage could be reached, it was determined that a motor that large was unnecessary, and the team switched to a design with a 75mm (about 2.95 in) OD to match common standards. The second design was a bolted case, with a 75mm (about 2.95 in) OD, 70mm (about 2.76 in) ID, 0.25mm (about 0.01 in)

aluminum walls, and 0.9 meters long. The nozzle was made of graphite and was held by a bolted nozzle holder. Both the top cap and nozzle were designed for 2 O-rings to seal the motors. This motor had a safety factor of 3. This motor was designed when it was still assumed that the grain would be custom made, and that the needed thrust would still need to carry the rocket to 5000 feet (about 1.52 km), so it is significantly larger than the final design.

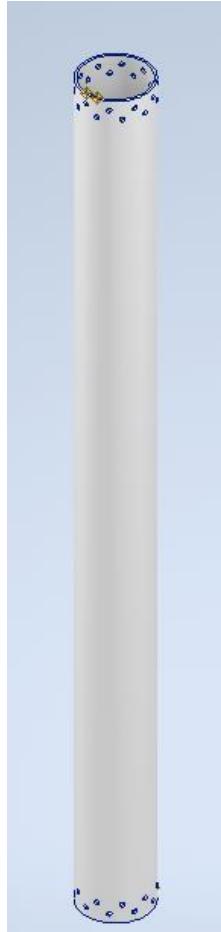


Figure 35. 2nd body tube design

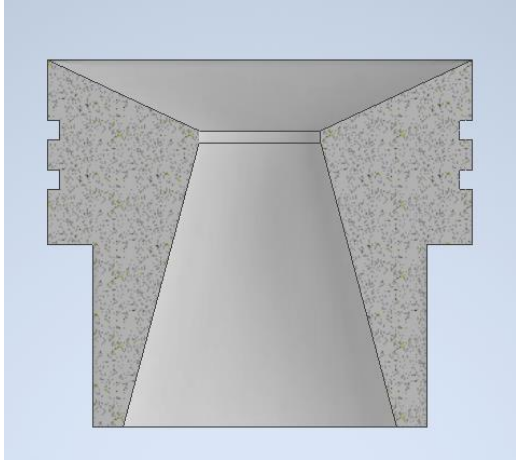


Figure 36. 2nd Nozzle Design

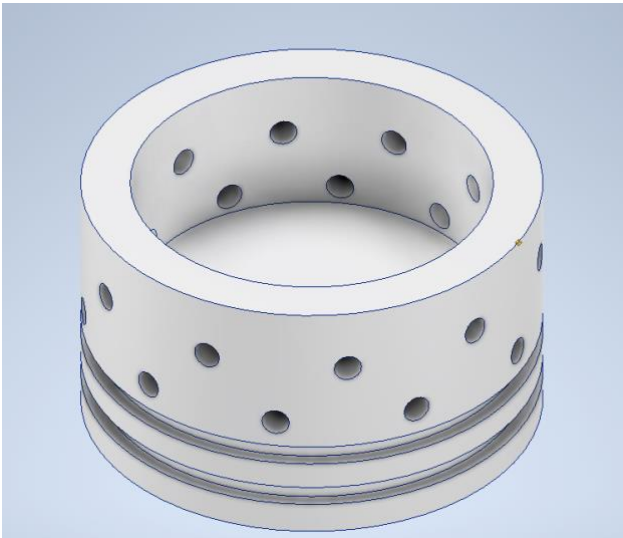


Figure 37. 2nd Top Cap Design



Figure 38. 2nd Nozzle Holder Design

The 3rd design was made when it was determined that the team would be unable to use custom made grains due to safety concerns. This significantly limited the design options, as the case had to closely match the specifications of available grains. This case also incorporated threading for securing the top cap and nozzle holder, which was later deemed infeasible. The case was also aluminum, 3in OD, 2.75 ID, 1/8in casing thickness, 25.35in long, and used 2 144 O-rings on each side to seal the case. The top cap and the nozzle holder were also aluminum, and the nozzle was made of graphite. This case was designed for a maximum pressure of 1000psi with a safety factor of 3. This design also incorporated filleted corners between the nozzle and nozzle holder to reduce stress, and shoulders to fit the liner. A hole was also included in the top cap to collect data from the motor for analysis.

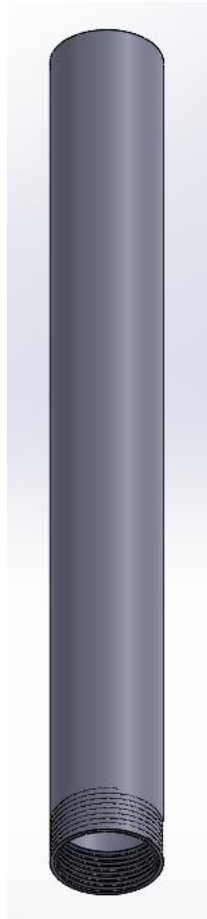


Figure 39. 3rd motor casing design

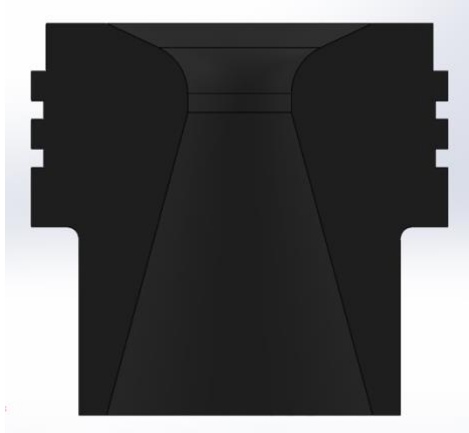


Figure 40. 3rd Nozzle Design

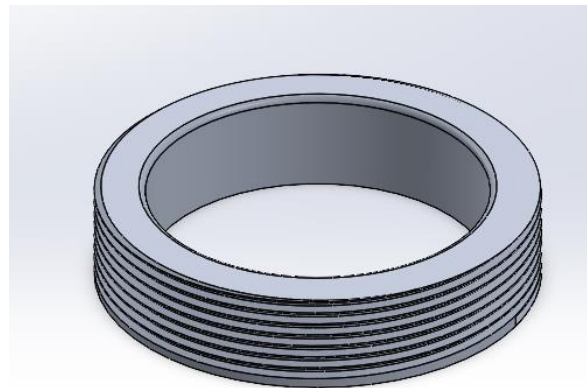


Figure 41 3rd Nozzle Holder Design

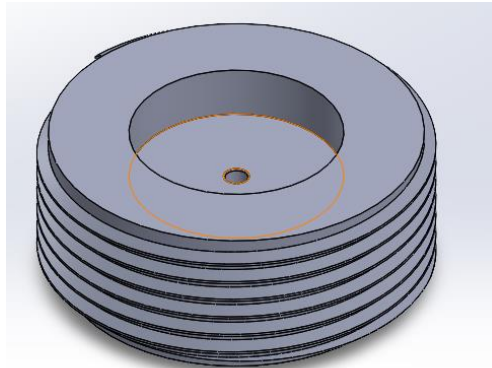


Figure 42. 3rd Top Cap Design

The fourth design went back to a bolted case, as it was determined that threading was infeasible due to manufacturing constraints. The 4th design was identical to the 3rd design except the threading was replaced by bolts and was 19.61in tall. The bolts chosen for this design were 0.3125in diameter, slightly larger than those of the first bolted design, because it was determined

that the tear through strength of the smaller bolts was too low for the desired safety factor. The case was secured by 14 bolts on each side, arranged in two rows of alternating placements. The hole in the top cap was also not included in the design, as in-flight motor data was a removed goal.

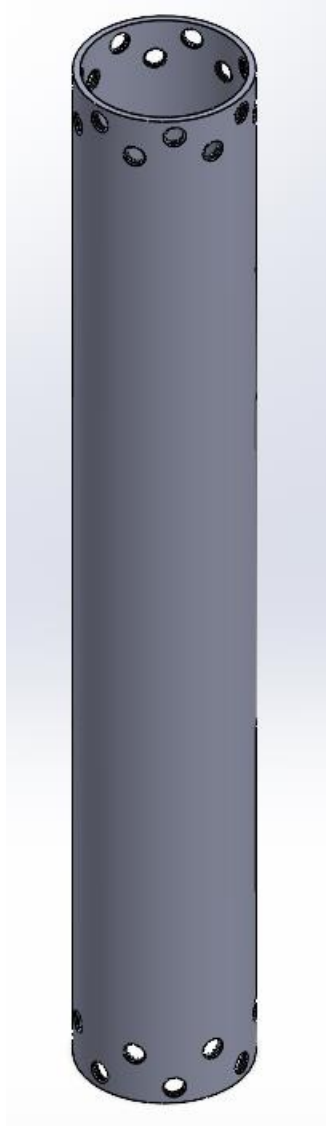


Figure 43. 4th Motor Casing Design



Figure 44. 4th Nozzle Design

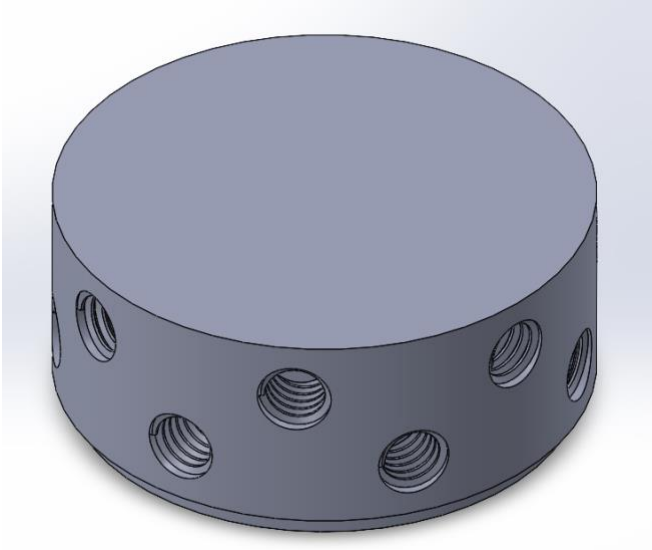


Figure 45. 4th Top Cap Design

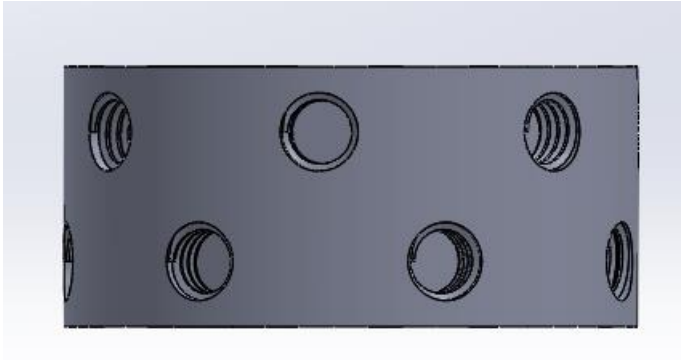


Figure 46. 4th Nozzle Holder Design

The 5th and final iteration was designed on the advice of experienced rocketry experts. It was determined that the best way to secure the nozzle pieces was the use of retaining rings. This case is made of Aluminum 6061 with a 3in OD, 2.75in ID, 1/8in wall thickness, and a height of 20.79in. The nozzle is made of graphite, with an OD of 2.75in, and a throat diameter of 0.6in, and a height of 2.81in, with grooves for 2 144 O-rings, and a shoulder for the phenolic liner. The nozzle also has a 65-degree half angle at the top, and a 15-degree half angle out, with an exit diameter of 1.75in. The top cap is made of Aluminum 6061 with an OD of 2.75in, grooves for 2 144 O-rings, a height of 1.67in, and a shoulder for the phenolic liner, with the advice that the engine did not need a top phenolic cap. The nozzle washer is made of 6061 Aluminum, with a 2.75in OD and a 2.25in ID, with a height of 0.5in. The design uses 2 internal retaining rings, and one external retaining ring to transfer force from the motor to the rocket. The safety factor for this motor was above 3, at an expected maximum pressure of 800psi.

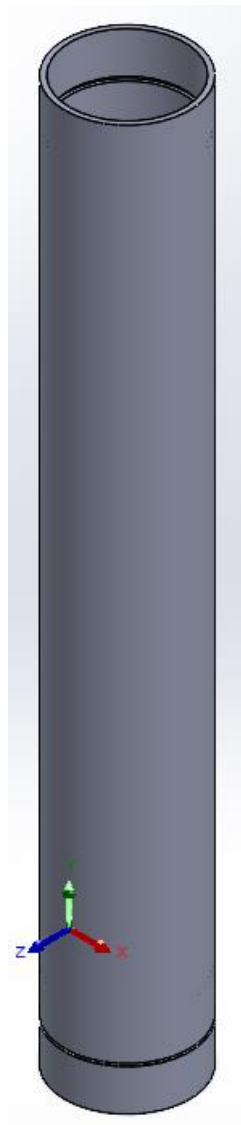


Figure 47. 5th Motor Casing Design

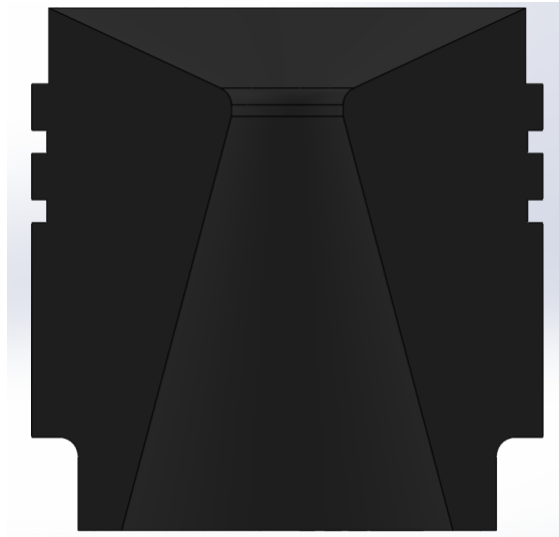


Figure 48. 5th Nozzle Design

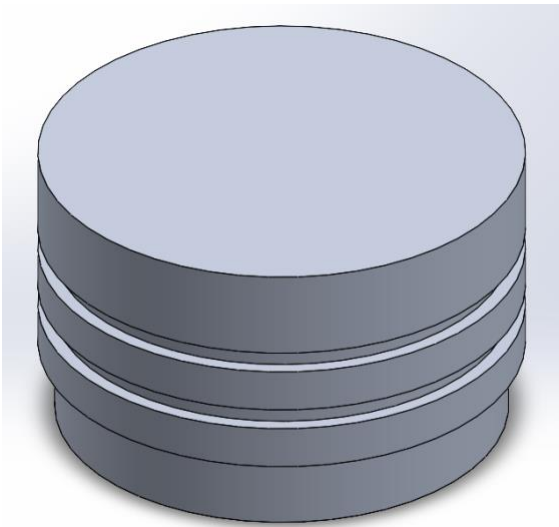


Figure 49. 5th Top Cap Design

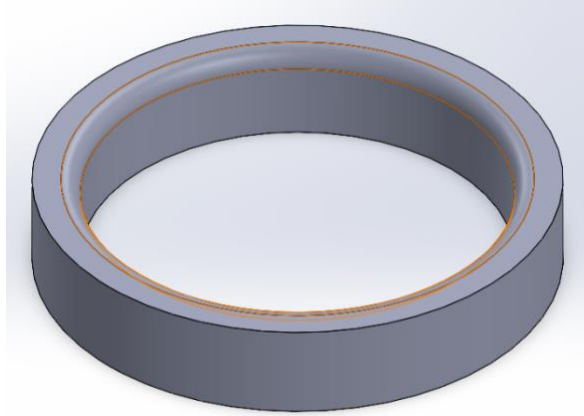


Figure 50. 5th Nozzle Holder Design

Because graphite is porous, water can seep into the nozzle during a hydrostatic test, which would evaporate and damage the nozzle during flight. Because of this, an aluminum nozzle replica was designed for use in hydrostatic testing with the same parameters as the graphite nozzle, except with a 1/4 NPT tapped hole through the center instead of the converging-diverging nozzle.

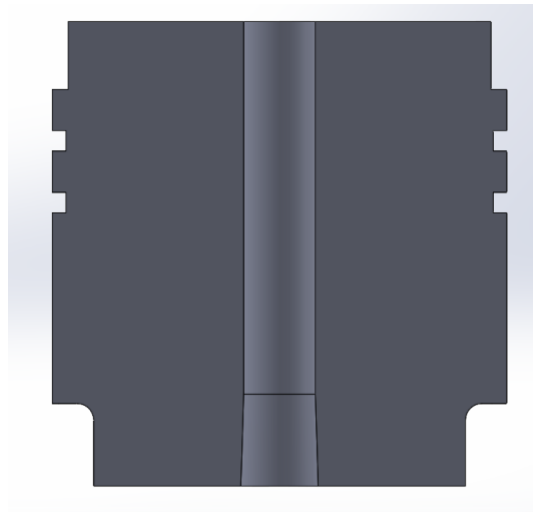


Figure 51. Hydrostatic Nozzle

Analysis

The casing was modeled using SolidWorks FEA simulation at a case pressure of 800psi, which the maximum stress is shown to be 10,390 psi (71.65MPa), which is well below the yield stress of 6061 Aluminum at 35,000 psi (240MPa).

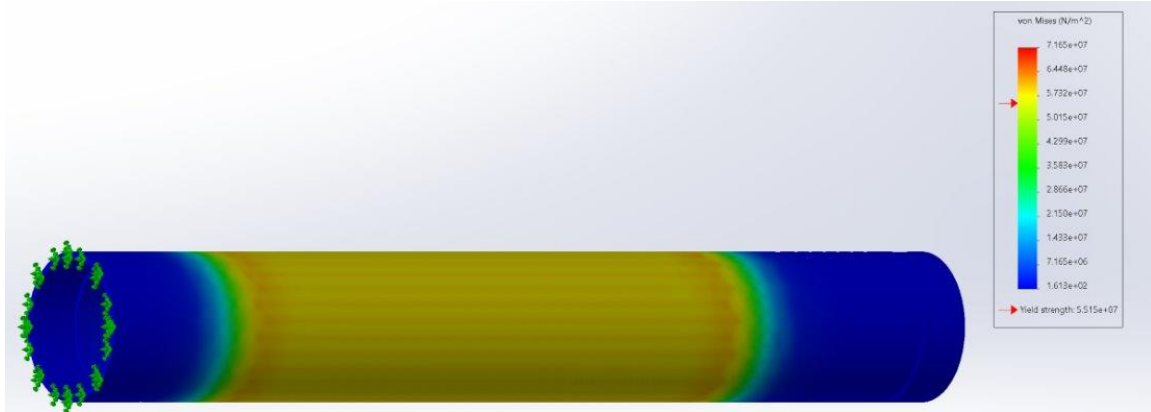


Figure 52. FEA Casing Simulation

Thermal analysis was conducted in Solidworks to ensure that all motor components could withstand the intense heat and thermal loads introduced during the firing of the rocket motor. Due to a variety of software simulations and sources of uncertainty in the behavior of the motor, several simple assumptions were needed to be made in the way the thermal simulation was set up. A CAD file of the motor assembly was loaded into a Solidworks thermal simulation environment. To simulate the thermal loads created during the burn time of the motor, a cylinder the size of the COTS motor was modeled and added into the assembly. This would be used as a “dummy” motor and would be simulated to radiate heat in accordance with the specifications of the COTS motor. The appropriate boundary conditions were added to the simulation to simulate the thermal load from the motor, the insulating walls of the aero-body surrounding the motor assembly, and the nozzle opening that would be exposed to air.

This test setup was met with a major limitation as the heat from the motor would not be a constant temperature nor be evenly distributed across the motor’s surface area. With this limitation in mind, A success would be determined by if the entire motor casing remained under the maximum service temperature for its component material for the duration of the motor’s burn time. Several simulations resulted in this being achieved with a safety factor of over 3, leading to satisfactory results in the thermal simulation.

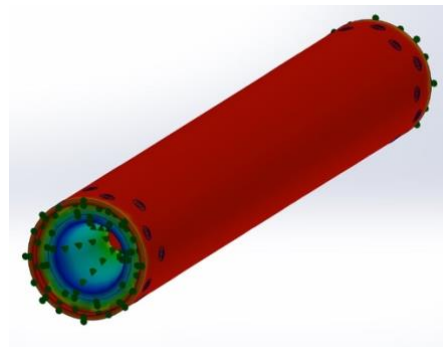


Figure 53. Thermal Simulation Setup

These simulations, along with student research and analysis, supported the material choices for each of the components on the propulsion system. Multiple types of motor casing and liner materials were researched and examined based on criteria such as affordability, durability, and thermal resilience throughout the school year. Employing techniques learned from UVA courses like MAE 3140 Heat and Mass Transfer, an initial assessment was conducted. Eventually, after consideration of the research findings and thermal analysis, preliminary casing and liner options were selected, aiming to strike an optimal balance between cost-effectiveness and performance. The motor casing was to be constructed from **6061-T6511 Aluminum Alloy**, chosen mainly for its excellent machinability & forming, making it well suited for manufacturing. Additionally, its thermal conductivity, reaching up to 1100°F, aligns with the motor requirements and its low cost and density contribute to overall affordability and weight management. The material for the rocket nozzle was chosen to be **Graphite**, chosen for similar reasons to the Aluminum Alloy. It has good thermal conductivity and high temperature resistance to withstand the heat generated during propulsion. Additionally, it has a much lower cost compared to other materials. However, graphite is highly anisotropic, making machining challenging and requiring specific manufacturing techniques. Despite that, it was determined that its low cost and characteristics were worth this extra consideration. Initially, for the motor's liner, Phenolic was chosen to be the material in the top section, while Brown Kraft Paper was to be used for the cylinder walls. This was because both materials are known to be excellent thermal insulators. However, it was determined that the top of the motor was not anticipated to experience prolonged exposure to high temperatures, making a motor lining unnecessary for the top section. It was also determined that the material for the cylinder walls would be **Phenolic RCS-03035L**. Phenolic has historically been an excellent thermal insulator and exhibits good heat resistance. It also has greater structural stability compared to paper, something critical for maintaining the integrity of the walls.

Prototype

Aerodynamics and Structures

Purpose

The purpose of this prototype is to display the feasibility of the teams' designs, provide evidence of functionality in several systems, and test the teams' cooperative manufacturing capabilities with several dependently integrated parts.

Description and Implementation

The Aerodynamics and Structures prototype consists of the manufactured and integrated forms of the Fins, Nosecone, Body, and Couplers components with the goal of providing a testing platform for future teams while ensuring proper integration. The creation of a prototype functions as an execution of the finalized design and serves to illustrate potential issues in the fabrication and integration of idealized components. Components were manufactured individually by subteams and later integrated into the final prototype, allowing for parallelization of the assembly process. The rocket prototype constructed of fiberglass, phenolic, and carbon fiber components to ensure RF permeability and weight savings, with fixed joints being secured with epoxy to avoid the stress concentrations associated with fasteners. Additive manufacturing in the form of ABS 3D printing was used in the fabrication of separation pistons, as well as in the creation of jigs and molds to aid in the construction of the fin and nosecone components respectively. The vast majority of components in the Aerodynamics and Structures prototype consist of student-designed and fabricated components, with the only exceptions being the phenolic body tube substructures and the fiberglass coupler tubes in order to ensure a tight tolerance integration of critical systems.

Manufacturing and Fabrication

Nosecone

The construction of the nosecone starts with three main materials:

1. 1) 3D printed mold
2. 2) Carbon Fiber Reinforced Plastic (CFRP)
3. 3) Epoxy and hardener for the wet layup process

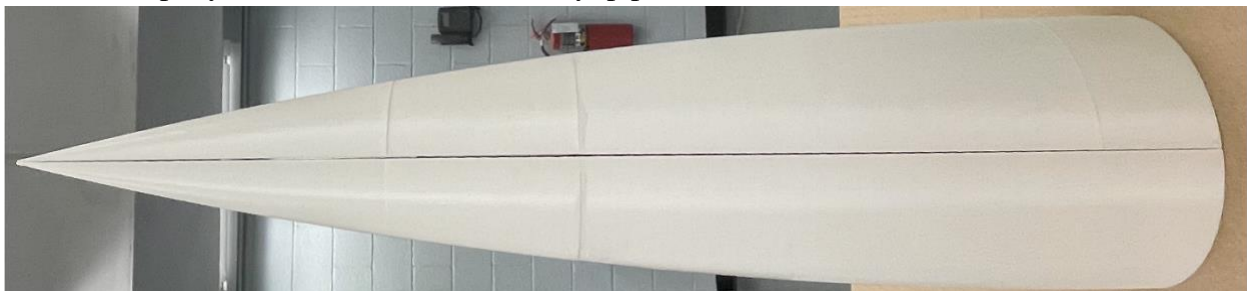


Figure 54. 3D printed mold of the nosecone

The construction of the nosecone comprises various materials addressed above and safety equipment. The 3D model gave us control over the ogive shape, and the dimensions, as shown in Figure 54. The material used for the outer surface is carbon fiber reinforced plastic (CFRP), which has a high strength-to-weight ratio and corrosion resistance. Other materials and equipment, such as Dremel tools with tungsten carbide blades, curing stands, etc., were also used in manufacturing. The two stands were handmade for this process to ensure a stable while doing the wet layup process and for curing the material.



Figure 55. Extended nosecone mold (Height 10 cm)

The manufacturing began by printing the 3D mold using the Engineering school and the library 3D printers. Initially, the nosecone was designed to be 65.82 cm (about 2.16 ft), and that was already printed using the E school 3D printers. Later, due to the additional changes made to accommodate coupler and body integration adjustments, the nose cone hand extended 10 cm (about 3.94 in) in height. Therefore, the extension to the initial mold was printed using 3D printers in the UVA library at no additional cost. The extension is shown in Figure 55.

Two curing stands were handmade before we started the CFRP wet layup method. The curing stand was specifically designed for two purposes:

1. Cleaner manufacturing
2. Stability during the wet layup method
3. For the curing purpose.

Stability during wet layup was essential for us, and the nosecone needed to be held high from the inside to avoid contact of the nosecone with the base and avoid any deformation to the CFRP by the weight of the nosecone itself. The excess material hanging from the mold may create some deformation after contact with the base for a long time. The curing table also helped us apply the material to the mold after it was soaked in epoxy. Later, we left the applied layer of carbon fiber and the mold on the curing table for more than 24 hours.



Figure 56. Manufacturing of nosecone using carbon fiber wet layup method

With the curing stand in place, we proceeded with the CFRP wet layup method, a process that required utmost care and precision. The epoxy and hardener were mixed in a ratio of 3:1, Ensuring the perfect consistency for the task at hand. The carbon fiber cloth was cut into a rectangular shape and laid flat on the prepared table, ready to be soaked in mixed epoxy and hardener. The mixture was evenly applied on the carbon fiber cloth, ensuring complete saturation. This cloth was then carefully placed on the first half of the mold, with any excess mixture of epoxy meticulously squeezed out. The process was then repeated for the other half of the mold, each step executed with precision and attention to detail.

The applied layer was left to cure for more than 24 hours. Once it was cured, we cut the excess cloth using a carbide tipped bit on a Dremel tool to prep the surface of the Nosecone for the following process. The same process was applied for the second and third layers of carbon fiber wet layup. Once all three layers were cured (Figure 57), we again used the Dremel tool to trim the excess cloth closer to the desired dimension to sand the edges of two halves of the nosecone to have an even surface. This step was essential to ensure a snug and closer fit of the edges to assemble the two halves and integrate the coupler and the body.

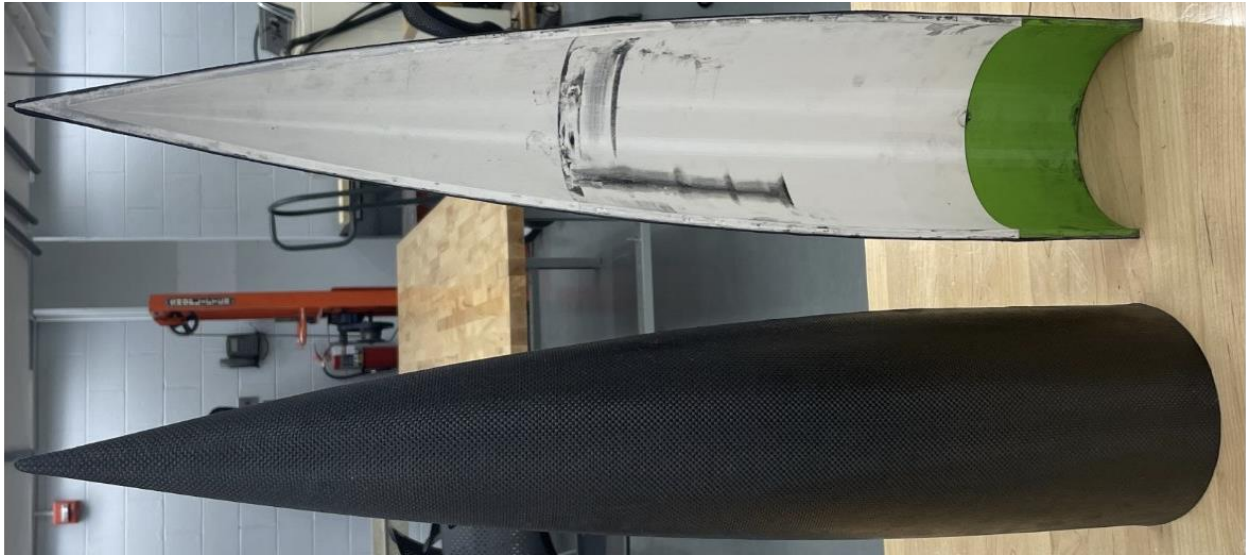


Figure 57. After 3 layers of CFRP wet layup

The final steps involved epoxying the two halves together and using the final CFRP wet layup method. One of the challenges we faced during the final process was aligning the two halves together, which required further sanding of the surface. Joining the two halves took over 24 hours to cure. The final layer was crucial to having a rigid connection between the two halves of the nosecone; hence, carbon fiber cloth was applied over the joints. The nosecone was set for a final curing process for over 24 hours. To ensure a continuous profile over the structure after the final layer was added, all ridges were sanded before a final layer of epoxy was applied to encase the entire structure. This ensured maximal aerodynamic efficiency.

Fins

To create viable fins to keep the rocket stable during launch and throughout the flight, the main materials chosen were a solid carbon fiber plate and epoxy resin attachment to the main rocket body. These materials were chosen due to the ease of manufacturing a solid plate and recommendations by the board members from the Tripoli Launch Site. The fins were cut using a water jet from a solid 6.35 mm (about 0.25 in) carbon fiber plate to the following shapes:

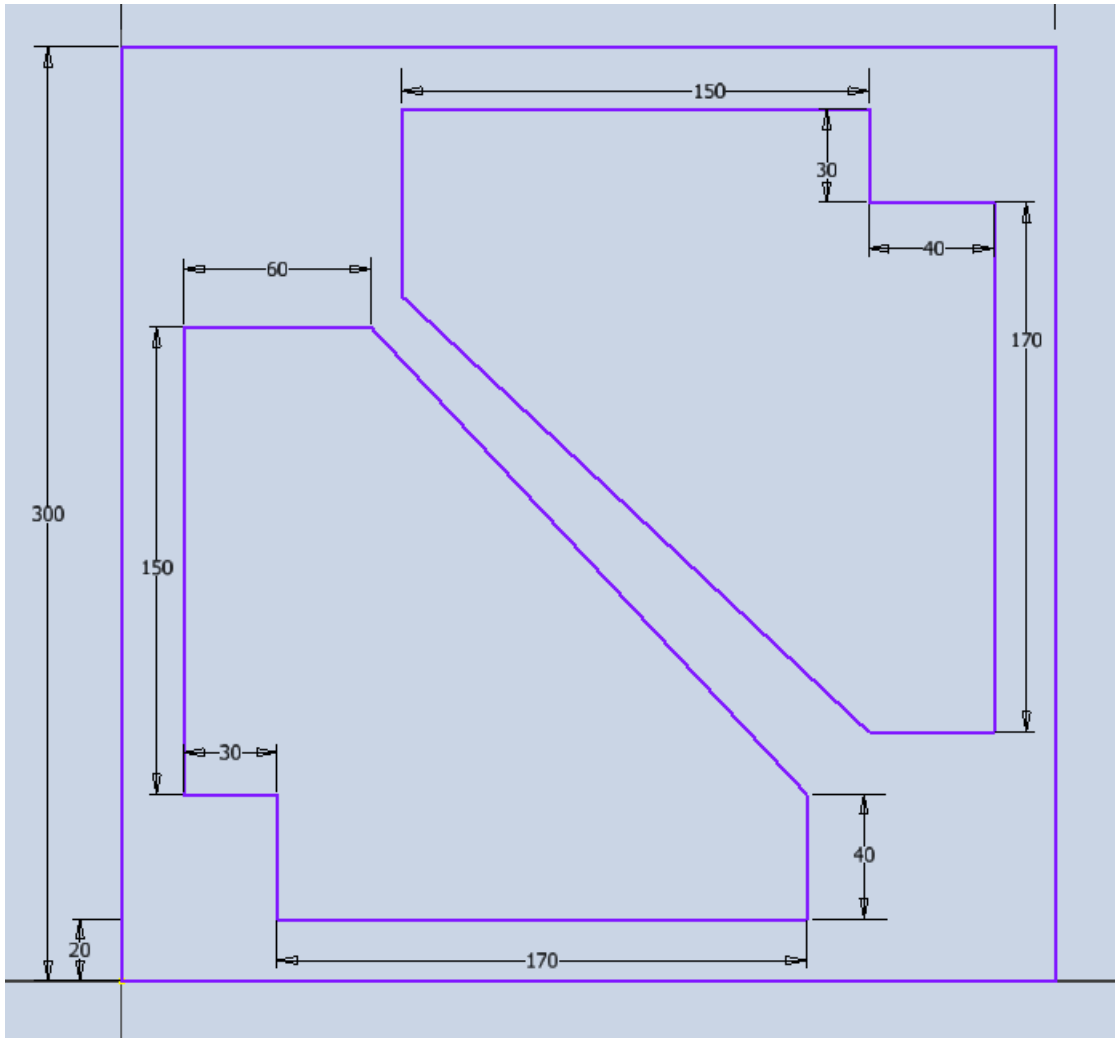


Figure 58. Numbers are in mm, the outer purple square is the outline of the carbon fiber plate, and the inner triangles are the cross section of the fins cut, note that the fin profiles are pushed in towards the center to compensate for the blooming effect, a slight difference from previously.

By using the water jet, the fins were cut very precisely (Appendix A). However, accounting for a blooming effect that occurs on the initial cut, we had to adjust the cut to begin in an area of the plate away from the actual fin cut area. Blooming occurs when the high-pressure water and particulates initially penetrate a layered surface, and, instead of cutting straight down, they shoot in between the layers and out the side of the plate, making a small, deformed bubble area ill-fit for a fin on the back of a rocket as it compromises structural integrity and aerodynamic design:

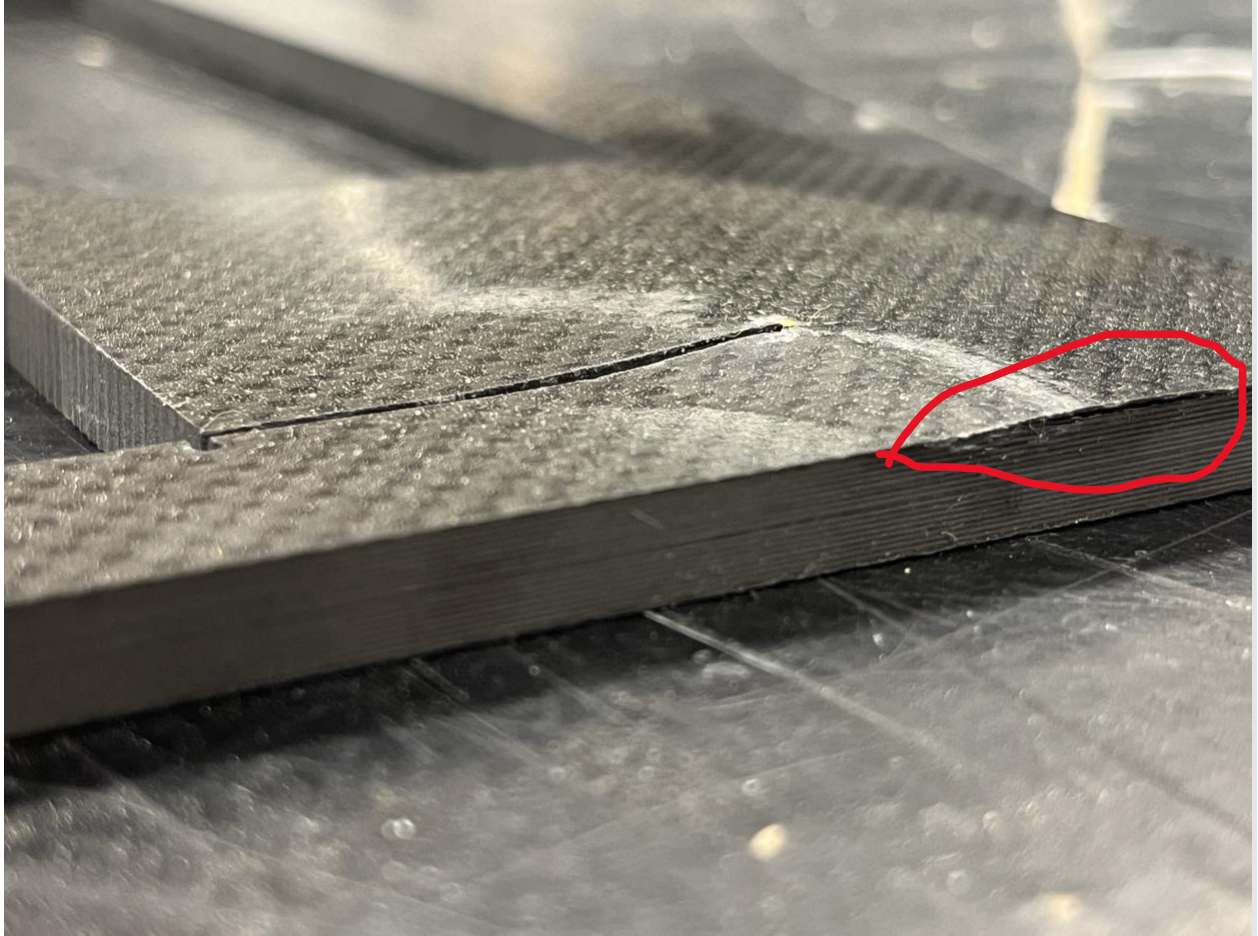


Figure 59. The bloom effects on the cut carbon fiber plate, note the open layers in the red circle and the bubble formation on the surface of the carbon fiber plate.

With the fins cut, the next step was to sand the leading and trailing edges of the fins to $\sim 15^\circ$ as a half angle. The fins were sanded using a Dremel with a sanding tip and then finished by hand. Proper precautions were taken by using a filtered mask during the mechanized sanding and then sanding by hand outside.



Figure 60. Designed vs actual sanded fin

Once sanding was completed, the fins needed to be integrated into the body. The body bottom section had four 170 mm (6.69 in) x 6.4 mm (0.25 in) slots cut into it using a Dremel with a drill tip. The fins were inserted into these slots with epoxy on the bottom edge to attached directly onto the motor mount tube. Epoxy was then used to attach the fins to the body's outer shell, and the fins were held in place with a 3D printed fin alignment jig we designed:



Figure 61. Fins in the slots aligned and hardening with the 3D printed fin alignment jig

Integration

Once the fin and aft body components were complete, these were integrated along with the fiberglass motor mount tube, three fiberglass centering rings, rail buttons, motor retainer, and avionics coupler section. The order of assembly was carefully planned out so that each component could be integrated before the epoxy cured for 24 hours. A schematic of this section is shown below:

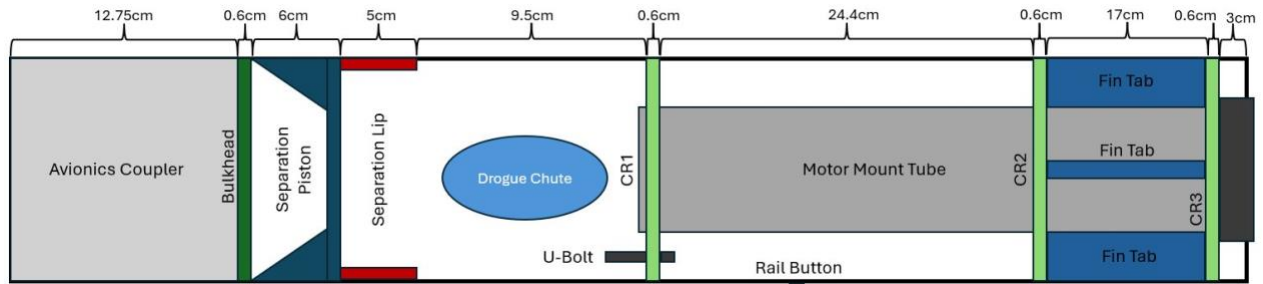


Figure 62. Aft Body Section

The order of assembly necessary to complete this process was as follows. First, each surface to be epoxied required sanding by hand, and the centering rings and couplers were sanded to friction fit with the body tube. The U-bolt was attached to centering ring 1, and the shock cord was tied. Each component's location was marked on the inside of the body tube to simplify the assembly process. Centering ring 2 was first epoxied to the motor mount tube, then the motor mount tube was inserted inside the body section at the appropriate location. Centering ring 3 was also inserted to keep the motor mount tube steady. Next, the rail button was inserted and centering ring 1 was epoxied in place. Centering ring 3 was then removed and then each fin was set temporarily in place one at a time with fast-setting GB-Weld. The fin jig was then attached, and epoxy was applied to where the fins met the inside of the body tube, the outside of the motor mount tube, and the bottom side of centering ring 2. Centering ring 3 was epoxied in place, as well as the motor retainer, and finally fin fillets were created along the edge of each fin. The fins remained set in the fin jig for one day before it was removed. The separation lip for the avionics coupler was also epoxied at the appropriate location, and the separation piston was inserted, thus completing the assembly of the aft body section.

Body

The body's construction consisted of phenolic tubing, fiberglass, and epoxy resin. Before any work could be done on the body itself, it was necessary to construct a mandrel-like apparatus where the body tubing would be able to rotate while keeping in a fixed position. This began with obtaining a pipe that was longer than the tubing while also having a smaller diameter. The pipe would be used as the base of the mandrel. Furthermore, a water jet was used to cut out wooden washers that were designed to have approximately the same outer diameter as the inner diameter

of the tubing. Equally important, the diameter of the inner circle of the washer was designed to have a diameter equal to the outer diameter of the pipe. Once the wooden washers were cut out, it was realized that the outer diameter of the washers were slightly too big, and the diameter of the inner circle was slightly too small. This issue was remedied by sanding the outer and inner ring of the wooden washers until the pipe could be fed through while also fitting inside the phenolic tubing. Once the process of constructing this mandrel-like apparatus was finished, the fiberglass layup process was ready to begin.

Each body tube section was cut to specific lengths with the use of a band saw. Once the section was properly cut, the wooden washers were placed at equal and opposite points within the tubing. The metal pipe was then fed through the inside of the tube and through the inner circle of each washer, allowing for fixed rotation. The fiberglass sleeve was then pulled over the tubing and cut at a length in which it was longer than the tube, leaving 10-15 inches of excess fiberglass sleeve at each end of the tube section. Once cut, the excess portions of the fiberglass sleeve were pulled snug at each end, and zip-tied down to the metal pipe. The ends of the metal pipe were then positioned on two flat surfaces equal in height, and application of the resin was set to begin.



Figure 63. Fiberglass sleeve fixed over phenolic tubing.

105 epoxy resin was mixed with fast hardener at a ratio of 5 parts resin to one part hardener. More specifically, for each tube section, 210g of epoxy resin was mixed with 42g of hardener. Once poured into a plastic cup, the resin-hardener mixture was actively hand-mixed for a minute. Brushes were then used to apply the resin-hardener mixture onto the fiberglass-covered tubing, rotating the tube after each section was finished with application. Once the resin-hardener mixture was finished being applied, clear mylar film was wrapped around the entire tube and secured with tape. Plastic putty knives were then used to evenly disperse the resin by scraping any excess portions towards each end of the tube section and out from beneath the mylar film. Additionally, any air pockets or bubbles were also ironed out during this part of the process.

Mechatronics and Controls

Electronics

Purpose

All processes done on a rocket are controlled through a flight computer, something that we pursued to develop as a Student Researched and Developed (SRAD) rather than solely relying on one bought Commercial-Off-The-Shelf (COTS). Beginning with this process was to develop the physical mechanism, the printed circuit board (PCB), and formulate a rough idea of what the coding structure for the processes would be to begin constructing our own flight computer and deployment system using an Inertial Measurement Unit (IMU) and a pressure sensor. A block code diagram was developed to describe the process that would occur on the flight computer once a functional code is developed.

Description and Implementation

Before circuit design could begin, several system requirements needed to be determined: the objective of the avionics system, the data needed to achieve it, where that data would be sent, and the types of electronics required. We determined that the system's main objective was to trigger the drogue and main parachute ejection charges. The system's secondary goals were to monitor the rocket's structural integrity and conduct an atmospheric survey. To achieve this, the system needed to record atmospheric pressure, temperature, and humidity, as well as the rocket's orientation, acceleration, velocity, and structural deformation (via strain gauges). Data would then be sent to ground control via radio and written to an on-board storage device. Generally, it was decided that the avionics system would include a microcontroller, sensors, a radio transmitter, a microSD shield, and various small components (e.g. capacitors).

Following this initial survey, we searched for specific sensors, PLCs, and radios that would be suitable for rocketry and aligned with the team's expertise. Components were prioritized based on a combination of their weight, footprint, cost, and availability of documentation. An Arduino Nano was selected as the microcontroller, which would interface with sensors from the Adafruit sensor suite and a LilyGo TTGO LoRa 32 radio transmitter. The Nano was chosen because it could handle our processing requirements, weighed only seven grams, covered just over eight square centimeters, and had extensive documentation available - team members also had experience with Arduino. The Adafruit sensor suite was chosen for the same reasons, as well as the fact that it seamlessly integrated with the Arduino Nano. The LilyGo transmitter was reliable, lightweight, and compact; it was also already available as the MAE department had several on-hand. Moreover, the LilyGo operates in the 900 Mhz band, which is the most powerful radio that we could legally use without HAM radio certification.

A block code diagram was created to outline all functions and chronological steps that the code would pass through during the flight, beginning from initialization of safeties (LED and beeper) and data collection and telemetry, then moving into detecting pressure and acceleration data, then processing this data to detect when the parachute will be deployed. A COTS flight computer will be implemented as a primary system, serving as a reliable basis for comparison for the SRAD flight computer's parachute deployment detection. Once the SRAD proves to be capable of reliably deploying the parachute at the proper altitude, it will act as the primary flight computer.

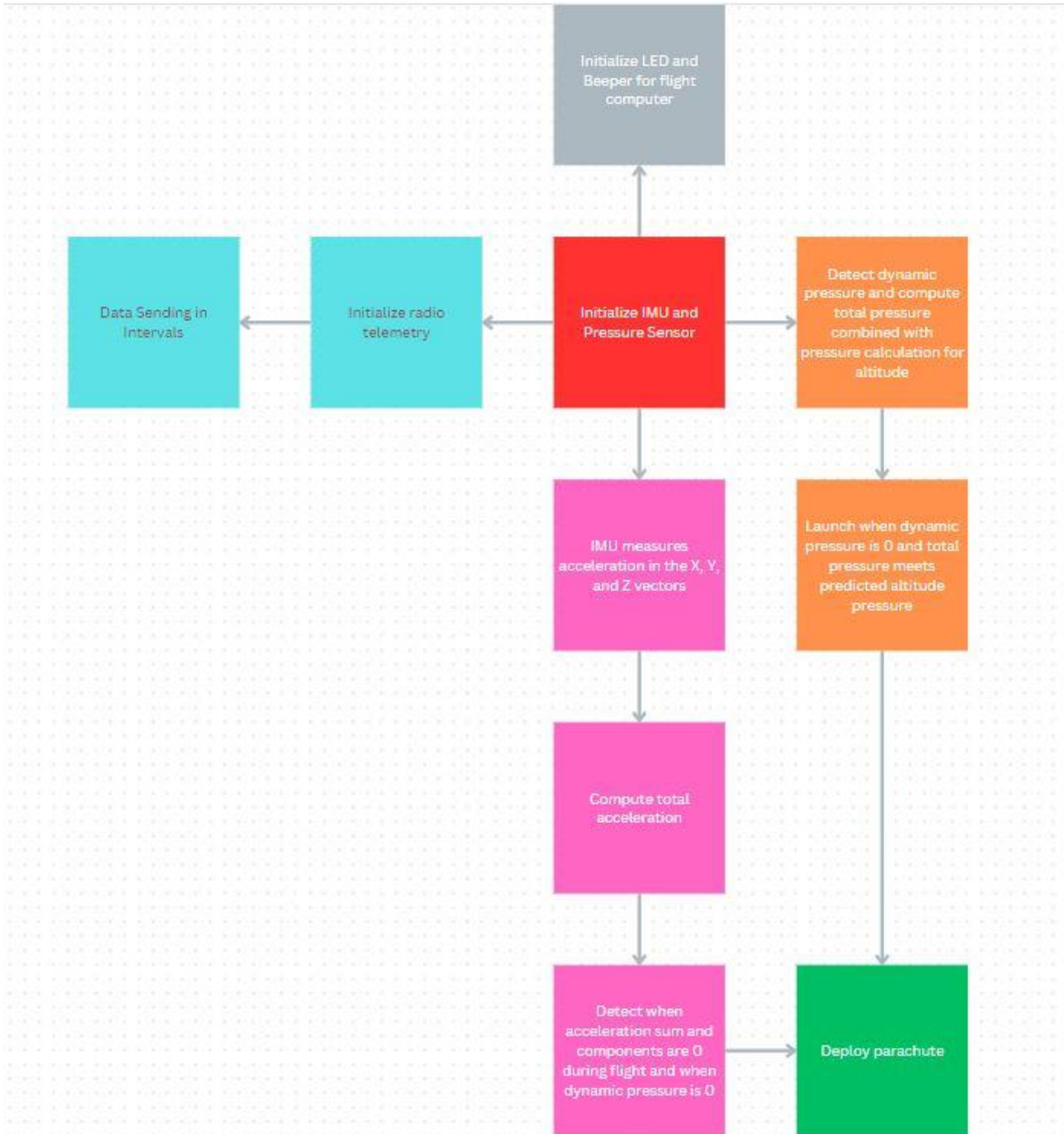


Figure 64. Block code diagram detailing flight computer processes

Testing and Results

Moving forward from our designing, we ran practical testing to confirm the feasibility of these designs. For the construction of the flight computer and its data transmission, both sensors were set up and verified to be able to display accurate data. With data collecting capabilities verified, we moved forward to creating a means of radio telemetry, accomplished with two T-Beam Meshtastic ESP32 LoRa Wireless Module radios.

T-BEAM V1.1 Meshtastic

MCU: ESP32 **Flash:** 4MB **Serial Chip:** CH9102
Wireless protocol: Wi-Fi + Bluetooth 4.2 **PMU:** AXP192
Onboard functions: 3 Buttons (Power+IO38+Reset)
Power Supply Mode: Support USB / 18650 battery

NEO-6M GPS Modules: Support GPS protocol
Onboard RTC crystal, Support interrupt/wakeup

Long Range Low Power LoRa Transceiver:
High sensitivity: -148 dBm, Transceive rate: 300 kbps
Optional Version: SX1278 / SX1276

Frequency model comparison:

	433Mhz	868Mhz / 915Mhz / 923Mhz
Hardware	SX1278	SX1276
Software	Meshtastic 433 Mhz Version	Meshtastic 868/915/923 Mhz Version

Figure 65. T-Beam Meshtastic ESP32 LoRa Wireless Module radio capabilities and specifications

These radios were provided by our program and are a great choice due to them being connected to a Mesh network, which allows for an external form of GPS tracking and telemetry. Both radios were configured, and code was developed to test transmission from a “sender” radio to a “receiver” radio. This was successful and proved the concept that once both sensors and the radios were connected to the main PCB, the data can be collected and transmitted. With the

testing of code, we verified that both static (set messages) and dynamic (alternating messages) were capable of being transmitted, along with sending messages between both radios and a tertiary system using the Meshtastic network.



Figure 66. Live GPS tracking of LoRa module



Figure 67. LCD of LoRa receiver module displaying static message (sender module's name) and dynamic message (number of packets sent by sender module)

Following the initial selection of our electronic components, we created a plan to assemble a small-scale test circuit using components already available through the school. The test circuit, to be built on a breadboard, would serve as a practical platform for testing student-developed data processing and apogee-detection algorithms, as well as to validate our selection of the Arduino/Adafruit platform. The testbed was composed of an Arduino Uno, two BMP280 pressure/temperature sensors, and an MPU9250 accelerometer/gyroscope, which were linked via the I2C digital communication protocol. For simplicity, this first circuit was powered via the

connection between a laptop and the Arduino. A circuit diagram of the test circuit is shown below - note that the thermocouple's removal did not affect the rest of the circuit.

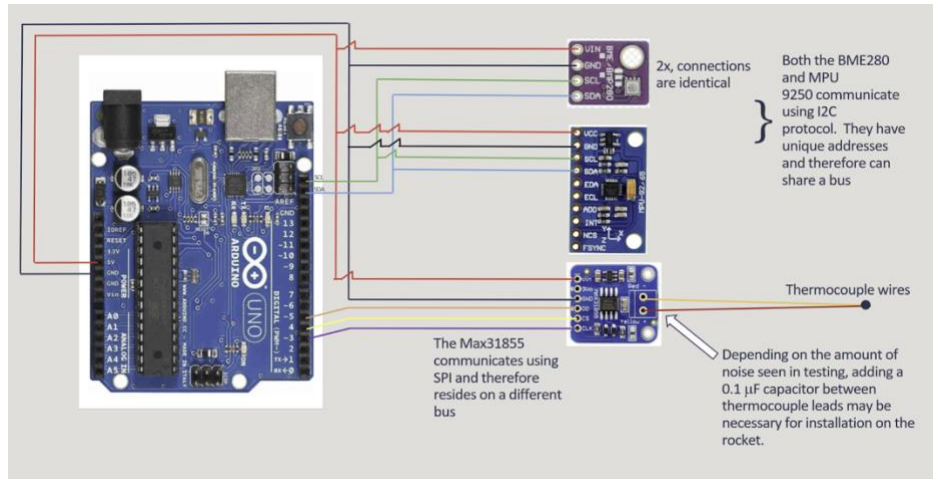


Figure 68. The circuit diagram for our first prototype.

Our test was successful in that we had no difficulties wiring the circuit, using the I2C communication protocol, or writing code to gather, clean, and analyze the sensor data. Originally, a MAX31855 thermocouple was to be included in the test circuit as shown above; however, after experiencing difficulties soldering the thermocouple leads and deciding not to monitor the temperature of the motor case, we opted to remove it. The design complexity associated with motor temperature monitoring was deemed excessive after the team was forced to use an off-the-shelf motor.

Following the successful test, we reevaluated our big picture system requirements. No issues were found with our proposed student-developed avionics system; however, for safety reasons our advisors necessitated that our rocket also carry a commercially proven parachute deployment system. Thus, the scope of our avionics circuit design changed to include both an off-the-shelf (OTS) and a student-developed (SRAD) solution. Under the guidance of our advisors, we decided that the OTS system would have primary control over parachute deployment. To validate our SRAD apogee-detection algorithms, we wanted to be able to compare their detection of apogee to that of the commercial system; to accomplish this, we elected to fuse the OTS and SRAD avionics system into one circuit. Before circuit design could proceed, we needed to select a specific OTS solution for our mission. The Entacore AIM Dual Deployment Altimeter was chosen for several reasons. First, it was an all-in-one altimeter, datalogger, and parachute ejection-charge ignition system. Moreover, it was compact, low-cost, lightweight, and simple to use and test.

With our new system requirements and components determined, a second circuit was prototyped. This circuit combined the Arduino/Adafruit system, the LilyGo, and the Entacore AIM into one platform. The operational amplifier (op-amp) and its surrounding resistors are the circuitry that allowed the Nano to interface with the OTS system and record its behavior. Additionally, proper external power supplies were included. The circuit diagram is shown below:

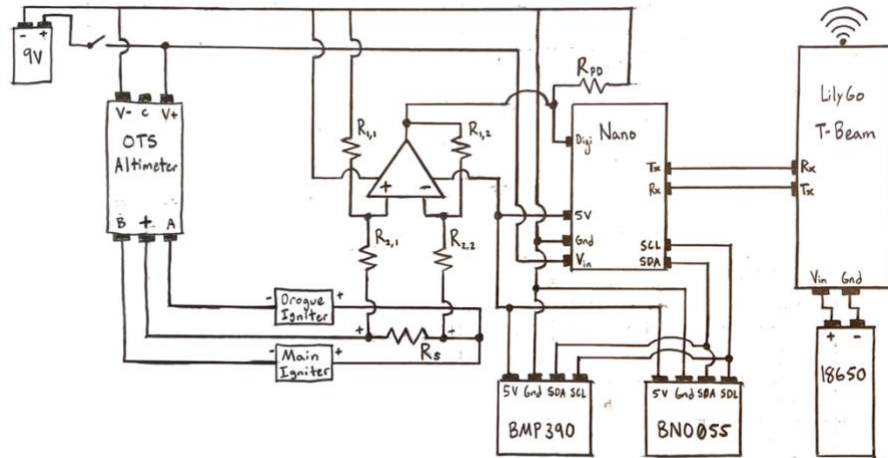


Figure 69. The circuit diagram for our second prototype which integrated an OTS apogee-detection system.

To timestamp the OTS system's detection of apogee, we decided to use a method of current detection on the ejection charge igniter lines: this enabled the Nano to save that timestamp for comparison to that of our SRAD algorithm's detection of apogee. Current-sensing using an op-amp and shunt resistor (R_s) was chosen due to its simplicity and cost relative to other methods of current sensing, such as hall effect sensors. The additional resistors ($R_{1,1}$, $R_{1,2}$, etc.) are required because we chose to perform high-side (pre-load) current sensing. This was necessary if we were to record both drogue and main parachute deployment using just one op-amp, which we elected to do to save weight and simplify the circuit. The pull-down resistor (R_{PD}) on the op-amp's output was used to ensure that the Nano did not gather erroneous readings, since the op-amp would only output a voltage when it sensed current. Note that the Nano and OTS system share a 9V power supply - since a 9V battery met the requirements to power both devices, we elected to use only one to save weight (this decision was eventually changed in our final circuit). An 18650 battery was used for the LilyGo as required by the manufacturer. Finally, we upgraded the sensors to the BMP390 (temperature, pressure, and humidity) and BNO055 (complete IMU) - this ensured more accurate data and ease of operation.

To validate the new circuitry introduced in the second prototype, we carried out two small-scale tests. First, we checked that the Entacore AIM could reliably source enough current from our 9V battery to heat the NiCr wire igniters. Second, we tested our ability to gather sensor data and send it from the Nano to the LilyGo via UART. Both tests were successful.

For our ignition test, we connected the Entacore AIM to our 9V battery and simulated apogee by manipulating its pressure sensor with a suction applied via a straw. Upon detection of apogee, the Entacore AIM was able to repeatedly heat the NiCr igniters to upwards of 600°F; it sent an average of 5A of current through the igniters during three trials (measurements were taken with a multimeter). This test served two main purposes: to confirm that the Entacore AIM was in working condition, to validate our battery selection, and to get an average value for ignition current. The current value was needed to determine the required op-amp and shunt resistor specifications.

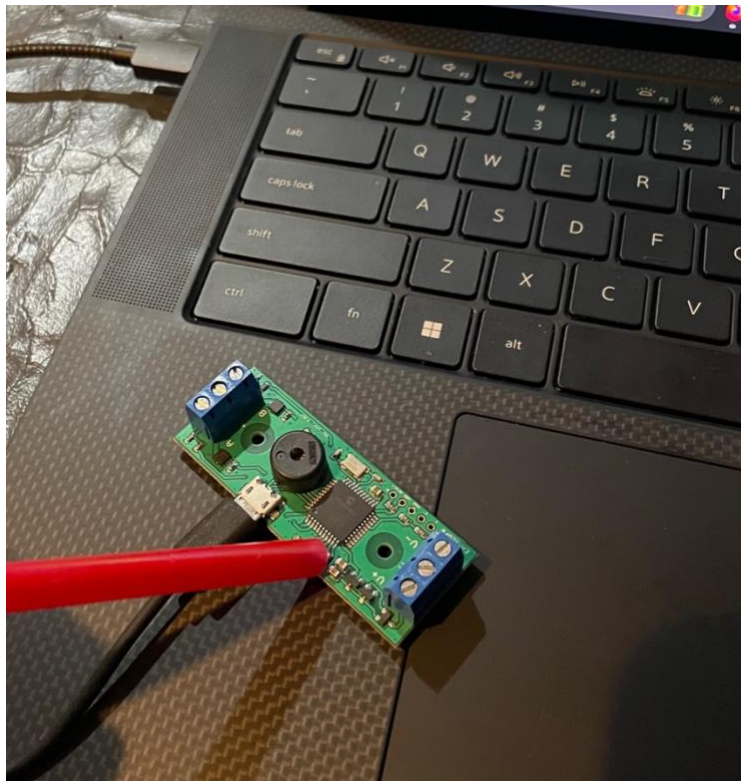


Figure 70. An example of the method used to simulate apogee during our tests that involved the Entacore AIM.

Our test of sending data from Nano to the Lilygo was simple but gave us the confidence to move forward with our design - a BMP390 was wired to the Nano (which was wired to the LilyGo), each device was connected to a laptop, and pressure readings were communicated with

no issue. All the tests and prototype circuits discussed in this section allowed us to validate our design, but more importantly, they acted as hands-on learning experiences for the team.

Avionics Bay

Purpose

The avionics bay design depicted in the assembly file is a preliminary representation intended to showcase the overall structure and layout of the bay. It serves as a foundational framework upon which the complete avionics system can be built and integrated. However, it is important to note that the illustrated design does not encompass all the components that would be utilized in the final manufactured version. Due to time constraints, a prototype was not made. However, the plans for the prototype can be discussed. The electronics team will decide on the internal components of the prototype, and in conjunction with them the layout of the avionics bay will be decided. One important detail is the transmitter needs to be separated from the rest of the bay to prevent electromagnetic interference on the sensors of the bay

Description and Implementation

One notable absence in the illustration is the onboard controller. While a placeholder box indicates a general area where the controller would sit, the dimensions of this box are not accurate, as the specific dimensions of the controller are currently unknown. The primary focus of the assembly file is to showcase the supports and dimensions of the avionics bay itself, providing a basic design upon which additional components can be integrated. The 36cm (about 1.18 ft) threaded rods, offer flexibility in arrangement. The bay itself is 30 centimeters (about 11.81 in) in height and 15 centimeters (about 5.91 in) in diameter.

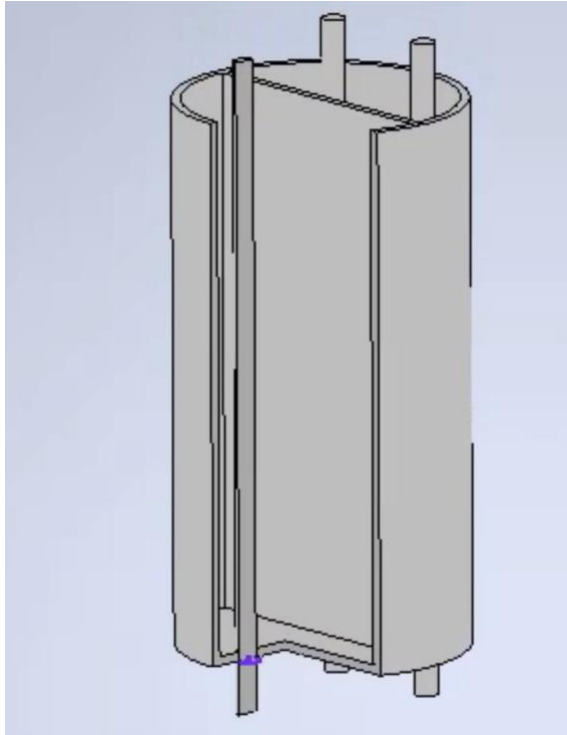


Figure 71. Avionics bay CAD.

Manufacturing and Fabrication

For ease of manufacturing, the three rods are standard $\frac{1}{2}$ inch threaded rods that can be bought from a “home improvement retailer” store. The internal separating wall can be made out of 3D printing material such as PLA, for maximum structural integrity polycarbonate would be best for printing. The wall should be thick enough to hold the electronic components without breaking from the forces of the rocket, but not thick enough to add unnecessary weight. The thickness of the wall would have been one of the factors to experiment with on a future prototype. The outer wall of the bay seen in the CAD is the outer wall of the rocket and is not part of the avionics bay.

Testing and Results

To test the prototype of the avionics bay (once manufactured in conjunction with the electronics team), tests should be conducted to test the structural integrity and functionality of the electronics. To test the structural integrity the bay should undergo dynamic testing using the forces calculated from the simulations using a factor of safety of 1.5. This is a standard factor of safety that NASA uses, however, the factor of safety can be lowered. To test the functionality of the electronics, there should be a test conducted where the bay changes elevation and accelerates rapidly. During this test, the bay should transmit and save data to the internal SD card. If the data

from the sensors is off, it should be checked if they are properly shielded from the transmitter. If problems persist for individual sensors then those sensors should be checked. If the problem persists with all the sensors a more thorough investigation should be conducted with the electronics team to diagnose the issue. If the structure holds on the structural test and the electronics work correctly, then the bay prototype will be ready for flight

Parachute Deployment and Separation

Purpose

The purpose of the test cycles for the deployment and separation system were to ensure that our initial design met the specifications set in the design stage, namely being electronically powered, ensuring total separation within the coupler system, and ensuring that the rocket's internal and external components would remain undamaged post-ignition.

Description and Implementation

The prototyping of the black powder charges didn't require any specialized methods, but given the inherent risk associated with using black powder and electronics, safety was paramount. For each test involving controlled ignition of the black powder, multiple masses were used incrementally, starting at 0.5 grams below the calculated mass, and increasing up to 1 gram over the target mass. Additionally, testing was done at a sufficient distance, and materials used to house the black powder were made of cardboard, so as to avoid shrapnel should an unexpected ignition take place.

Manufacturing and Fabrication

The final charges were made using a 10 cm length of nichrome wire coiled at a radius of approximately 3 millimeters, initial test found that an uncoiled length of nichrome took much longer to increase in temperature and didn't get as hot as the coiled variant. These copper leads were connected to a flip switch which connected to the battery terminal, ensuring that connecting the circuits would not lead to accidental ignition due to a switch failure or human error. The black powder was measured and placed into nitrile pouches, after which the nichrome leads were inserted into the pouches and tied off with electrical tape to ensure no spillage would occur.



Figure 72. Charges used in final test with spare coupler

Testing and Results

The first test done was to ensure that the nichrome wire would show a temperature increase when a current passed through it. This was done by first coiling the wire, connecting it to two copper leads, and then hooking the leads up to our 9-volt power source. After a bright glow was emitted from the nichrome wire, the next test involved igniting a mass of cardboard rated to ignite at 400 Fahrenheit, which is also the ignition point of the 3FG black powder to be used in the charge.

Once the preliminary tests were successful, a test section modelling the coupler was created, with a plastic top that sealed with a friction fit. Given a radius of approximately 4 cm, we were able to determine that roughly 1.5 to 2.5 grams would be sufficient for separation. This also gave us an opportunity to test the validity of our equation used to determine the black powder mass.

While separation didn't occur at 1.5 grams, it was achieved at 2.5, this is most likely due to initial calculations ignoring friction forces between the housing components. Given this correction, it was determined that the final separation charges should be approximately 4.5 grams of 3FG black powder. Additionally, at higher masses, there was also a delay between switching

on the power and combustion occurring. This is most likely due to the 3FG black powder being relatively coarse, slowing down the combustion cycle.

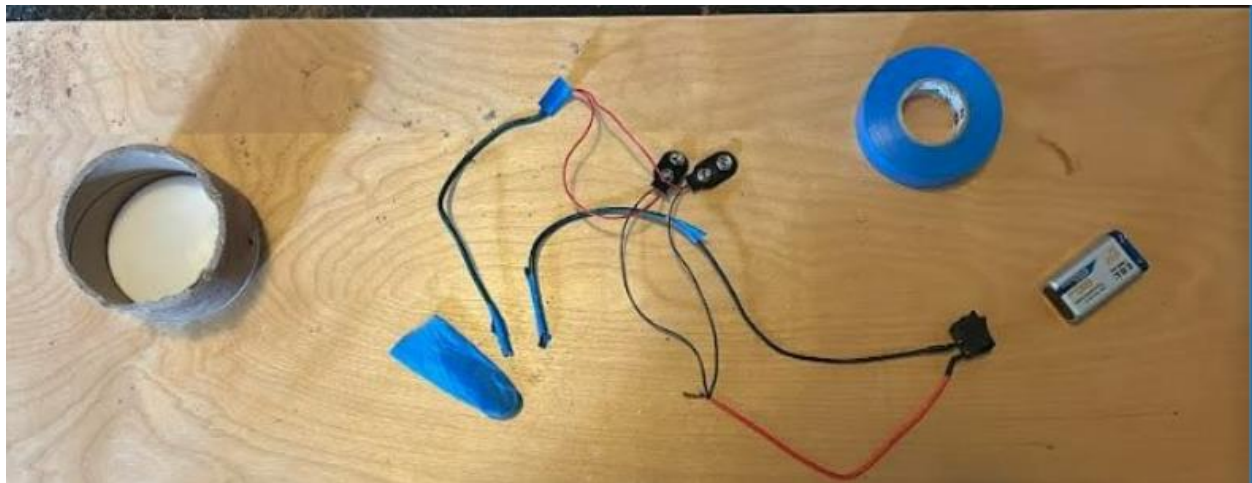


Figure 73. Scaled coupler prototype, nitrile pouch holding black powder, nichrome filament connected to battery terminals and switch, 9-volt battery used as power source (*left to right*)

Our final test involved using one of the 3D printed separation pistons, as well as a section of body tube that was made of the same fiberglass as the rocket's main body. To look at how the explosion would affect the rocket's bulkhead, a paper membrane was placed on the end opposite the separation piston. The separation was a success, with full separation occurring, and no damage to any components of the simulated coupler, besides some minor debris, which wouldn't be able to reach any internal components because of the bulkhead regardless.

Given the test cycle's success, the ignition system has met all the design specifications; creating full separation, being able to connect to an electrical power source, and not damaging any components of the rocket.

Payload

Purpose

The purpose of the 3D printed glider prototypes was to test the glider's flight abilities. The results were then compared to the theoretical model and updated accordingly. The primary goal of these prototypes was to provide insight on the characteristics that affected the glider's flight abilities that weren't accounted for in the theoretical model. The secondary goal was to compare the performance of BWB design to the RPW design to quantify which design is better.

Description and Implementation

Our main method of prototyping the gliders was through 3D modeling in SolidWorks followed by 3D printing of the SolidWorks model's parts, and either gluing or taping the parts together into the full model. We tested our models by throwing them from high surfaces and qualitatively analyzed their ability to glide with smooth and controlled flight. The testing areas were public, and we tested carefully to avoid injury of people or damage to objects nearby. Three iterations of the conventional glider's SolidWorks designs are shown in Figures 74, 75, and 76. Additionally, views of the CAD models contrasted with pictures of the 3D printed prototypes can be seen in Figures 77 and 78.

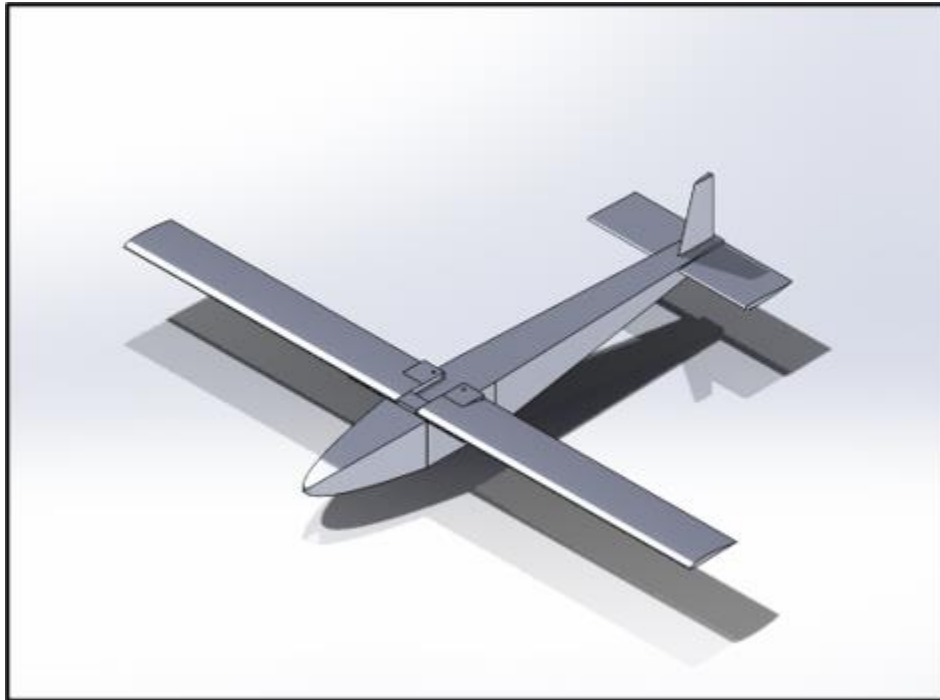


Figure 74. Initial design of conventional glider. The glider was designed in SolidWorks and is composed of multiple parts: wings, pins, main body, ailerons, rudder, and nose cone. The SD-7037 airfoil cross section was used.

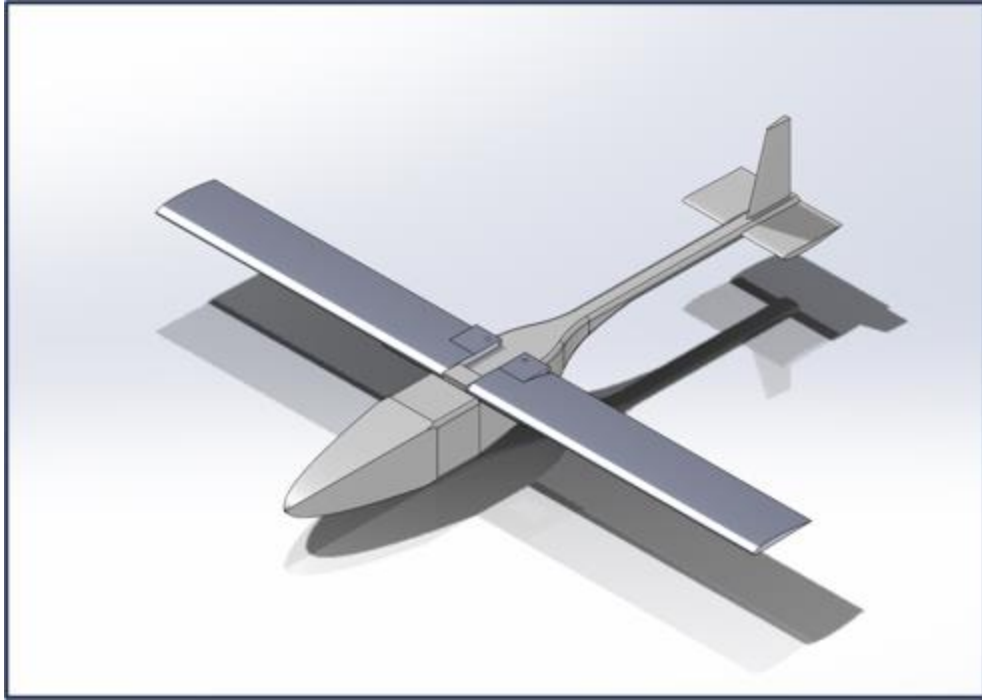


Figure 75. Revised design of conventional glider. The changes made from the last model were focused on pushing the center of mass forward.

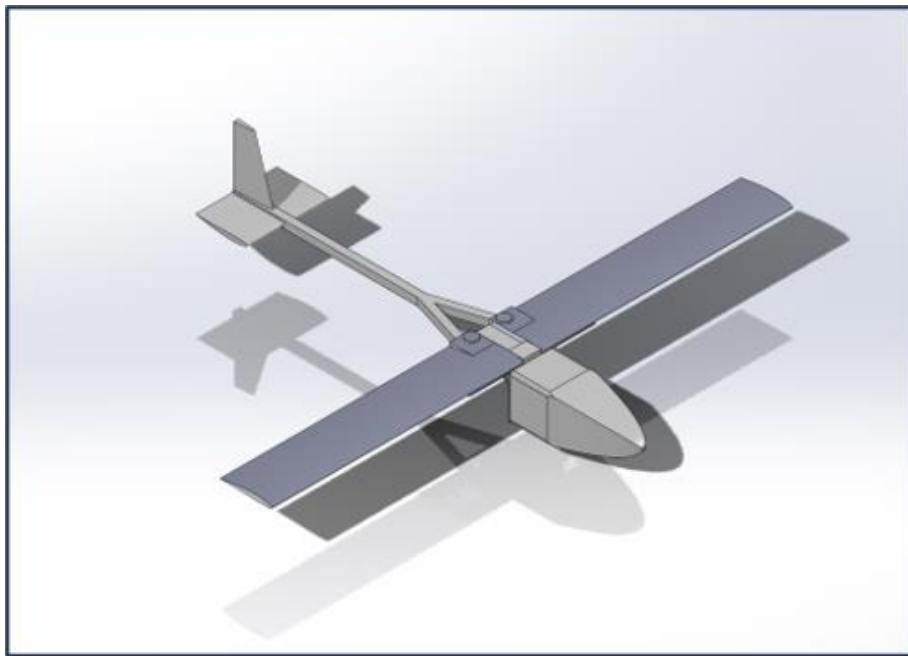


Figure 76. Further revised conventional glider design. Further revisions were also aimed at pushing the center of mass forward.

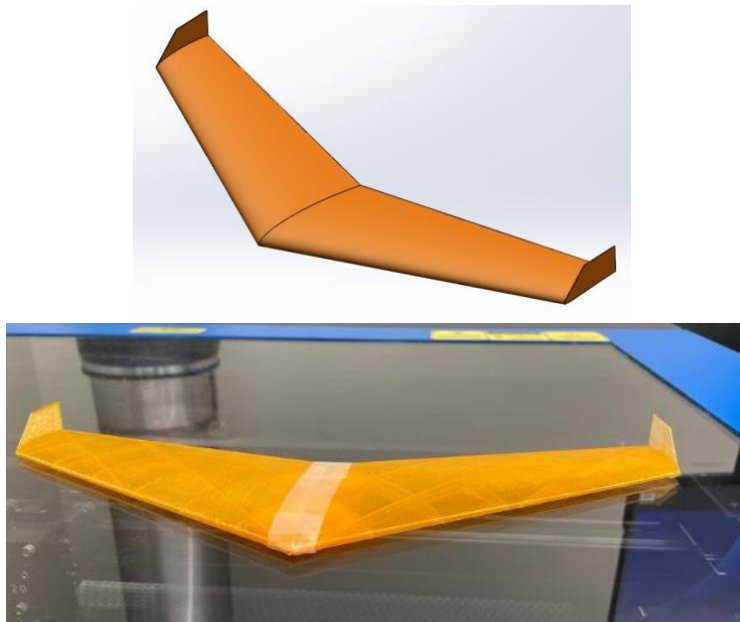


Figure 77. BWB CAD model (left) vs 3D printed model (right).

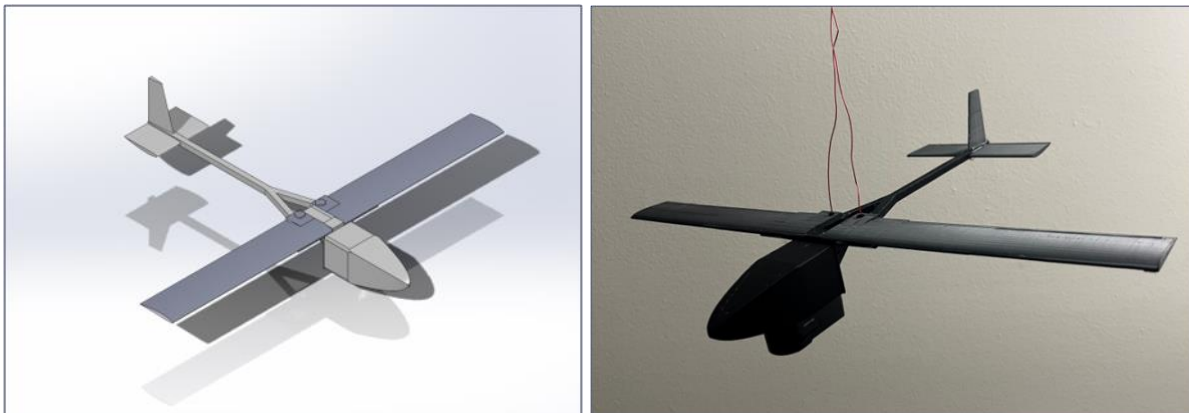


Figure 78. Conventional CAD model (left) vs 3D printed model (right). Note: the camera is glued to the underside of the nose cone in the 3D printed model here.

Fabrication and Materials Selection

Deciding on a glider presents multiple design factors relating to fabrication: the material and design must be strong enough to avoid failure yet light enough to function as a glider, the fabrication process must be able to produce fine details and smooth shapes reliably, and the fabrication process must have a high turnover rate for multiple design and test iterations. Another factor to consider is that to optimize the design of the glider a CAD software was used, and thus

a mechanism of fabrication that can translate easily between CAD models and a real-life prototype was desired. A few possible options include machining parts out of aluminum, using balsa wood and then potentially adding a skin made of a paper-like material, and 3D printing the gliders out of plastic. Machining parts out of aluminum would certainly have provided strong enough parts, however due to the small size of the glider aluminum might've been too heavy of a material. Additionally, machining aluminum quickly with fine details seems rather complex and could become relatively costly and time consuming when ordering aluminum stock and machine training is factored in. Additionally, while aluminum would be a good option for a larger, reusable glider, the glider we focused on only needs to hold up during flight conditions and thus we don't need the biggest advantage of aluminum, its strength, for the glider to remain intact upon impact with the ground. Thus, for these reasons aluminum was not the best choice. The next material, balsa wood, has the main advantage of being relatively cheap and lightweight. This made it promising as it could work with the size of the glider we were working on.

However, getting precise details into a base of balsa wood, like with aluminum, seems complex so it might have been difficult to achieve the optimal design we were looking for. The final option, 3D printing, made the most sense for our project. 3D printing provides a particularly easy transition between CAD and a final product; all one has to do is save the CAD model as a different file type, run it through the 3D printing slicer software, and then print it. 3D printing also allows for relatively quick turnaround due to its ability to craft a full prototype in the background on a timescale of the order of 10 hours. 3D printing is an additive process, and unlike using balsa wood or aluminum stock and carving out the shapes we want, it would create the shapes we want by melting a plastic filament and adding layer by layer from scratch. This allows 3D printing to create very intricate objects with fine and coarse details. Using cheap plastics such as PLA or ABS, in addition to design freedom, e.g. the ability to design hollow parts, allows 3D printing to create extremely lightweight structures. Fortunately, our school has 3D printing available as a service for students, and as it turned out two members of the payload team owned hobbyist 3D printers already. The filament used ended up being PLA as it was readily available and has standard properties which were good enough for the models we created. Thus, 3D printing allowed for convenient, timely, cheap, and intricate fabrication of components and thus was the optimal choice for our capstone.

3D printing comes with a few special considerations. The first is the printing orientation. As it is a constructive fabrication process, the parts must be printed from scratch and must be able to avoid tipping over in whatever orientation they are printed in. The biggest difficulty for this was printing the wings; they were printed with the cross-section of the airfoil flat on the bed of the 3D printer. Had we printed the wing flat on the bed, much of it would've been floating off of the bed of the printer and this could've led to defects. Another consideration was the infill pattern of the wings. In the BWB design, a hollow wing with a criss-crossing infill pattern was utilized to create a strong but lightweight structure. In the conventional model, the wings were

made hollow with no infill. Finally, if certain structures like overhangs or abrupt changes in geometry in certain directions are to be printed, supports (that will be physically removed later) must be added into the models in order to prevent defects due to gravity in the final 3D printed product.

Testing Results

Our testing results were promising. With the test of the BWB design, the model seemed to glide smoothly although it only worked when flipped upside down. The suspected reason for this is an error with the angle of twist, and future proposed models should be able to correct this issue. We tested the conventional glider twice; the first test resulted in a nosedive. This prompted us to move the center of gravity backwards and to increase the aileron size, and a subsequent test resulted in a spiral due to the center of gravity being too far back. The next proposed iteration will involve a center of gravity somewhere in between these two locations in order to find the best balance. The conventional glider broke upon impact after each test; this is acceptable as the final mission only requires the glider to resist structural failure during flight. Furthermore, printing was cheap and quick so rebuilding the glider was not a problem. Finally, making the glider strong enough to withstand impact with the ground could decrease its gliding performance by adding size and weight. It is worth noting that the conventional testing was done with the camera attached, thus adding weight and drag to the glider, while the BWB testing was done without the camera.

Propulsion

Purpose

The purpose of the prototype is to demonstrate the feasibility of designing, manufacturing, and integrating several essential parts of a solid rocket motor. This prototype will let us highlight the structural integrity of the motor as one assembled unit then identify and address any unforeseen modes of failure through the implementation of various testing methods such as a hydrostatic test, or a static fire test.

Description and Implementation

The prototype was built to a 1:1 scale and mirrors the dimensions and specifications of the fifth and final motor design. It is 20.7 inches long with a 3-inch outer diameter and a 2.75-inch inner diameter. The fully assembled motor system is shown in the figure below.

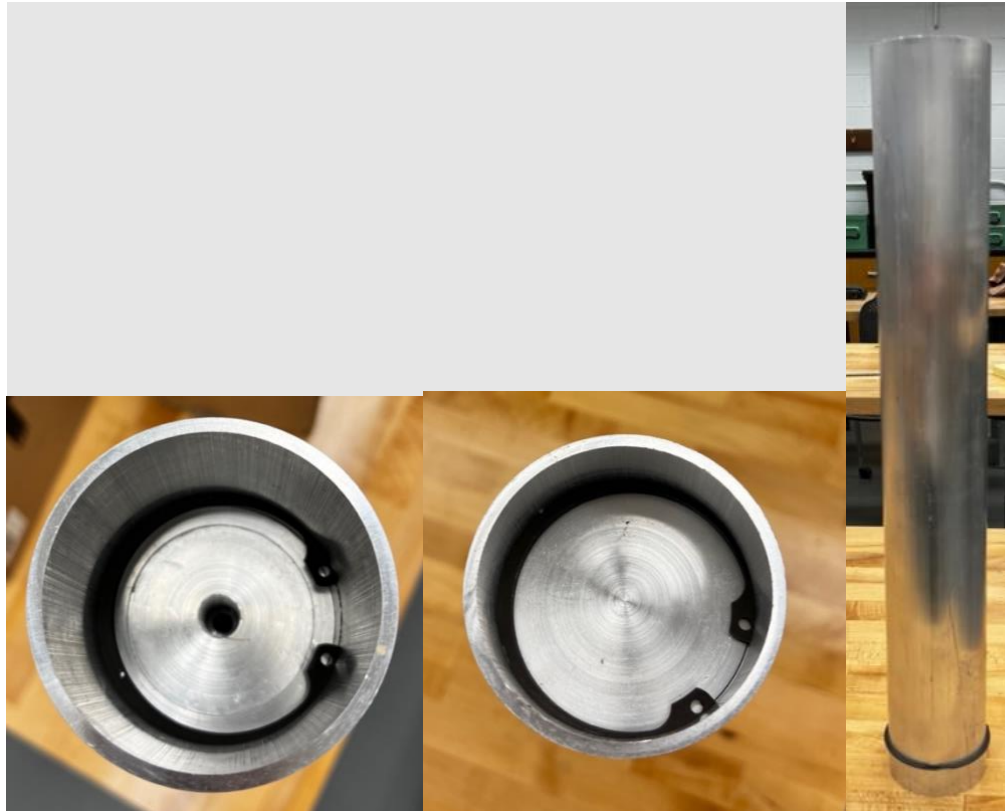


Figure 79. Bottom view (left), top view (middle), and side view (right) of the motor

The class decided to forgo a static fire test and integrated launch to focus on student research, development, and experimentation. A mixture of pushback from UVA Environmental Health & Safety and time constraints led to this decision. This meant that certain key components weren't required in the final prototype. Every component in the design was fabricated except for the propellant grains and graphite nozzle. The prototype includes the top closure, the nozzle washer, a hydrostatic nozzle, the casing, and the phenolic liner, all of which are crucial for its functionality. The hydrostatic nozzle replaced the graphite nozzle; it reflects the same outer geometry of the graphite nozzle but doesn't have the converging-diverging internals. Instead, it consists of a through-hole that is threaded at the aft end for the hydrostatic plumbing system. Images of the top closure, hydrostatic nozzle, and nozzle washer are shown below.



Figure 80. Hydrostatic nozzle and washer (left) and top closure (right) with O-rings

The casing, hydrostatic nozzle, nozzle washer, and top closure were manufactured from 6061 aluminum. Meanwhile, the liner was purchased through Rocket Motor Components, a popular online high-powered rocketry vendor. Additionally, the 1060-1090 spring steel internal and external retaining rings were bought from McMaster-Carr. Lastly, the O-rings were also supplied from McMaster-Carr and made from Buna-N, a nitrile rubber. Each of these materials were chosen so that the prototype could be used for all tests and could even be fully integrated into a rocket launch by future students given a successful static fire test.

Moving forward, the data and insights gathered from testing will inform further refinements to our motor system design, allowing other students to use it for solid propellant research or experimentation, which will act as a steppingstone in bringing a strong rocketry presence within UVA.

Manufacturing and Fabrication

The primary manufacturing method for the prototype was subtractive manufacturing. Using aluminum 6061 round stock and a lathe, the top closure, nozzle washer, and hydrostatic nozzle were created. The circular and symmetrical nature of these components made lathing the ideal method of manufacturing. The motor casing was purchased to meet the required inner and outer diameters. The shop manager handled the task of carving the internal and external grooves present on the motor casing, as the process was too complex for students to perform. The remaining shaping and geometric modification was performed by a group of students within the propulsion subgroup. During manufacturing, it was found that the inner diameter of the casing was ~ 0.020 inches smaller than 2.75 inches. This led to the outer diameters for the rest of the parts to be reduced accordingly so each part properly fit. The tolerances for the O-rings and snap

rings were given in the technical data sheet provided by McMaster-Carr. The fit for the internal components in the casing were close to a locational clearance fit. The locational clearance fit allowed for the internal components to be pushed into the casing without too much force. Adding O-rings to the closures made it significantly more difficult to assemble the pieces, which is beneficial for keeping the gasses trapped. Knowledge on tolerances, fits, and precise manufacturing skills were essential throughout the process of fabricating the prototype.

The only process students performed which did not use the lathe was cutting the phenolic liner for the motor casing's interior. This was done with a bandsaw, and after cutting to size, the liner was sanded to allow for a smoother fit inside the motor casing. Sanding the liner would have likely not been necessary if the inner diameter of the casing was 2.75 inches because the liner's outer diameter is 2.73 inches. Before full assembly, each of the internal components, except for the snap rings, were lubricated. Then, the top closure, nozzle washer, hydrostatic nozzle and phenolic liner, along with the purchased spring steel internal and external retaining rings and O-rings, were combined as shown in Figure 79 and Figure 80.

Testing Results

A variety of testing techniques were planned to ensure the safety and viability of the designed propulsion system. These tests came in the form of both physical tests.

Hydrostatic testing was employed to determine two things about the motor design: (a) that the motor could handle the calculated internal pressure that the propellant burning would have produced and (b) to check the system for leaks. Thus, the chosen method of testing these points of failure was the hydrostatic test. This is a method of testing where water is pumped into a pressure vessel at a predetermined pressure and time. The maximum pressure the pressure vessel was expected to accrue during launch was 510 psi. Had the test gone through, we expected to reach pressures in excess of 800 psi. The test was scheduled to be undertaken at the Aerospace Research Lab at UVA. The schematic shown in Figure 81 shows how the pressurized water flowed out of the pump, through the system, and into the motor.

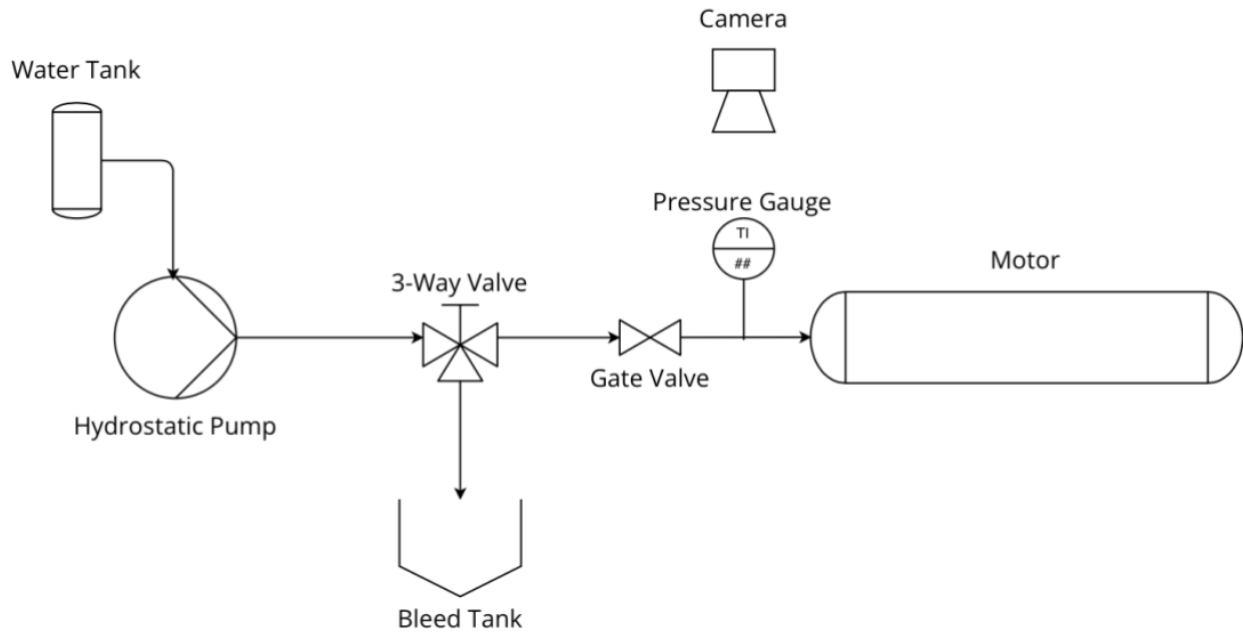


Figure 81. Schematic for Hydrostatic Test

Another important testing method is a static fire test of the propulsion system. The static fire test is a method where the prototype motor is loaded with a sample of the same propellant that will be used at launch, then fixed to a rigid test stand, ignited, and allowed to burn until all the sample propellant is consumed. A load cell attached to the side opposite the burn measures the total thrust. The measured thrust and burn time can then be used to find the burn rate coefficient of the propellant grains if desired, which is a value of paramount importance in the process of developing and testing new formulas and grain geometries. The values gathered from the static fire could then be compared with the simulations in OpenMotor. Accuracy of the actual pressure and thrust curves could be determined given how close the values from the actual test are to the simulations.

Since the university does not yet have its own test stand, the static fire was planned with the rocketry team at VCU after they completed the construction of theirs. Having a test stand and facility of our own would open several new opportunities for future projects and allow for the students to gain experience in testing methods that are used in industry.

Due to scheduling issues, these tests did not happen.

Risk and Liability

The staggering number of separate components required for the capstone project presented many risk and liability issues. Failure during flight would be possible in many unique ways, all of which had to be individually analyzed by relevant sub teams. Some of these included failure to separate, premature separation, failure of components such as the fin, nose cone, or avionics bay due to unexpected loads or random vibration, and instability during flight. These risks were mitigated during the design and fabrication phase and during the testing phase, succeeding successful assembly. Many of these risks were unique to each team. The Propulsion team encountered many risks relevant both to the danger of the materials intended for use as well as the fidelity necessary for their components. The Mechatronics and Controls team faced risks involving the loss of communication during flight, and therefore had to integrate redundancy into the design. The Aero-Structures team faced risks both during the fabrication process, as well as some of the more severe in-flight risks, such as loss of stability or the incompleteness of the rocket body. Risk was also inherent to the fabrication process itself. Many steps were taken to ensure safety, including the use of PPE such as masks, the use of well-ventilated spaces (Fig X.), and by speaking with relevant overseeing bodies. Risk during the fabrication process also extended to affect the capstone's timeline. The completion of many components were contingent upon one another, and so back-up plans—such as the use of prefabricated body tubes or nose cone—had to be put in place. This allowed the capstone to progress while also permitting sub teams to complete their work. Risk relevant to the project's timeline extended to entities beyond the class; safety training had to be completed for the use of some necessary tools, and the inability to access this training was a risk almost entirely out of the capstone's control. The class established open lines of communication with the relevant individuals, but many scheduling conflicts arose. The results of any of these failures could be extremely wide-ranging. Some small failures would not permit us to complete the final assembly of the rocket, while others would pose physical dangers to students working on the rocket. Ultimately, risk assessment matrices (Fig X.) were used during each design review to mitigate all these risks, and to ensure that every step was performed as safely as possible. These matrices included the consequence and likelihood of risks both pre-mitigation and post-mitigation. Responsibility for a negative result would be difficult to pinpoint; many issues could have been avoided if a more rigorous schedule was set and abided by, but ultimately each sub team had to claim responsibility both for the completion of their component and in their own risk assessment. Each team also had a Safety Lead which was responsible for overseeing any issues which might arise, but communication ultimately proved vital in ensuring everyone was aware of the risks posed during each step.



Figure 82. Assembly Performed in Aaron's Well-Ventilated Garage

		Pre-Mitigation							Post-Mitigation				
Likelihood	5				A	B							
	4			D									
	3				C					A			
	2								C	B			
	1							D					
		1	2	3	4	5			1	2	3	4	5
		Consequence							Consequence				

Figure 83. Example Use of Risk Assessment Matrix

Ethical Issues

Throughout the development of our rocket, our team has abided by the National Society of Professional Engineers’ Code of Ethics, a framework for the proper behavior of engineers that has been taught to us many times throughout the course of our time at the University of Virginia. The canons state that engineers should, “hold paramount the safety, health, and welfare of the public”, “perform services only in areas of their competence”, “issue public statements only in an objective and truthful manner”, “act for each employer or client as faithful agents or trustees”, “avoid deceptive acts”, and “conduct themselves honorably, responsibly, ethically, and lawfully so as to enhance the honor, reputation, and usefulness of the profession.” Within our project, there lies the innate capacity to cause harm, as actions taken in malice or ignorance can endanger our own team and the public. Major ethical concerns come with the choice of payload, the construction of the rocket frame, and its propulsion system. The payload of a sounding rocket is primarily used for experimental purposes, with the goal of collecting data and analyzing it for research. With this, there stands the ethical concern that comes with our freedom to choose, whether it be our choice of propellant, our choice of payload, or even our choice of how we construct the many parts of our rocket. These choices come with the consequences that it may have to the safety of our team, the public, and the environment.

Impact on Society

Oftentimes, large scale projects for rocket and space missions can cost upwards of tens to hundreds of millions of dollars. In a field where testing in both Earth and space environments is often essential, these projects can take a significant amount of time, so a mission is not wasted due to a fault in a system. Sounding rockets can offer a significantly cheaper alternative to testing new technologies for use in future missions (McDonell & Ahuja, 2023). With scaled down versions, the cost, and risk, decreases which can allow more people such as students and

researchers to gain experience. This hands-on experience is especially valuable in a field where there are often fewer due to the high cost and high risk of the projects typically available.

From this, student-oriented competitions such as the Intercollegiate Rocket Engineering Competition (IREC), emerge and are important ways students can get involved in work related to their fields of interest while gaining hands-on experience. Since this project was initially towards the goals set by the IREC competition, it is appropriate to emphasize the importance of such a competition. At a student level in a university, this competition can play an important role in introducing students to the rocketry field. In turn, this also helps students gain experience and training while often being able to interact with industry professionals along the way.

Overall, this project allowed students to be involved in all stages of a rocket from design to fabrication. Through this project, students were able to develop new design, manufacturing, and testing skills that may not have been available in a non-industry or professional setting otherwise. While not ultimately launched, this project demonstrates the usefulness of small scale, hands-on projects in learning environments. For example, this project allowed students to demonstrate skills learned in the classroom in a practical way, experience that may be useful in future industry endeavors. Without the availability of similar projects to this rocket and without support of outside organizations such as the Experimental Sounding Rocket Association (ESRA) which runs IREC, students may not have the opportunity to participate in, and gain experience from, hands-on projects that reflect industry standards in a field of their interest.

Impact on the Environment

Due to factors beyond our control, we were not able to launch our rocket, leading to a very minimal overall environmental impact. However, there were still aspects of our project where we had to take precautions to minimize our impact on the environment.

Throughout the entire manufacturing process, each sub team took steps to work to mitigate any potential environmental damage. The teams primarily worked indoors in well-ventilated rooms with personal protective equipment to minimize risk to ourselves. When teams did fabricate parts of the rocket outdoors, we made sure to work in areas where we would not disturb plants or wildlife, and we made sure to thoroughly clean up after ourselves when finished, leaving the area as we found it.

Another source of environmental impact stems from the resources used to ship all of our materials. This part of our project had the greatest environmental impact since most sub teams opted to custom-build their sections of the rocket rather than purchase pre-made parts, leading to more materials ordered and more fuel and resources expended to ship these materials. Although we knew that fabricating the rocket this way would have a more negative environmental impact, we decided that the hands-on learning experience we gained from constructing each section ourselves was worth the environmental risk.

A portion of our project that we were not able to complete due to environmental and safety concerns was the propulsion team’s development of ammonium perchlorate composite propellant (APCP). Despite providing thorough documentation and planning to try to safely manufacture APCP, UVA Environmental Health & Safety perceived the risk to our safety and the manufacturing environment to be too high and did not allow us to develop our own propellant formula. We are now using AeroTech Classic L798 propellant, which poses less risk to our personal health and that of the surrounding environment.

Had we completed our rocket and been ready to launch by our original timeline, we still would not have been able to launch due to dry weather conditions in Virginia and too great a potential for wildfires. A small spark from our rocket launch could have ignited a forest fire, which could have had detrimental effects to the surrounding land and environment. This is a risk that we would not have been able to mitigate any other way than not launching, and even though we were not in this situation, it was still an important exercise to consider launch conditions in preventing harm to the surrounding environment.

Overall, our project had a fairly inconsequential impact on the environment, but it is still important to keep this aspect in mind throughout the engineering design process, and this project allowed us to gain valuable experience in doing so.

Cost and Engineering Economics

Table 5: Budget and expense breakdown for aerospace structures.

Aero-Structures Budget		
Sub-team	Total Spent	Percent of Total Budget
Nosecone	\$1,052	28%
Body	\$1,375	36%
Couplers	\$535	14%
Fins	\$468	12%
Misc.	\$360	9%
Total	\$3790	100%

Table 6: Budget and expense breakdown of mechatronics.

Mechatronics Budget		
Sub-team	Total Spent	Percent of Total Budget
Parachutes	\$250.50	38%
Payload	\$0	0%
Electronics	\$403.50	62%
Total	\$654	100%

Table 7: Budget and expense breakdown of propulsion (propellant grains included in motor design).

Propulsion Budget		
Sub-team	Total Spent	Percent of Total Budget
Motor Selection & Testing	\$890	56%
Motor Design	\$709	44%
Thermal & Structural Analysis	\$0	0%
Total	\$1,599	100%

Codes and Standards

This project adhered to two sets of codes and standards, those set by UVA, which provided the funding for the project, and those set by the Tripoli Rocketry Association (TRA), the officials regulating the proposed launch site. Both sets of codes and standards influenced the design process of the rocket, the effect of which will be examined individually by the organization.

The main UVA codes and standards influencing this project were SEC-003 and SEC-005, the chemical and student safety codes. SEC-003 specifically covers the standards for handling and usage of hazardous chemicals, which in this context pertained mostly to the design and testing of the propulsion systems of the rocket. This code requires that any individual that handles hazardous chemicals in a UVA environment pass Chemical Safety and Waste Training. Through our talking with the UVA environmental and health safety office, as detailed in previous sections, we were advised to not pursue in-house propellant options, and instead either buy a prebuilt motor, or pre-made propellant and motor housing. Alongside this, all members working with possibly hazardous chemicals received the training as required by SEC-003. SEC-005 details the safety requirements relating to labs, makerspaces, shops, and studios, which were facilities used by almost every team and student involved in this capstone project. SEC-005 requires that each student abide by the safety programs in place for each work area they use and complete machine-specific training when needed.

The Tripoli safety code outlines the general procedures and required features for rockets to launch at their site and dictated some general design constraints from these requirements. The main design and protocol changes that were made to accommodate this safety code, as highlighted previously, were the height per rocket class and launch radius limits, which lead to our decision to postpone and eventually cancel our launch. Other than the design changes, the Tripoli safety code also required a member of our team to become a level two certified Tripoli rocketry member to launch a rocket of the size built in this project.

Conclusion

We successfully designed all the components necessary to launch the rocket. We were able to fabricate the body of the rocket, including the nosecone, fins, and couplers, as well as prototypes for the gliders. Several factors led to our decision not to launch. Primary among these was that we felt by launching we would need to change our initial design for the rocket to such an extent that it would no longer be truly our design, and not sufficiently student researched and developed to be a capstone project for thirty students. We weighed what we felt was important in an engineering capstone – on the one hand, having a rocket that was almost entirely student developed, with research and original ideas, but not being able to launch or entirely fabricate it due to launch site and health and safety restrictions. On the other hand, restricting the scope of our project to a rocket that was mostly off the shelf, following all of the competition conventions, but being able to fabricate and launch it. In the end, we decided that to fulfill our capstone, the most important thing was to conduct research and try to do something new and interesting, not necessary to produce results, so we went with the former option. This turned out to be the right decision, because although we ordered parachutes in December after refining our design, they did not arrive until April 25, two weeks after our initial launch date. If we had tried to change our design and launch, we would not have been able to launch anyway and also had an uninteresting design. Therefore, the product satisfied our original requirements in theory, but we don't know whether they would have been satisfied in practice. Next steps include completing fabrication, including for the avionics bay, the PCB, the finalized motor, and then finding somewhere to launch that would allow us to launch with the design we created. If that was not possible without verifying our components, we would look into verifying each of our components through external testing methods. Our hope is that the next class to attempt to design a rocket sees the deviations from the original plan that happened with our rocket and ensures that they determine all of the design restrictions before beginning their design in a serious manner. Once they have all of the restrictions, they should discuss whether or not they can create a project that will be sufficient in scope for their capstone, and choose a different course of action if it is not.



Figure 84. Final Assembled Rocket.

Acknowledgements

The students of the Class of 2024 Spacecraft Design Capstone would like to acknowledge several important groups in individuals for making this capstone possible. Firstly, the class

would like to thank Professor McPherson for his considerable efforts in assisting the Mechatronics and Controls team in their design and fabrication process, as well as his reliable guidance and presence throughout the year. We would also like to acknowledge and thank Professor Haibo Dong in his organizing of the capstone, as well as the University of Virginia in making this possible. We would also like to sincerely thank both Ben and Elaine Russell for their continued guidance and support, without which this capstone could not have progressed as far as it has. Their expertise was instrumental in ensuring the capstone achieved the goals we set for ourselves. We also thank Sean Hanlon and Tripoli Central Virginia for their guidance on the project's safety. Finally, the capstone would like to acknowledge the University of Virginia for providing a space with which fabrication could be completed.

References

- Acosta, A. (2019). *Rice Eclipse Noctua II Technical Report*. Rice University.
- Crowell Sr., G. A. (1996). *The Descriptive Geometry of Nose Cones*. https://nakka-rocketry.net/articles/Descriptive_Geometry_Nosecones_Crowell_1996.pdf
- Dewey-Hagborg, H. (n.d.). *Introduction to the Serial Peripheral Interface | Arduino Documentation*. Retrieved May 4, 2024, from <https://docs.arduino.cc/tutorials/generic/introduction-to-the-serial-peripheral-interface/>
- Fraley, E. (2018). *Design, Manufacturing, and Integration of Fins for 2017-2018 OSU ESRA 30k Rocket*. Oregon State University.
- Gupta, S. (n.d.). *Current Sensing Techniques using Different Current Sensors*. Retrieved May 4, 2024, from <https://circuitdigest.com/article/how-to-measure-current-in-a-circuit-with-different-current-sensing-techniques>
- McDonnell, D. & Ahuja, K. (2023). A Historical Review of Sounding Rockets and their use in Hypersonics Research. *AIAA SCITECH 2023 Forum*. (p. 0769). <https://doi.org/10.2514/6.2023-0769>
- Milligan, T. (2017). *What is the best fin shape for a model rocket?* Peak of Flight Newsletter, Issue 442.
- Nakka, R. (2022a, September 1). *Solid Propellant Burn Rate*. <https://www.nakka-rocketry.net/burnrate.html>
- Nakka, R. (2022b, October 19). *Rocket Motor Design Charts*. <https://www.nakka-rocketry.net/design1.html#Deter>
- Nakka, R. (n.d.). *Richard Nakka's Experimental Rocketry Site*. Retrieved May 4, 2024, from <https://www.nakka-rocketry.net/>
- National Society of Professional Engineers. (2019, July). *NSPE Code of Ethics for Engineers*. Ethics. <https://www.nspe.org/resources/ethics/code-ethics>
- Pektas, A. (2019). Effects of Different Fin Shapes on Apogee and Stability of Model Rockets. DOI: 10.1109/RAST.2019.8767439
- Sankalp, S. (2022). *Computational analyses of tail fin configurations for a sounding rocket*. <https://doi.org/10.1007/s42401-021-00116-8>

Spaceport America Cup. (2023). *Intercollegiate Rocket Engineering Competition Rules & Requirements Document*.

https://www.soundingrocket.org/uploads/9/0/6/4/9064598/sa_cup_irec_rules_and_requirements_document-2023_v1.0_20221202.pdf

What is an RF Capacitor? (n.d.). Retrieved May 4, 2024, from

<https://www.kemet.com/en/us/technical-resources/what-is-an-rf-capacitor.html>

Zambetti, N., Hylan, J., & Soderby, K. (n.d.). *Inter-Integrated Circuit (I2C) Protocol | Arduino Documentation*. Retrieved May 4, 2024, from

<https://docs.arduino.cc/learn/communication/wire/>

Zhao, N., Liao, W., & Sino, H. (n.d.). *High-Side Current Sensing with Wide Dynamic Range: Three Solutions | Analog Devices*. Retrieved May 4, 2024, from

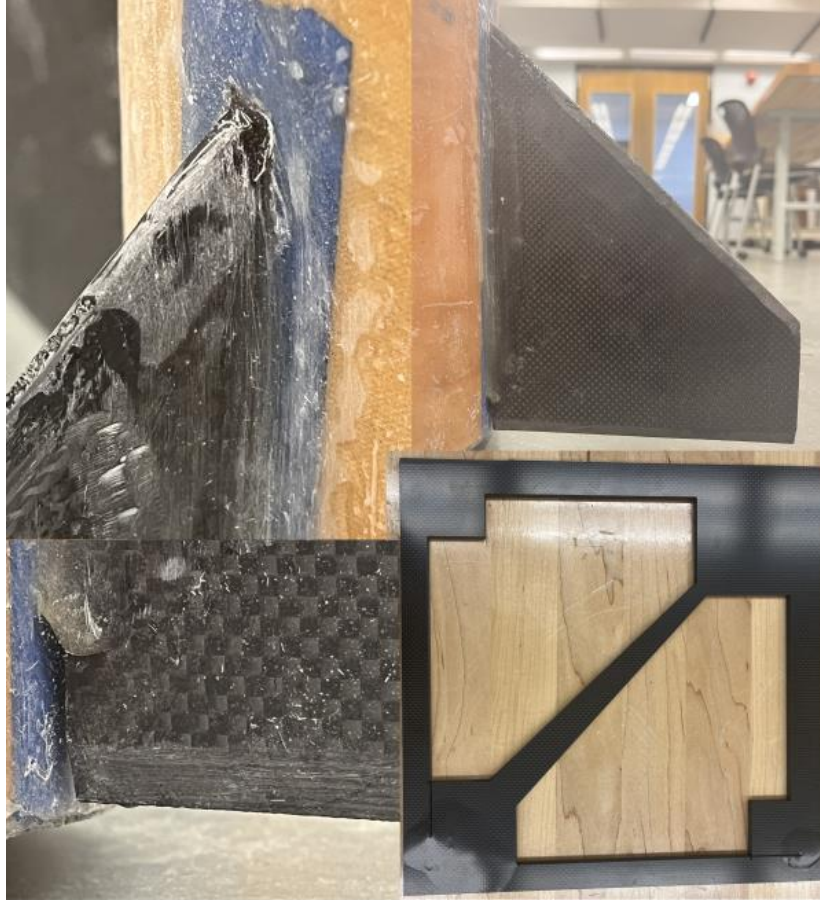
<https://www.analog.com/en/resources/analog-dialogue/articles/high-side-current-sensing-wide-dynamic-range.html>

9V Success. (n.d.). Retrieved May 4, 2024, from <https://www.missileworks.com/9v-success>

Current Sensing Methods in Power Electronics Applications. (n.d.). Retrieved May 4, 2024, from <https://encyclopedia.pub/entry/47796>

Appendices

Appendix A: Fin photos clockwise: leading edge, full fin, cut carbon fiber plate, trailing edge.



Appendix B: Matlab Live Script for Fin CoP & Flutter Velocity Calculation.

Fin calculation v1.1

Parameter definitions

General Parameters

```
% eff. shear modulus G_E [Pa = N/m2 = kg/(m*s2)]:  
G_E = 10E6;  
% speed of sound a [m/s]:  
a = 330;  
% Air pressure at sea level p_0 [Pa = N/m2 = kg/(m*s2)]:  
p_0 = 1.01325E5;  
% Flight altitude h [m]:
```

```
h = 3048; % 3048 m = 10000 ft
% Rocket CoG [m]:
X_CG = 1.87;
```

Dependent parameters:

```
% Air pressure at altitude p [Pa = N/m2 = kg/(m*s2)]:
p = p_0*(1-(9.8067*h)/(1004.7*288.16))^(1004.7*0.028970/8.3145);
```

Rocket Parameters

Nose & Body:

```
% Length of nose L_N [m]:
L_N = 0.623;
% Length of body tubes L_B [m]:
L_B = 2.21;
% Length of transition L_T [m]:
L_T = 0.1;
% Diameter at base of nose d [m]:
d = 0.157;
% Diameter at front of transition d_F [m]:
d_F = 0.157;
% Diameter at rear of transition d_R [m]:
d_R = 0.157;
% Radius of body at aft end R [m]:
R = 0.0785;
% Distance from tip of nose to front of transition X_P [m]:
X_P = 1;
```

Fins:

```
% Number of fins N []:
N = 4;
% Fin thickness at root chord t_RC [m]:
t_RC = 6.35*1E-3;
% Fin thickness at tip chord t_TC [m]:
t_TC = 6.35*1E-3;
% fin root chord C_RC [m]:
C_RC = 0.18;
% Fin tip chord C_TC [m]:
C_TC = 0.06;
% Fin semispan S [m]:
S = 0.145;
% Set fin to be clipped delta (X_LRT will be ignored)
set_clipped_delta = true;
% Distance between fin root leading edge and fin tip leading edge parallel to
% body X_R [m]:
X_LRT = 0.16;
% Distance between fin root chord trailing edge to rearmost part of rocket
% X_RB [m]:
```

```

X_RB = 0;
% leading edge half angle phi_LE [°]:
phi_LE = 15;
% trailing edge half angle phi_TE [°]:
phi_TE = 15;
Dependent parameters for the fins:
% chord c [m]:
c = (C_RC+C_TC)/2;
% Panel aspect ratio A []:
A = S/c;
% taper ratio lambda []:
lambda = C_RC/C_TC;
% Distance from nose tip to fin root chord leading edge X_B [m]:
X_B = L_N + L_B - C_RC - X_RB;
% Length of fin mid-chord line L_F [m]:
L_F = sqrt(S.^2 + (X_LRT + C_TC./2 - C_RC./2).^2);
% CHECK if dimensions are ok (parallel part of tip chord airfoil > 0)
X_P_TC = C_TC - t_TC./2*cos(deg2rad(phi_LE)) - t_TC/2*cos(deg2rad(phi_TE))
if X_P_TC <= 0
    warning('Fin tip chord too short or edge half angle too small, collision of
both tapered sides.')
end

if set_clipped_delta
    X_LRT = C_RC-C_TC;
    disp(['Fin set to clipped delta. Using X_LRT = ',num2str(X_LRT)]);
end

```

Calculation of flutter velocity v_f

```

% medium thickness is used
v_f =
a.*sqrt(G_E./((39.3*A.^3./((t_RC+t_TC)./(2*c)).^3.*(A+2)).*(lambda+1)./2*(p/p_0))

```

Center of Pressure calculation

Nose Cone Terms:

```

C_N_N = 2;
X_N = 0.666*L_N; % for cone
%X_N = 0.466*L_N; % for ogive

```

Conical Transition Terms:

```

if d_R == d_F
    C_N_T = 0;
    X_T = 0;
else
    C_N_T = 2*((d_R/d)^2-(d_F/d)^2);

```

```
X_T = X_P + L_T/3*(1+(1-d_F/d_R)/(1-(d_F/d_R)^2));
end
```

Fin Terms:

```
C_N_F = (1+R./(S+R)).*(4.*N.*(S./d).^2)./(1+sqrt(1+(2.*L_F./(C_RC+C_TC)).^2));
X_F = X_B + X_LRT./3.*(C_RC+2*C_TC)./(C_RC+C_TC)+1/6.*((C_RC+C_TC)-
(C_RC.*C_TC)./(C_RC+C_TC));
```

Finding the Center of Pressure

```
C_N_R = C_N_N + C_N_T + C_N_F;
% Find CP Distance from Nose Tip:
X_CP = (C_N_N.*X_N + C_N_T.*X_T + C_N_F .* X_F)./C_N_R
```

```
% goal of distance between CG and CP: 0.3 m
delta_X_CG_CP = X_CP - X_CG
```

Print information for Excel sheet

```
for i = 1:1
    fprintf(['S',repmat(' %.3f', 1, length(S)),'\n t_RC',repmat(' %.3f', 1,
length(t_RC)),'\n t_TC',repmat(' %.3f', 1, length(t_TC)),'\n
C_RC',repmat(' %.3f', 1, length(C_RC)),'\n C_TC',repmat(' %.3f', 1,
length(C_TC)),'\n X_LRT ',repmat(' %.3f', 1, length(X_LRT)),'\n phi_LE
',repmat(' %.3f', 1, length(phi_LE)),'\n phi_TE',repmat(' %.3f', 1,
length(phi_TE)),'\n X_CP ',repmat(' %.3f', 1, length(X_CP)),'\n
delta_X_CG_CP',repmat(' %.3f', 1, length(delta_X_CG_CP)),'\n v_f
',repmat(' %.3f', 1, length(v_f)),'\n'], S, t_RC, t_TC, C_RC, C_TC, X_LRT,
phi_LE, phi_TE, X_CP, delta_X_CG_CP, v_f)
    %fprintf('S %.3f\n t_RC %.3f\n t_TC %.3f\n C_RC %.3f\n C_TC %.3f\n X_LRT %.3f\n
phi_LE %.3f\n phi_TE %.3f\n X_CP %.3f\n delta_X_CG_CP %.3f\n v_f %.3f\n', S(i),
t_RC(i), t_TC(i), C_RC(i), C_TC(i), X_LRT(i), phi_LE, phi_TE, X_CP(i),
delta_X_CG_CP(i), v_f(i))
    %fprintf('S %.3f\n t_RC %.3f\n t_TC %.3f\n C_RC %.3f\n C_TC %.3f\n X_LRT %.3f\n
phi_LE %.3f\n phi_TE %.3f\n X_CP %.3f\n delta_X_CG_CP %.3f\n v_f %.3f\n', S,
t_RC(i), t_TC(i), C_RC, C_TC, X_LRT, phi_LE, phi_TE, X_CP, delta_X_CG_CP, v_f(i))
end
```

Appendix C: Nosecone Shapes.

Table C1: The equations used for the three shapes for the design and analysis of the nosecone (Crowell, 1996).

Shape	Equation	Diagram
-------	----------	---------

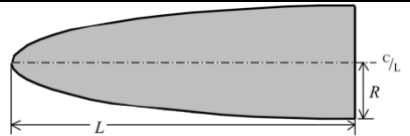
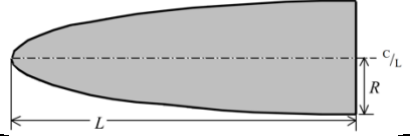
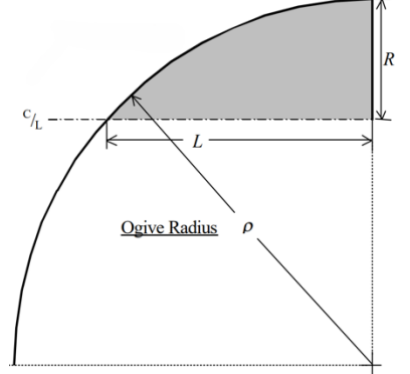
Parabolic	$y = R \left(\frac{x}{L} \right)^{\frac{1}{2}}$	
Elliptical	$y = R \sqrt{1 - \frac{x^2}{L^2}}$	
Ogive	$\rho = \frac{R^2 + L^2}{2R}$	

Table C2: First iteration nosecone CFD results

Shape	Nosecone height (cm)	Drag Force (N)
Parabolic	49.5	126.7743
	66	119.2123
	82.5	125.8847
Elliptical	49.5	122.7709
	66	112.54
	82.5	118.7675
Ogive	49.5	116.5434
	66	110.0935
	82.5	102.309

Table C3: Second iteration nosecone CFD results

Shape	Nosecone Height (cm)	Drag Force (N)	Fineness Ratio (Height/Diameter)
Elliptical	62.6872	91.9532	4
	65.82156	91.6439	4.2
	68.95592	91.0074	4.4
	72.09028	91.4997	4.6
	75.22464	91.3602	4.8
	78.359	87.6225	5

Ogive	62.6872	91.3812	4
	65.82156	82.3081	4.2
	68.95592	82.4527	4.4
	72.09028	87.6562	4.6
	75.22464	84.9722	4.8
	78.359	82.1871	5

Appendix D: Couplers Equation Development.

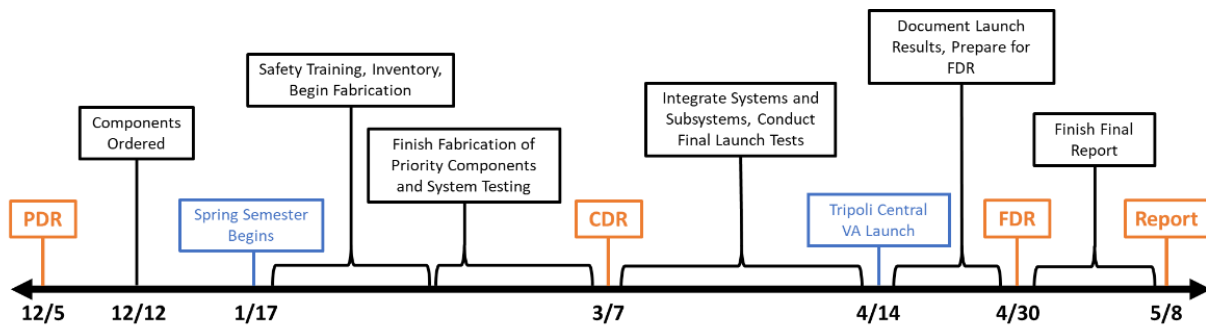
Minimum BP Charge Estimate: <https://www.desmos.com/calculator/ljvfp37c>

Median BP Charge Estimate: <https://www.desmos.com/calculator/dxdio15ohj>

Maximum BP Charge Estimate: <https://www.desmos.com/calculator/ha4r0kcyts>

Secondary Calculations: <https://www.desmos.com/calculator/ds5ztfmsyr>

Appendix E: Timeline Developed for PDR.



Appendix F: Timeline Developed for CDR.

